NASA CONTRACTOR REPORT

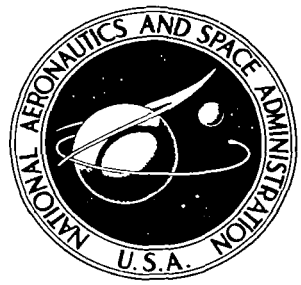

NASA CR-2

NASA CR-2887

MODELING AND PARAMETER UNCERTAINTIES FOR AIRCRAFT FLIGHT CONTROL SYSTEM DESIGN

J. D. McDonnell, R. A. Berg,
R. M. Heimbaugh, and C. A. Felton

Prepared by
DOUGLAS AIRCRAFT COMPANY
Long Beach, Calif. 90846
for Langley Research Center

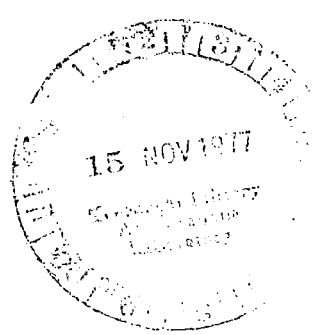

NATIONAL AERONAUTICS AND SPACE ADMINISTRATION • WASHINGTON, D. C. • SEPTEMBER 1977

1. Report No.	2. Government Accession No.	3. Recipient's
NASA CR-2887		

4. Title and Subtitle	5. Report Date
Modeling and Parameter Uncertainties for Aircraft Flight Control System Design	September 1977
	6. Performing Organization Code

7. Author(s)	8. Performing Organization Report No.
J. D. McDonnell, R. A. Berg, R. M. Heimbaugh, and C. A. Felton	MDC J4555
	10. Work Unit No.

9. Performing Organization Name and Address	11. Contract or Grant No.
Douglas Aircraft Co. 3855 Lakewood Blvd. Long Beach, California 90846	NAS1-14151
	13. Type of Report and Period Covered Final Report

12. Sponsoring Agency Name and Address	14. Sponsoring Agency Code
National Aeronautics and Space Administration Langley Research Center Hampton, Virginia 23665	

15. Supplementary Notes

Langley technical monitor: Robert S. Dunning

Final report.

16. Abstract

As aircraft designs trend toward further applications of control-configured vehicle concepts, the aircraft control systems will increasingly rely on stability and dynamic augmentation to obtain normal flying qualities and reasonable structural margins. Although the control system designer would choose to have a perfect dynamic description of the vehicle that is being developed, he knows that a level of uncertainty of plant dynamics will exist.

This report gives typical values of plant dynamic uncertainties for some recent aircraft design and development programs. Histories of pertinent aerodynamic, inertial, and structural parameter variations are given for a period of time from program initiation to aircraft certification. These data can be used as typical of future vehicles so that control system design concepts can be evaluated with due consideration to their sensitivity to uncertainties in plant dynamics.

17. Key Words (Suggested by Author(s))	18. Distribution Statement
Aircraft Design Control Systems Aerodynamic Coefficients Structual Vibration Estimates Confidence Mathematical Models	Unclassified-Unlimited Subject Category 05

19. Security Classif. (of this report)	20. Security Classif. (of this page)	21. No. of Pages	22. Price*
Unclassified	Unclassified	131	$6.00

*For sale by the National Technical Information Service, Springfield, Virginia 22161

CONTENTS

ILLUSTRATIONS

TABLES

NOTATION

SYMBOL	DEFINITION	UNITS
A	Aspect ratio, $\frac{b^2}{S}$	---
b	Wing span	meters (feet)
C_D	Drag coefficient, $\frac{\text{drag}}{\bar{q}S}$	---
C_{D_q}	$\frac{\partial C_D}{\partial (q\bar{c}/2U)}$	1/radian
C_{D_u}	$\frac{U}{2}\frac{\partial C_D}{\partial u}$	---
C_{D_α}	$\partial C_D/\partial \alpha$	1/radian
$C_{D_{\dot{\alpha}}}$	$\frac{\partial C_D}{\partial (\dot{\alpha}\bar{c}/2U)}$	1/radian
$C_{D_{\delta_e}}$	$\partial C_D/\partial \delta_e$	1/radian
C_L	Lift coefficient, $\frac{\text{Lift}}{\bar{q}S}$	---
C_{L_q}	$\frac{\partial C_L}{\partial (q\bar{c}/2U)}$	1/radian
C_{L_u}	$\frac{U}{2}\frac{\partial C_L}{\partial u}$	---
C_{L_α}	$\frac{\partial C_L}{\partial \alpha}$	1/radian

NOTATION

SYMBOL	DEFINITION	UNITS
$C_{L_{\dot{\alpha}}}$	$\frac{\partial C_L}{\partial (\dot{\alpha}\bar{c}/2U)}$	1/radian
$C_{L_{\delta_e}}$	$\partial C_L/\partial \delta_e$	1/radian
C_ℓ	Rolling-moment coefficient, $\frac{\text{rolling moment}}{\bar{q}Sb}$	---
C_{ℓ_p}	$\frac{\partial C_\ell}{\partial (pb/2U)}$	1/radian
C_{ℓ_r}	$\frac{\partial C_\ell}{\partial (rb/2U)}$	1/radian
C_{ℓ_β}	$\frac{\partial C_\ell}{\partial \beta}$	1/radian
$C_{\ell_{\delta_a}}$	$\frac{\partial C_\ell}{\partial \delta_a}$	1/radian
$C_{\ell_{\delta_r}}$	$\frac{\partial C_\ell}{\partial \delta_r}$	1/radian
$C_{\ell_{\delta_{sp}}}$	$\frac{\partial C_\ell}{\partial \delta_{sp}}$	1/radian
C_m	Pitching-moment coefficient, $\frac{\text{pitching moment}}{\bar{q}Sc}$	
$C_{m_{i_H}}$	$\frac{C_m}{i_H}$	1/radian

NOTATION

SYMBOL	DEFINITION	UNITS
C_{m_q}	$\frac{\partial C_m}{\partial(q\bar{c}/2U)}$	1/radian
C_{m_u}	$\frac{U}{2}\frac{\partial C_m}{\partial u}$	---
C_{m_α}	$\frac{\partial C_m}{\partial \alpha}$	1/radian
$C_{m_{\dot{\alpha}}}$	$\frac{\partial C_m}{\partial(\dot{\alpha}\bar{c}/2U)}$	1/radian
$C_{m_{\delta_e}}$	$\frac{\partial C_m}{\partial \delta_e}$	1/radian
C_n	Yawing-Moment coefficient, $\frac{\text{yawing moment}}{\bar{q}Sb}$	---
C_{n_p}	$\frac{\partial C_n}{\partial(pb/2U)}$	1/radian
C_{n_r}	$\frac{\partial C_n}{\partial(rb/2U)}$	1/radian
C_{n_β}	$\frac{\partial C_n}{\partial \beta}$	1/radian
$C_{n_{\delta_a}}$	$\frac{\partial C_n}{\partial \delta_a}$	1/radian
$C_{n_{\delta_r}}$	$\frac{\partial C_n}{\partial \delta_r}$	1/radian

NOTATION

SYMBOL	DEFINITION	UNITS
$C_{n_{\delta_{sp}}}$	$\frac{\partial C_n}{\partial \delta_{sp}}$	1/radian
C_y	Sideforce coefficient, $\frac{\text{sideforce}}{\bar{q}S}$	---
C_{y_p}	$\frac{\partial C_y}{\partial (rb/2U)}$	1/radian
C_{y_r}	$\frac{\partial C_y}{\partial (rb/2U)}$	1/radian
C_{y_β}	$\frac{\partial C_y}{\partial \beta}$	1/radian
$C_{y_{\delta_a}}$	$\frac{\partial C_y}{\partial \delta_a}$	1/radian
$C_{y_{\delta_r}}$	$\frac{\partial C_y}{\partial \delta_r}$	1/radian
$C_{y_{\delta_{sp}}}$	$\frac{\partial C_y}{\partial \delta_{sp}}$	1/radian
$\bar{c}$	Wing mean aerodynamic chord	meters (feet)
f	Fore and aft structural deflection	meters (feet)
f	Natural Frequency	hertz

NOTATION

SYMBOL	DEFINITION	UNITS
F_H	Aft fuselage bending factor	---
g	Acceleration of gravity 9.807 (32.174)	$\frac{\text{meters}}{\text{sec}^2}$ (ft/sec^2)
h	Altitude	meters (feet)
h	Vertical structural deflection	meters (inch)
I_{XZ}	Product of inertia	Kg-$meter^2$ ($slug-ft^2$)
I_X	Rolling moment of inertia	Kg-$meter^2$ ($slug-ft^2$)
I_Y	Pitching moment of inertia	Kg-$meter^2$ ($slug-ft^2$)
I_Z	Yawing moment of inertia	Kg-$meter^2$ ($slug-ft^2$)
ℓ	Lateral deflection	meters (inch)
i_H	Horizontal stabilizer incidence	radians
M	Mach number	---
m	Mass	kg (slugs)
n	Normal load factor $\approx \frac{\text{lift}}{\text{weight}}$	g
P	Roll rate	rad/sec

NOTATION

SYMBOL	DEFINITION	UNITS
q	Pitch rate	rad/sec
q	Modal displacement	meters (inch)
$\bar{q}$	Dynamic pressure, $1/2\ \rho U^2$	newtons/meter^2 (lb/ft^2)
r	Yaw rate	rad/sec
S	Wing area	meters^2 (ft^2)
s	Laplace operator	1/sec
U	Velocity along longitudinal axis ($\approx$ true airspeed)	meters/sec (feet/sec)
u	Perturbation velocity along longitudinal axis	meters/sec (feet/sec)
v	Perturbation velocity along lateral axis	meters/sec (feet/sec)
W	Velocity along normal axis	meters/sec (feet/sec)
w	Perturbation velocity along normal axis	meters/sec (feet/sec)
α	Angle-of-attack	radians
α	Pitch deflection	radians

NOTATION

SYMBOL	DEFINITION	UNITS
β	Sideslip angle	radians
Δ	Increment	---
δ_a	Aileron deflection	radians
δ_e	Elevator deflection	radians
δ_r	Rudder deflection	radians
δ_{sp}	Spoiler deflection	radians
θ	Pitch angle; roll deflection	radians
κ	Ratio of two-dimensional lift-curve slope at appropriate Mach number to $2\pi/\beta$; or, ratio of incompressible two-dimensional lift-curve slope to 2π	---
$\Lambda_{c/2}$	Sweepback angle of 50-percent chordline	radians
ρ	Density of air	kilograms/meters^3 (slugs/feet^3)
ϕ	Bank angle	radians
ϕ_{β_j}	Modal wordrate at location β of the airframe for the jth mode (-)	
ψ	Yaw angle	radians
ψ	Yaw deflection (structural)	radians

NOTATION

ABBREVIATIONS

ATP	Authority to proceed
CCV	Control configured vehicle
CERT	FAA certification date
C.G.	Center of gravity
D	First dynamics analysis
FF	First flight
G. M. or $\overline{m}$	Generalized mass (newtons-second/meter)
GVT	Ground vibration test
MLW	Maximum landing weight
MZFW	Maximum zero fuel weight
MEW	Manufacturer's empty weight
OPITEMS	Operational items = crew + unusable fuel + oil + food, water and emergency equipment + miscellaneous
MTOGW	Maximum takeoff gross weight = MEW + OPITEMS + PAYLOAD + FUEL
SIC	Structural influence coefficient
T	Time duration to certification

NOTATION

SUBSCRIPTS

A	Total airplane
FINAL	Final value
H	Horizontal tail
o	Initial (trim) conditions
TO	Tail off
$\begin{matrix} i \\ j \end{matrix}$ or α	Parameter number mode number
B	Location on airframe

SUPERSCRIPTS

E	Elastic
E/R	Elastic-to-rigid ratio
R	Rigid

NOTE: Dot over symbol denotes derivative with respect to time

MODELING AND PARAMETER UNCERTAINTIES FOR AIRCRAFT FLIGHT CONTROL SYSTEM DESIGN

by

J. D. McDonnell, R. A. Berg, R. M. Heimbaugh,
and C. A. Felton

Douglas Aircraft Company
McDonnell Douglas Corporation
Long Beach, California

SECTION 1
INTRODUCTION

Aircraft designs are continuing their evolution in structural and aerodynamic innovations that require artificial means of stability and dynamic augmentation to obtain normal flying characteristics and acceptable structural margins. The motivation, of course, is to continue the reduction in direct operating costs for commercial aircraft and to continue to improve the mission effectiveness/costs of ownership of military vehicles. The recent rapid rise in fuel costs has made commercial applications of some control-configured-vehicle (CCV) concepts desirable in the near term, perhaps on a derivative aircraft. Thus, it is not only imperative that dynamics of the aircraft in flight turn out as predicted, since stability margins will be lower (and in some cases, zero or negative), but that the flight control systems for those aircraft provide desired characteristics when the aircraft's actual dynamic description has some expected variability about its predicted behavior.

The data presented in this report are intended to provide a start of a typical data base for use in flight controls work that is directed toward the kinds of systems noted above, i.e., those that are flight-critical or tending toward it.

The data show typical historical variability in the steady aerodynamic and selected dynamic structural parameters of jet transports at one flight condition. Historical values of many dimensionless stability derivatives

include original analytical estimates, wind tunnel updates, and final flight determined values. Structural dynamic parameters as originally estimated are shown, and the impact of configuration changes as a function of time are given. Final corrected values based on modal ground vibration test results are also given.

The data base constructed for this report has been derived from many sources and is representative of many analytical and experimental techniques. The parameters themselves range from significant dynamic contributors to those with little influence on aircraft flying characteristics. The data, therefore, indicate to the designer the historical uncertainties and variations that may be encountered in an advanced control system design and development program on a large subsonic transport aircraft. In a specific future design exercise, improvements in analytical or experimental techniques would have to be accounted for, as would greater uncertainties introduced as a result of new technology (and possibly less understood) devices and configurations.

Section II of this report discusses the sources of aerodynamic, structural and weight data and defines the formats for data presentation. The methods used to derive the data are discussed as are the results themselves. The general data format objective has been to show the historical variations of the various parameters as a function of time. The historical variations of the dimensionless aerodynamic derivatives are given so that the effects of independent error sources on rigid body dynamics can be estimated regardless of the specific notation of the user (i.e., three degree-of-freedom linear small perturbation equations, six degree-of-freedom non-linear equations of motion, transfer functions, state space notation, etc.).

Historical variations of structural dynamic characteristics are presented for the design evolution of large transport airplanes in terms of natural frequencies, the corresponding modal displacements of selected stations, and the corresponding generalized masses. The modal characteristics are discussed with respect to the control designer as to value and as to limitations.

The important field of unsteady aerodynamics as related to structural response and flutter and control-configured vehicle design were not a part of this study but should not be neglected in future studies.

Section III gives all of the actual data, while Section IV notes some possible applications of the data. Aerodynamic equations of motion and the definitions of the dimensional stability derivatives are given in the Appendix.

SECTION 2
DISCUSSION OF DATA AND METHODOLOGY

The data included in this report are from many sources and disciplines and cover time spans ranging up to four years. This section will discuss sources of data and presentation formats, and is divided into three parts where detailed discussions of aerodynamic parameter variations, and structural modal analysis are presented. Examples of data are given in this section to support the discussion, but the complete data set is given in Section III.

AERODYNAMIC PARAMETERS

The aerodynamic longitudinal and lateral-directional dimensionless derivatives given in Table 1 and 2 have been reconstructed as a function of time, where time in general goes back to initial configuration development for the particular airframe being considered. The relationship of these derivatives to aircraft dynamics is shown in the Appendix, where the aircraft equations of motion and their coefficients are defined in terms of the dimensionless derivatives.

Detailed Example of Stability Derivative Calculation

An example of the type of detailed calculation used for the determination of a single stability derivative is presented here. The selected parameter is the fundamental derivative, $(C_{L_\alpha})_A^E$ the airplane lift-curve slope, which can be calculated from the following expression:

$$(C_{L_\alpha})_A^E = (C_{L_\alpha})_{TO}^{E/R} (C_{L_\alpha})_{TO}^{R} - \left\{ F_H (C_{L_\alpha})_H^{E/R} (C_{L_{\alpha_H}})^R \right\} \left\{ 1 - \left[\left(\frac{\partial \epsilon}{\partial \alpha} \right)^R + \left(\Delta \frac{\partial \epsilon}{\partial \alpha} \right)^E \right] \right\}$$

Equation (1)

where

$(C_{L_\alpha})_A^E = \frac{\partial C_L}{\partial \alpha}$ for the entire airplane and includes static aeroelastic effects.

TABLE 1

LONGITUDINAL AERODYNAMIC PARAMETER UNCERTAINTIES

1. Drag coefficient (C_D)
2. Rate of change of drag coefficient with forward speed (C_{D_u})
3. Rate of change of drag coefficient with angle of attack (C_{D_α})
4. Rate of change of drag coefficient with elevator deflection ($C_{D_{\delta e}}$)
5. Lift coefficient (C_L)
6. Rate of change of lift coefficient with forward speed (C_{L_u})
7. Rate of change of lift coefficient with angle of attack (C_{L_α})
8. Rate of change of lift coefficient with angle of attack rate ($C_{L_{\dot{\alpha}}}$)
9. Rate of change of lift coefficient with pitch rate (C_{L_q})
10. Rate of change of pitching moment coefficient with forward speed (C_{m_u})
11. Rate of change of pitching moment coefficient with angle of attack (C_{m_α})
12. Rate of change of pitching moment coefficient with angle of attack rate ($C_{m_{\dot{\alpha}}}$)
13. Rate of change of pitching moment coefficient with pitch rate (C_{m_q})
14. Rate of change of lift coefficient with elevator deflection ($C_{L_{\delta e}}$)
15. Rate of change of pitching moment coefficient with elevator deflection ($C_{m_{\delta e}}$)
16. Rate of change of drag coefficient with pitch rate (C_{D_q})
17. Rate of change of drag coefficient with angle of attack rate ($C_{D_{\dot{\alpha}}}$)

TABLE 2

LATERAL-DIRECTIONAL AERODYNAMIC PARAMETER UNCERTAINTIES

1. Rate of change of yawing moment coefficient with sideslip angle (C_{n_β})
2. Rate of change of yawing moment coefficient with rudder deflection ($C_{n_{\delta_r}}$)
3. Rate of change of yawing moment coefficient with aileron deflection ($C_{n_{\delta_a}}$)
4. Rate of change of yawing moment coefficient with spoiler deflection ($C_{n_{\delta_{sp}}}$)
5. Rate of change of yawing moment coefficient with yaw rate (C_{n_r})
6. Rate of change of yawing moment coefficient with roll rate (C_{n_p})
7. Rate of change of side force coefficient with sideslip angle (C_{y_β})
8. Rate of change of side force coefficient with rudder deflection ($C_{y_{\delta_r}}$)
9. Rate of change of side force coefficient with aileron deflection ($C_{y_{\delta_a}}$)
10. Rate of change of side force coefficient with spoiler deflection ($C_{y_{\delta_{sp}}}$)
11. Rate of change of side force coefficient with yaw rate (C_{y_r})
12. Rate of change of side force coefficient with roll rate (C_{y_p})
13. Rate of change of rolling moment coefficient with sideslip angle (C_{ℓ_β})
14. Rate of change of rolling moment coefficient with rudder deflection ($C_{\ell_{\delta_r}}$)
15. Rate of change of rolling moment coefficient with aileron deflection ($C_{\ell_{\delta_a}}$)
16. Rate of change of rolling moment coefficient with spoiler deflection ($C_{\ell_{\delta_{sp}}}$)
17. Rate of change of rolling moment coefficient with yaw rate (C_{ℓ_r})
18. Rate of change or rolling moment coefficient with roll rate (C_{ℓ_p})

$(C_{L_\alpha})_{TO}^{E/R} = \left[\frac{\left(\frac{\partial C_L}{\partial \alpha}\right)^{Elastic}}{\left(\frac{\partial C_L}{\partial \alpha}\right)^{Rigid}}\right]_{Tail\text{-}off}$ = the ratio of C_{L_α} with aeroelastic effects to C_{L_α} of the rigid airplane, in the absence of the tail.

$(C_{L_\alpha})_{TO}^{R} = \frac{\partial C_L}{\partial \alpha}$ for the rigid airplane in the absence of the tail.

F_H = factor that accounts for effect of aft fuselage bending on horizontal tail lift.

$(C_{L_\alpha})_{H}^{E/R} = \left[\frac{\left(\frac{\partial C_L}{\partial \alpha}\right)^{Elastic}}{\left(\frac{\partial C_L}{\partial \alpha}\right)^{Rigid}}\right]_{\substack{Horizontal \\ Tail}}$ = the ratio of C_{L_α} with aeroelastic effects to C_{L_α} of rigid structure, of the isolated horizontal tail.

$(C_{L_{\alpha_H}})^{R} = \frac{\partial C_L}{\partial \alpha_H}$ horizontal tail lift curve slope of the rigid airplane

$\left(\frac{\partial \varepsilon}{\partial \alpha}\right)^{R}$ = downwash gradient for the rigid airplane

$\left(\Delta \frac{\partial \varepsilon}{\partial \alpha}\right)^{E}$ = increment to account for aeroelastic effects on downwash gradient

The method of determination of the various components in the equation depends on the point in the design cycle at which the calculation is made. For this discussion, four stages in the design process will be considered:

1. Early preliminary design.
2. Later preliminary design, but before wind tunnel data are available
3. After wind-tunnel data are available
4. After flight-test data are available

It should be noted that wind-tunnel tests are usually conducted prior to the official program start but for the flight condition selected in the present study these tests must be of the high-speed variety in order to correctly represent compressibility effects.

In Stage 1 of the design effort the components of the equation which apply to the rigid airplane are found by relatively simple methods. For example, the derivatives $(C_{L_\alpha})^R_{TO}$ and $(C_{L_{i_H}})^R$ can be determined through the use of the USAF DATCOM (Reference 1), from which Figure 1 is reproduced. The aeroelastic correction terms, $(C_{L_\alpha})^{E/R}_{TO}$, F_H, $(C_{L_\alpha})^{E/R}_H$, and $(\Delta\partial\epsilon/\partial\alpha)^E$, may be estimated based on values from previous similar production designs.

During Stage 2 in the design more sophisticated methods are employed. Typical of these is the Weissinger lifting surface theory, Reference 2, which lends itself to the estimation of both rigid and elastic characteristics.

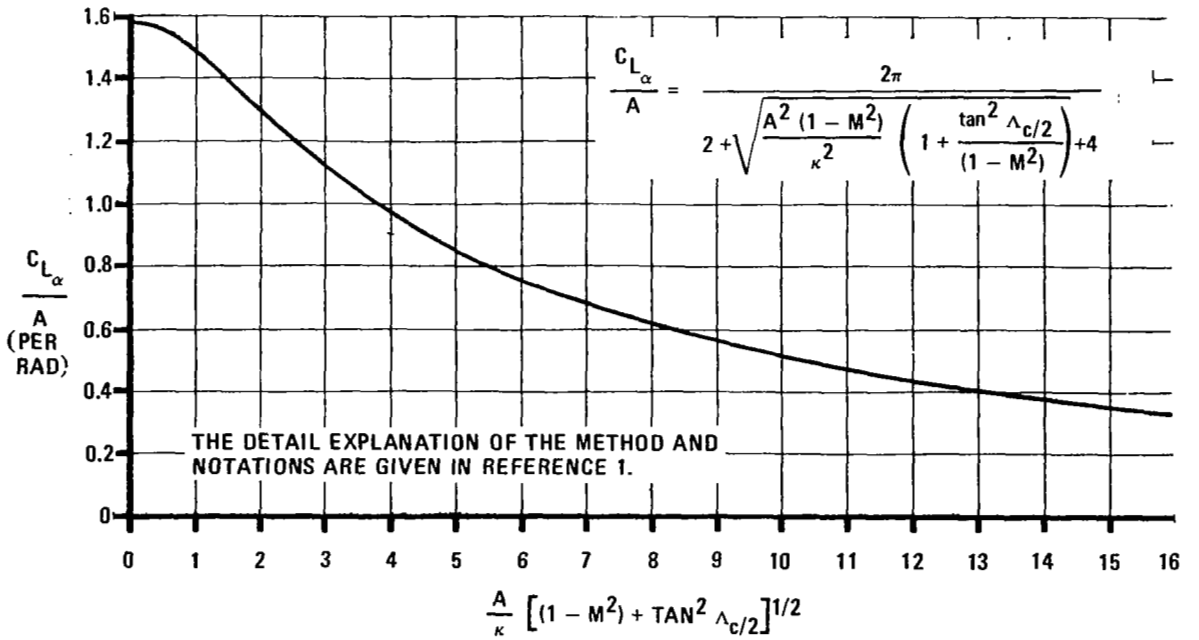

FIGURE 1. SUBSONIC WING LIFT-CURVE SLOPE

Highspeed digital computers are a virtual necessity for the application of this and similar complex methods. Other aeroelastic calculations for wing and tail surfaces are made by means of the Hedman vortex lattice lifting surface theory for elastic wings, presented in Reference 3.

The third stage of the design process benefits from the availability of wind-tunnel data. As previously noted, the tests must be appropriate for the flight condition of interest; i.e. high-speed wind tunnel data for cruise flight conditions for which compressibility effects are important, and high Reynolds number tests for high angle-of-attack flight conditions. Aside from the usual testing corrections that must be applied to wind tunnel data, other adjustments must be made to account for the fact that geometric dissimilarities often exist between the wind tunnel model and the configuration being analyzed. For the example derivative, $(C_{L_\alpha})^E_A$, wind tunnel tests provide the information for which the components $(C_{L_\alpha})^R_{TO}$, $(C_{L_{i_H}})^R$ and $(\partial\epsilon/\partial\alpha)^R$ are derived. Ground tests to ascertain the airplane stiffness characteristics are conducted during this period to verify the estimated values. If any significant discrepancies exist, the aeroelastic corrections are reevaluated using the methods previously described.

The final stage of the process follows the first flight and involves verification of the estimated values of the derivatives. Measurements made in flight test are obviously for the elastic aircraft, so the procedure is now reversed. In the case of the present example, the complete elastic derivative is measured, the elastic corrections are assumed accurate, and the elastic tail effectiveness $\left[F_H(C_{L_\alpha})^{E/R}_H (C_{L_{i_H}})^R\right]$ can be measured, thus permitting the rigid airplane characteristics to be calculated. Any necessary adjustments are made to these rigid airplane derivatives.

At this point some comments regarding stability derivatives and flying qualities may be appropriate. Prior to first flight in the development of an airplane, stability derivatives are carefully estimated as discussed in the preceding paragraphs. To the stability and control engineer the stability derivatives serve largely as the building blocks with which flying qualities are calculated. The flying qualities are then checked for com-

pliance against numerous criteria. Of course, the stability derivatives are also important to other engineering specialists, in particular, control system designers and others who utilize aircraft equations of motion in their work.

Once the flight test program is underway, many of the airplane flying qualities can be determined directly without the necessity of knowing the values of specific derivatives. The situation is somewhat different than before flight test; it is generally the flying qualities information that is available and the estimated stability derivatives are checked using the test data. Flight test results, however, are obtained for discrete flight conditions and flying qualities analyses over the remainder of the flight envelope require knowledge of the stability derivatives. Therefore, the stability derivatives are established at the flight test points and interpolations or fairings are made to develop continuous values. In this manner, a complete bank of aerodynamic data is compiled, from which the airplane flying qualities are generated for the entire flight envelope.

Referring again to Equation (1) it is apparent that several of the terms are not unique to the expression for $(C_{L_\alpha})_A^E$; they are involved in the determination of many of the other aerodynamic derivatives. Therefore, errors or uncertainties associated with these terms would cause a degree of correlation to exist between many of the derivatives. For example, the horizontal tail lift-curve slope $C_{L_{\alpha H}}$, the horizontal tail elastic-to-rigid correction factor $(C_{L_\alpha})_H^{E/R}$, and the aft fuselage bending correction factor F_H, are elements in the expressions for numerous longitudinal stability derivatives. In the data presented, the proliferation of an error in the $C_{L_{\alpha H}}$ estimate is rather dramatic. The error (caused by an underestimate of Mach number effects on $C_{L_{\alpha H}}$) is reflected in the estimates of seven separate stability derivatives: C_{L_α}, $C_{L_{\dot{\alpha}}}$, $C_{m_{\dot{\alpha}}}$, C_{Lq}, C_{m_q}, $C_{L_{\delta e}}$, and $C_{m_{\delta e}}$. The potential for this type of error correlation exists with many of the other parameters, including the lateral-directional variety.

Sources of Uncertainties

There are a number of sources for error or uncertainty associated with the estimated values of the various aerodynamic parameters. In the very early

stages of design there is considerable likelihood that the airplane configuration will be altered before the first flight occurs. In some cases these modifications taks place well into the period between program commencement and first flight. Depending on the type of change made to the configuration, there can be a considerable impact on the estimated value of the aerodynamic parameters.

Another uncertainty arises from inaccuracies that are inherent in analytical methods used to estimate the aerodynamic characteristics, including aeroelastic corrections. The degree of the uncertainty, when related as a percentage of the actual of final value, is magnified by the method of calculating most derivatives as the sum of two or more increments. When two increments are of opposite sign and the magnitudes are similar, small errors in either increment results in a large error in the total value. For example, tail increments are often added to airplane tail-off increments to obtain total airplane derivatives, and depending on the particular derivative, the two increments may be of opposite sign.

If the flight conditions of interest should change for any reason during the design process (e.g., modification of flight envelope), the coefficients of the equations of motion (dimensional stability derivatives) will change because, in general, they are functions of such flight parameters as Mach number, dynamic pressure, airspeed, altitude, and angle of attack.

Then, of course, there are the ubiquitous computational errors that occasionally go undetected for significant periods of time. Obviously, it is not possible to predict the occurrence of uncertainties stemming from such causes.

Discussion of Data

The flight condition for which the subject data were compiled was deliberately chosen to be one which is particularly prone to aerodynamic modeling errors. This proclivity for error arises from the transonic flow conditions that exist at high-speed cruise and to the relatively high dynamic pressure which has a major effect on the aeroelastic corrections. Any small misjudgements in the effects of compressibility can be exaggerated because of the rapid variations with Mach number that occur with many aerodynamic characteristics

in the transonic speed range. A typical variation with Mach number of a primary stability derivative, C_{L_α}, the airplane lift-curve slope, is shown in Figure 2. The symbol denotes the approximate cruise flight condition of this study.

It should be observed that it is difficult to generalize on the aerodynamic parameter uncertainties. A derivative which is estimated with great accuracy on one airplane may not fare as well on the next. For example, uncertainties that are attributed to configuration changes certainly cannot be generalized. However, some generalizations associated with estimation accuracies can be offered. Table 3 a provides an indication of the relative impact and the estimation accuracy normally expected for each of the aerodynamic parameters.

It should be emphasized that the categorizing of the parameters is approximate and will tend to vary with particular aircraft configurations and with flight conditions. It is emphasized that the estimation accuracy shown includes only the estimating methods normally used and does not consider uncertainties due to other causes. In Table 3 b the probable risk in flying qualities analyses and control system design is shown for each of the nine categories of Table 3 a. For example, a derivative with secondary impact that is estimated with only fair accuracy is no more or less likely to create problems than a primary derivative that normally is estimated with good accuracy.

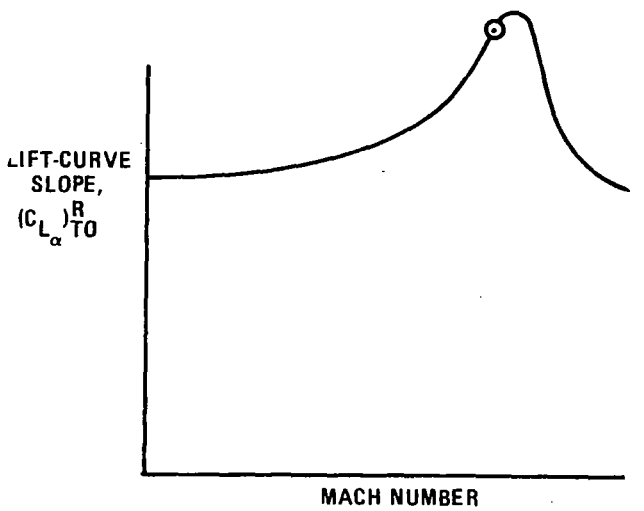

FIGURE 2. TYPICAL VARIATION OF LIFT-CURVE SLOPE WITH MACH NUMBER

TABLE 3

PARAMETER ESTIMATION ACCURACY AND POTENTIAL ERROR IN FLYING QUALITIES ANALYSES

(a)

		IMPACT ON FLYING QUALITIES		
		Primary	Secondary	Negligible
Expected Estimation Accuracy	Good	C_{L_α} C_{m_α} C_{m_q} $C_{m_{\delta e}}$ C_{ℓ_p} C_{n_r} $C_{n_{\delta r}}$	C_L C_D $C_{L_{\delta e}}$ $C_{\ell_{\delta r}}$ $C_{y_{\delta r}}$	--
	Fair	C_{n_β} C_{ℓ_β} $C_{\ell_{\delta sp}}$ $C_{\ell_{\delta a}}$	C_{L_q} $C_{L_{\dot\alpha}}$ $C_{m_{\dot\alpha}}$ C_{D_α} C_{ℓ_r} C_{n_p} $C_{n_{\delta a}}$ $C_{n_{\delta sp}}$ C_{y_β}	$C_{D_{\delta e}}$ C_{y_p} C_{y_r}
	Poor	--	C_{L_u} C_{m_u} C_{D_u}	C_{D_q} $C_{D_{\dot\alpha}}$ $C_{y_{\delta sp}}$ $C_{y_{\delta a}}$

(b) Potential Error in Flying Qualities Analyses:

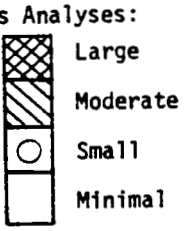

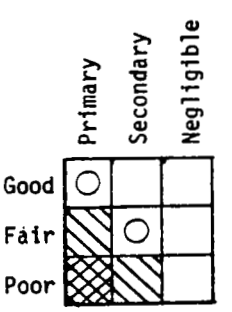

Historical values of each of the aerodynamic parameters are presented in Section 3. Most of the historical values are normalized by the final value of each parameter. However, in some cases in which the final level of the parameter is very small, the normalized value would be grossly distorted. In these cases the incremental difference between each value and the final value is deemed more meaningful and is therefore presented. In the case of the derivative C_{m_α}, the value depends on the selected moment reference center, which is another reason to present an incremental uncertainty. On each of the historical plots the abscissa is marked with the time of first flight (FF) and the FAA certification date (CERT), in addition to the authority to proceed (ATP, or program initiation) at the origin. Also noted on the plots is the time of the first complete dynamics analysis (D) of the airplane.

This date is significant because it represents the first firm requirement for some of the parameters. Included with each graphical presentation are brief comments regarding the usual impact of the particular parameter on the augmented airplane dynamics. Also included are comments relating to the final value uncertainty. A typical presentation is repeated here for convenience as Figure 3.

In viewing the data, certain of the parameters reveal a relatively large degree of uncertainty early in the design program. In most of the cases, this is attributable to configuration changes being made as the design is

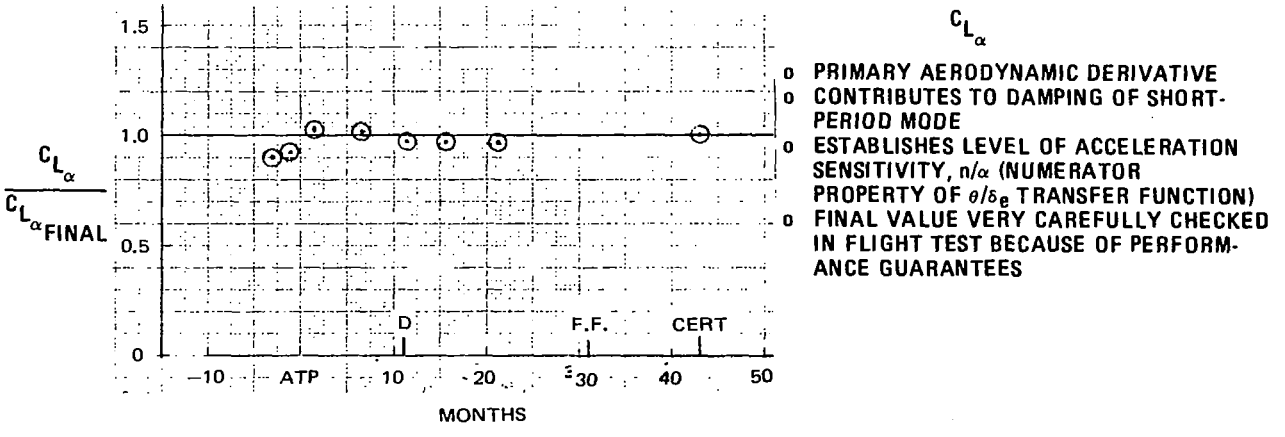

FIGURE 3. TYPICAL DATA FORMAT; $C_{L\alpha}/C_{L\alpha}$ FINAL

finalized. High levels of uncertainty near the outset of the program in some cases can be traced to the lack of early aeroelastic corrections; that is, the available estimates of the parameter are for the rigid airplane. Had there been a firm requirement for these parameters at this time some approximate elasticity corrections would have been applied. Similarly, compressibility correction were not applied during the initial design stages to some of the less significant parameters.

It will be noted that, in general, the data points do not tend to coincide chronologically for the various parameters. The point in time at which a derivative is estimated is affected by several factors, among which are the importance of the derivative and the difficulty of estimation. When a configuration change occurs during the design the more important derivatives are recalculated first. In fact, configuration changes are not made until the impact on certain parameters and aircraft flying qualities is ascertained.

Of the aerodynamic parameters presented in Section 3 all except two are partial derivatives. These two are the airplane lift and drag coefficients which are given because they appear in the coefficients of the equations of motion, sometimes referred to as the dimensional stability derivatives (see Appendix). The airplane lift coefficient is an independent variable in specifying a particular flight condition so no uncertainty can be assigned. As discussed earlier, however, if the flight condition of interest should change for any reason, not only the lift coefficient, but the entire set of equations of motion will be altered.

The aircraft drag coefficient is somewhat unique in this discussion because it is the basic aerodynamic design parameter for cruise flight. The initial value shown in Section 3 represents a guarantee and normally is not revised until flight test data are available. Every effort is made to achieve this design goal, including configuration changes which can range from minor refinements in the design to major drag reduction programs.

The uncertainties associated with the final values of the various aerodynamic parameters are difficult to assess when traditional methods are used in the analysis of flight test data, as in the subject case. The measurement accuracy of certain of the parameters receives great attention because of the relationship to performance guarantees. An example is presented in Figure 4

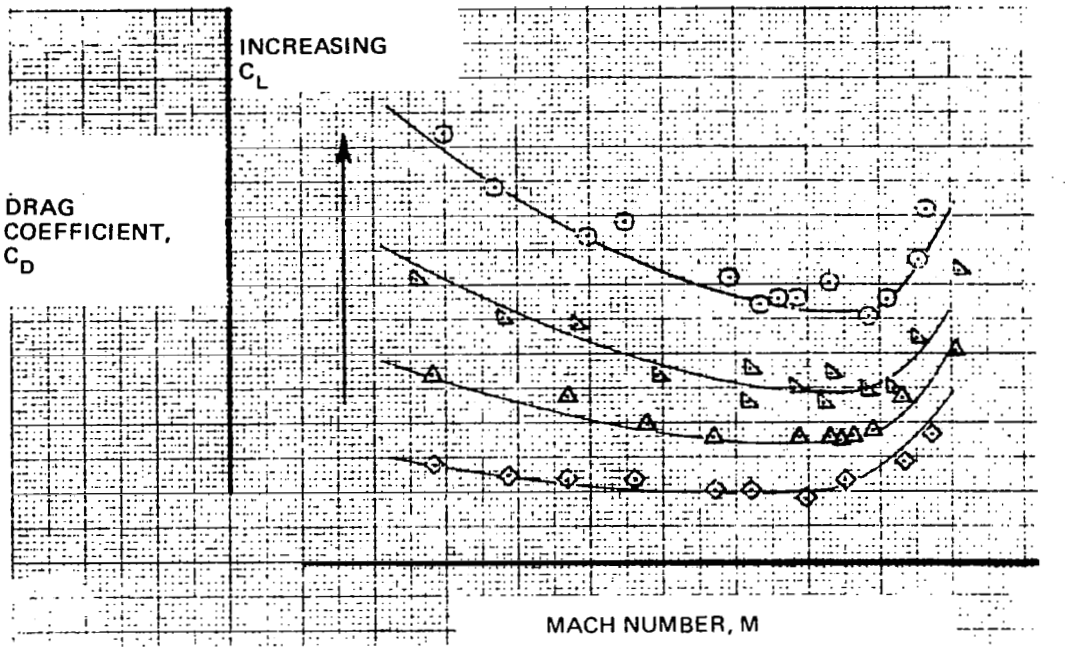

FIGURE 4. TYPICAL FLIGHT TEST DATA; DRAG COEFFICIENT

where drag coefficient, C_D, has been plotted versus Mach number at various levels of lift coefficient, C_L. The scatter in the data can be regarded as an indicator of the uncertainty in the final value; for the subject case, the standard deviation of C_D is 2 percent. The total error arises from several factors, the major one being the engine thrust measurement error.

There are other parameters which are also carefully checked against flight test data but are not normally analyzed with respect to measurement error. An example is presented in Figure 5 where the horizontal stabilizer effectiveness, C_{mi_H}, is shown as a function of Mach number. This parameter is simply related to the elevator control power term, $C_{m_{\delta_e}}$, so that the measurement accuracy of the two derivatives is comparable. In Figure 5, only data points near the subject flight condition are shown, and the calculated standard deviation over this Mach number range is 4 percent. An insight into the potential measurement error of C_{mi_H} can be gained by considering the expression used to calculate the individual points:

$$C_{mi_H} = \frac{\Delta\left(\frac{X_{cg}}{\bar{c}}\right) C_L}{\Delta i_H}$$

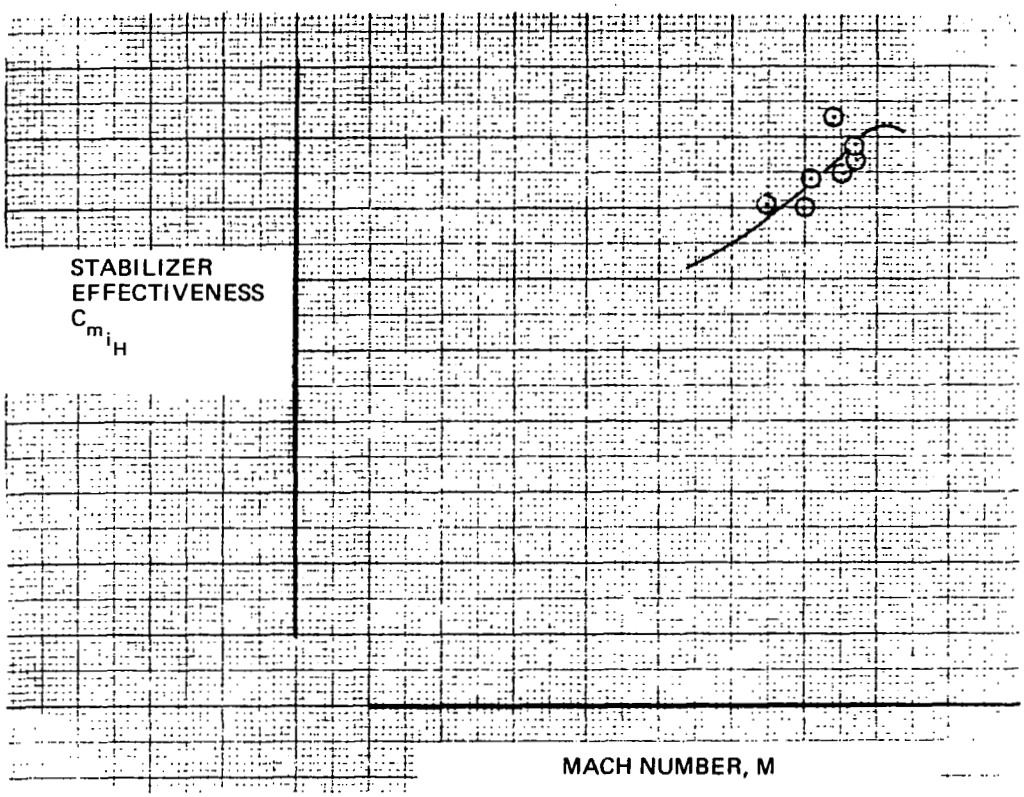

FIGURE 5. TYPICAL FLIGHT TEST DATA; STABILIZER EFFECTIVENESS

where the incremental values represent the differences between two trimmed centers of gravity. Errors can arise from several sources: the measurement of the stabilizer angle; the measurement of the cg location; the measurement of airplane weight and dynamic pressure that determine the lift coefficient; and the ability of the pilot to precisely trim the aircraft. The level of measurement error for C_{mi_H} is considered typical of a number of static derivatives.

In the case of the dynamic derivatives, the verification is normally accomplished by a comparison of response characteristics; i.e. frequencies, damping ratios, time to half or double amplitude, etc. If the match between the estimated and the measured characteristics is reasonable, the estimated derivatives are presumed to be correct; if not, adjustments are made to the derivatives in order to achieve a satisfactory match of the aircraft dynamics. For the most part, it is extremely difficult, if not impossible, to isolate the undertainties or errors associated with the measurement of individual dynamic derivatives.

WEIGHT AND INERTIAL PARAMETERS

Aircraft weight and inertias are key quantities in the aircraft equations of motion and have a history of variability during the aircraft's configuration development. Although the aircraft can be weighed quite accurately prior to first flight (to within $\pm$ 0.2 percent), the manufacturer's empty weight (MEW) and gross weight can change significantly after program initiation. Manufacturer's empty weight changes occur both because of changes in the specification (increase in range, say) and changes in material (engine weight change). If the designer's concern is control system dynamics, he will be more interested in gross weights than MEW's. Both are given, however, so that the user of these data will have some appreciation for the kinds of factors influencing his control system design.

The growth of MEW over the four-year period is shown in Figures 6 and 7, where it will be noted that the initial value was 7.7 percent less than the final value. The major jumps in MEW are accounted for in Table 4. Of the 7.7 percent difference, specification growth accounted for 4.7 percent and non-specification growth 2.0 percent. Figure 8 gives the changes in other design weights for the same period of time. Note from Figure 6 that the original maximum takeoff gross weight (MTOGW) was 90 percent of the final value.

Coincident with the weight increases are changes in moments of inertia. These are summarized in Table 5. It will be noted that the increase in gross weights can be utilized several ways. The operation can keep the fuel load constant and increase payload, in which case the pitching moment of inertia I_Y, shows a rather large increase (Table 5, Item 2). When the payload is held constant and fuel load is increased, the roll moment of inertia, I_X, shows a large increase, as shown in Table 5, Item 3.

STRUCTURAL PARAMETERS

Modal Vibration Analysis

The approach for determining the uncertainties associated with structural dynamic considerations arising from structural flexibility was to track historically the variations in the normal modes of vibration as described by

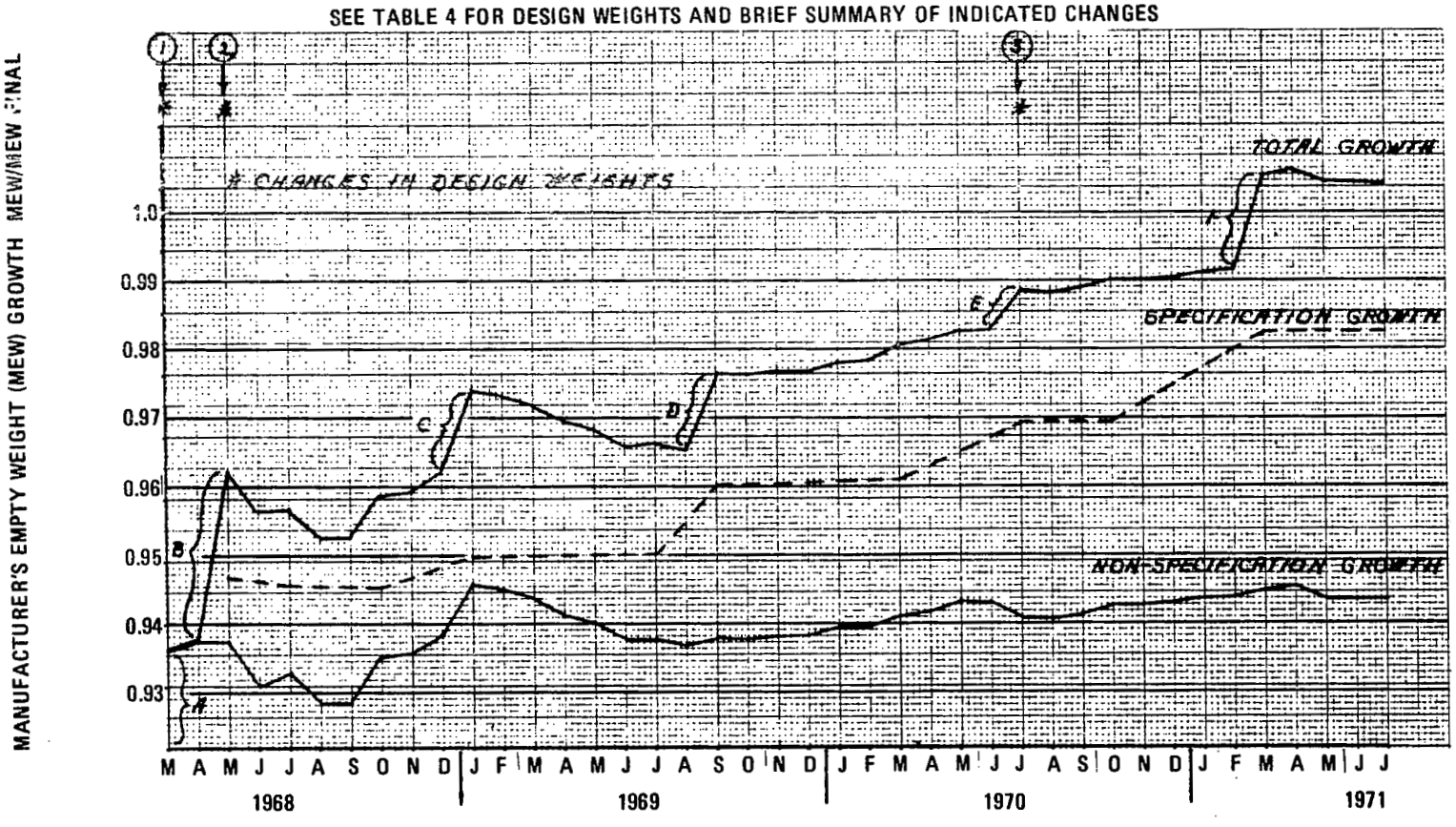

FIGURE 6. MANUFACTURER'S EMPTY WEIGHT GROWTH HISTORY

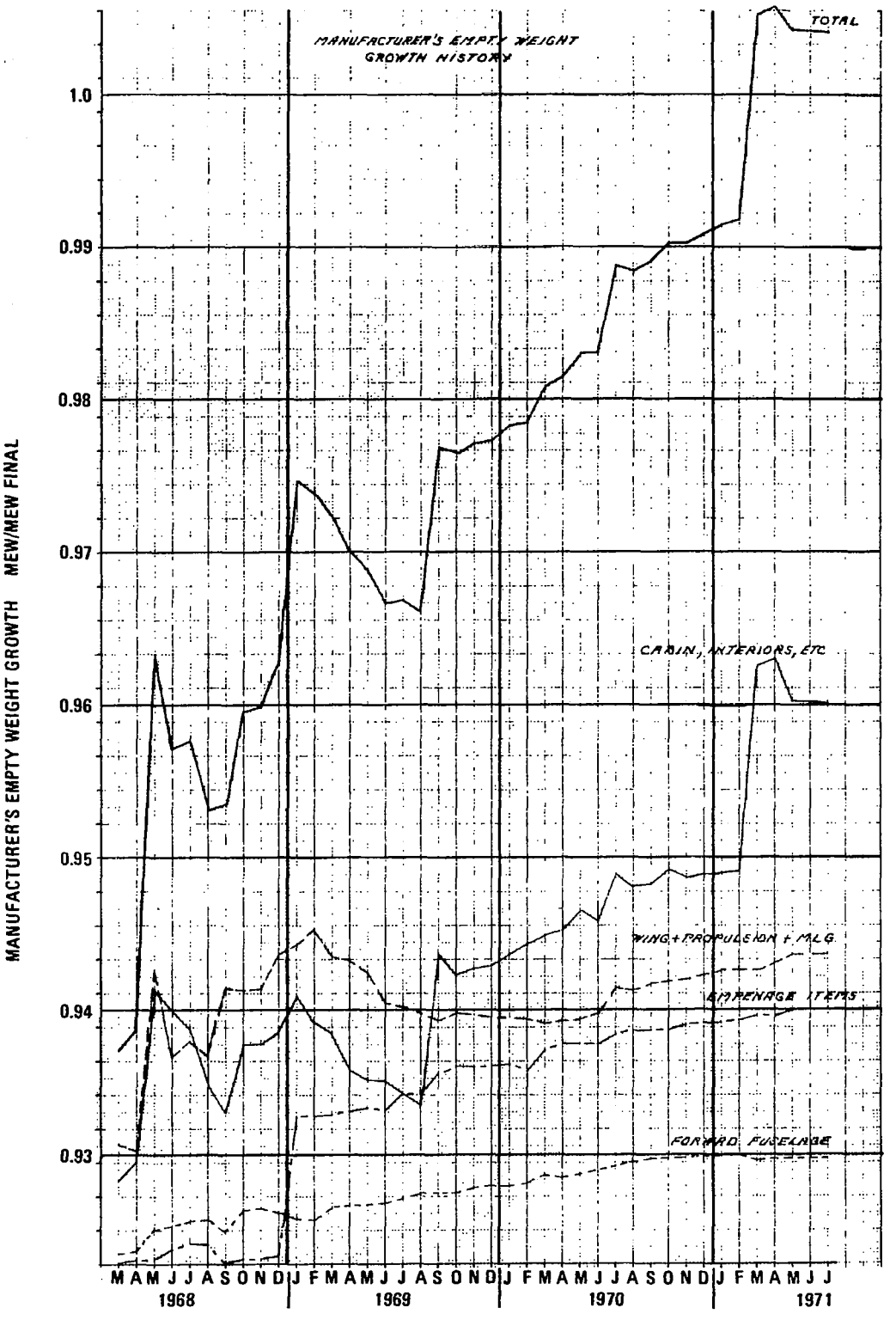

FIGURE 7. MANUFACTURER'S EMPTY WEIGHT GROWTH HISTORY

TABLE 4

MAJOR WEIGHT CHANGE SUMMARY

(see Figure 6)

A. Revised estimate for wing bending material, increased allowance for insulation and interior panels plus miscellaneous changes.

B. Increased engine weight, revised estimate for wing and landing gear to provide for an increase in takeoff gross weight plus miscellaneous changes.

C. Interior design changes, 0.102m (4-inch) fuselage stretch, addition of aft engine maintenance platform plus revised estimates for fuselage, wing and tail.

D. Customer requested interior changes plus revised estimates for miscellaneous structural and subsystem items.

E. Increased engine weight, revised estimate for wing and landing gear to provide for an increase in takeoff gross weight plus miscellaneous changes.

F. Incorporated more representative weights for galleys and passenger seats.

frequencies, modal displacements, and the resulting generalized masses. The method for computing the modes was begun by the usual lumping of the fuselage, empennage, and wing into a finite number of mass and spring elements. As the aspect ratio of the selected airplane was large, it was justifiable to represent the structure as interconnected slender beams. The root or connecting springs were computed from a finite element representation using a redundant force procedure.

The time period considered in this study covered 35 months starting with the formal authority to proceed (ATP) and ending with the ground vibration test (GVT) 1 month prior to first flight. Preceding this 35-month period there was approximately 6 months of preliminary design activity. This preliminary design phase was not covered by this study because structural uncertainties

(a) MAXIMUM TAKEOFF GROSS WEIGHT

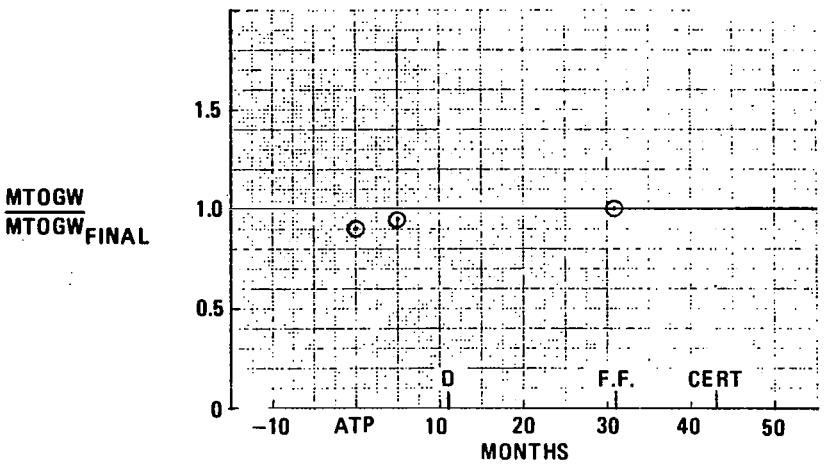

(b) MAXIMUM LANDING WEIGHT

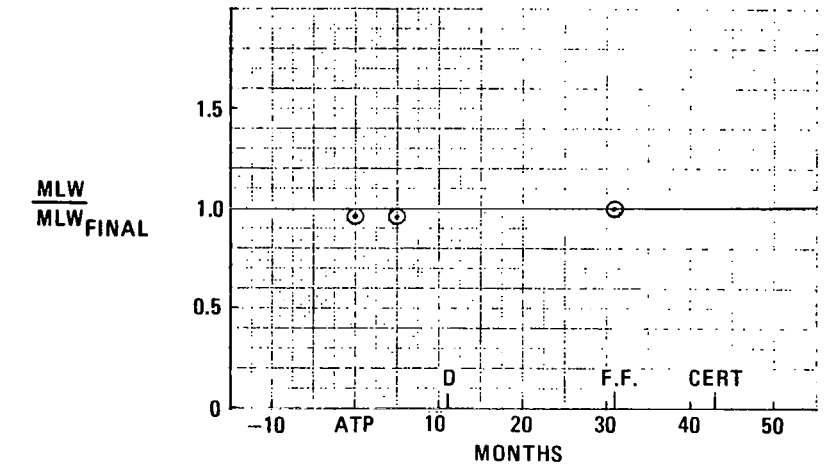

(c) MAXIMUM ZERO FUEL WEIGHT

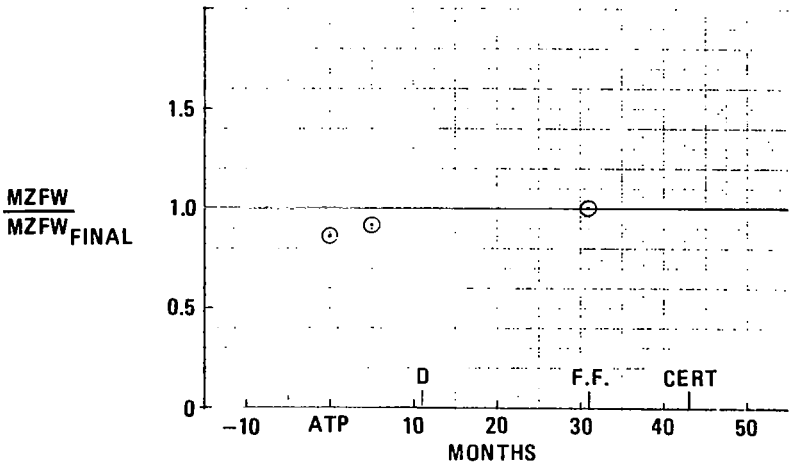

FIGURE 8. DESIGN WEIGHT HISTORY

TABLE 5

MOMENT OF INERTIA HISTORY

Assumed Growth	Inertia Value at Program Start / Final Inertia Value
1. Manufacturers Empty Weight (MEW) Growth of 8.8 percent	
$I_X/I_{X\ Final}$	0.95
$I_Y/I_{Y\ Final}$	0.92
$I_Z/I_{Z\ Final}$	0.93
2. Maximum Takeoff Gross Weight (MTOGW) Growth of 11 percent and Constant Fuel:	
$I_X/I_{X\ Final}$	0.96
$I_Y/I_{Y\ Final}$	0.88
$I_Z/I_{Z\ Final}$	0.92
3. Maximum Takeoff Gross Weight (MTOGW) Growth of 11 percent and Constant Payload:	
$I_X/I_{X\ Final}$	0.85
$I_Y/I_{Y\ Final}$	0.93
$I_Z/I_{Z\ Final}$	0.89

Final values are those calculated at first flight (31 months after program initiation). The product of inertia (I_{XZ}) does not change significantly.

would have been distorted by the large configuration changes resulting from changes in design specifications that were made during this phase.

During the evolution of the design from ATP to GVT eleven changes were made which were judged of sufficient significance to warrant computation of new modes. During that time, the modes were used primarily for flutter analyses with application to control system effects being made less frequently. For this study the modes were recomputed and the results compared to the final or certification results. The final results were computed based upon corrections as made from GVT results.

In particular, the dynamic representation of the airplane consisted of a masswise representation composed of 50 lumped bays. Each bay was capable of six "rigid body" degrees of freedom, three translations and three rotations. The entire mass of the airplane was lumped into these bays by calculating the mass properties of each bay about a selected reference station in the bay. Mass and stiffness symmetry was assumed allowing an analysis of half the airplane. Figure 9 shows the mass bay distribution used in the modal calculations.

Theoretical cantilevered vibration modes were calculated using the stiffness and mass data of the respective bays for the major components - wing, horizontal stabilizer, fuselage and vertical stabilizer. All modes were calculated using structural influence coefficients (SICs) which relate control point static deflections to applied forces. Complex joint structures such as wing-fuselage, fin-fuselage, and engine pylons, used structural influence coefficients obtained from finite element redundant force type analyses. Figure 10 illustrates the stiffness representation used in the vibration analyses.

Rigid body modes were used in conjunction with the above component modes to release the airplane and generate free-free orthogonal modes into symmetric and antisymmetric sets. In all cases, sufficient component modes were used in the free-free modal calculations to assure modal convergence of the airplane modes of concern, from zero to 10 hertz. All modal calculations were performed using a digital computer program.

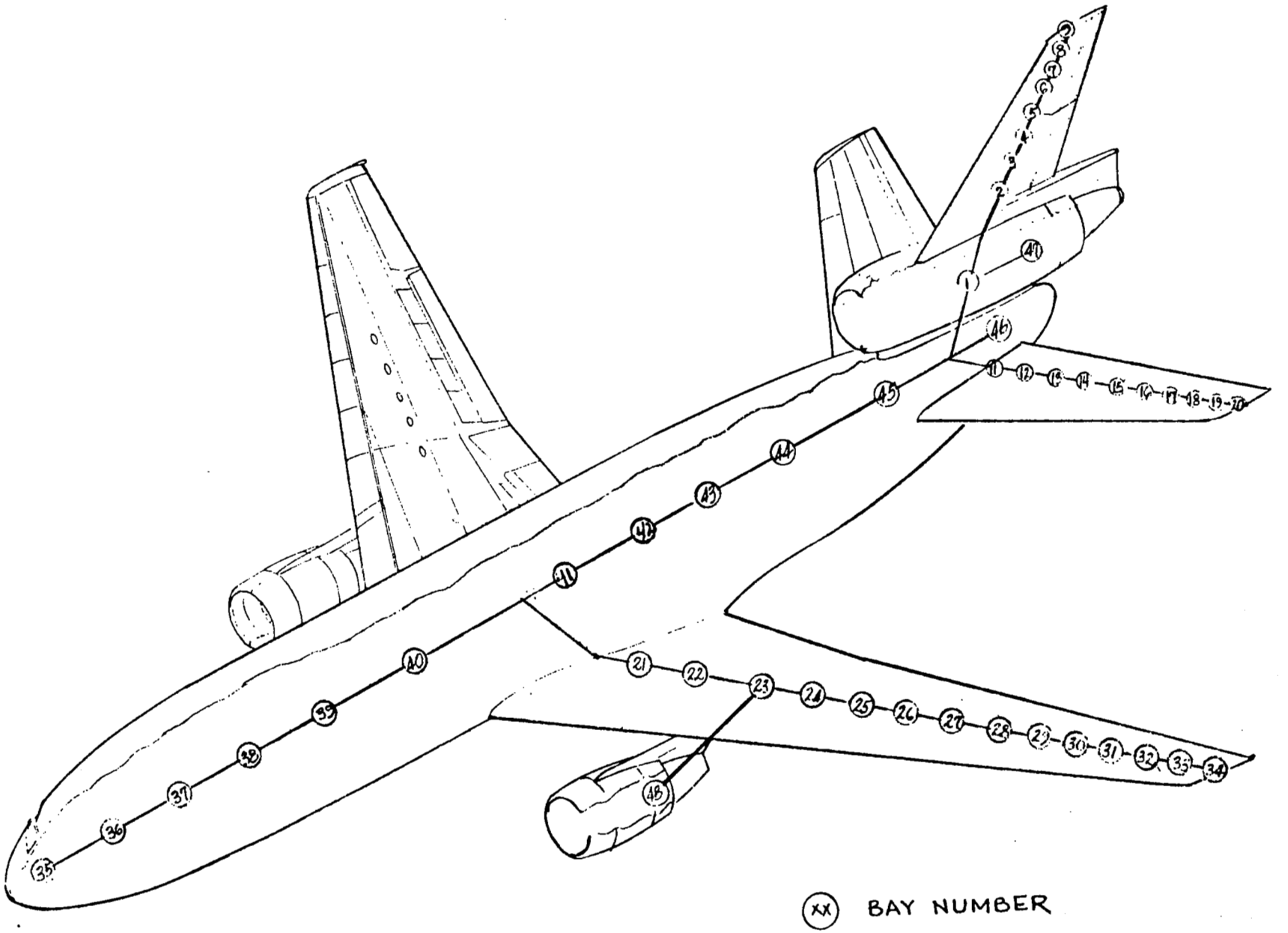

FIGURE 9. INITIAL-TO-FINAL MASS REPRESENTATION

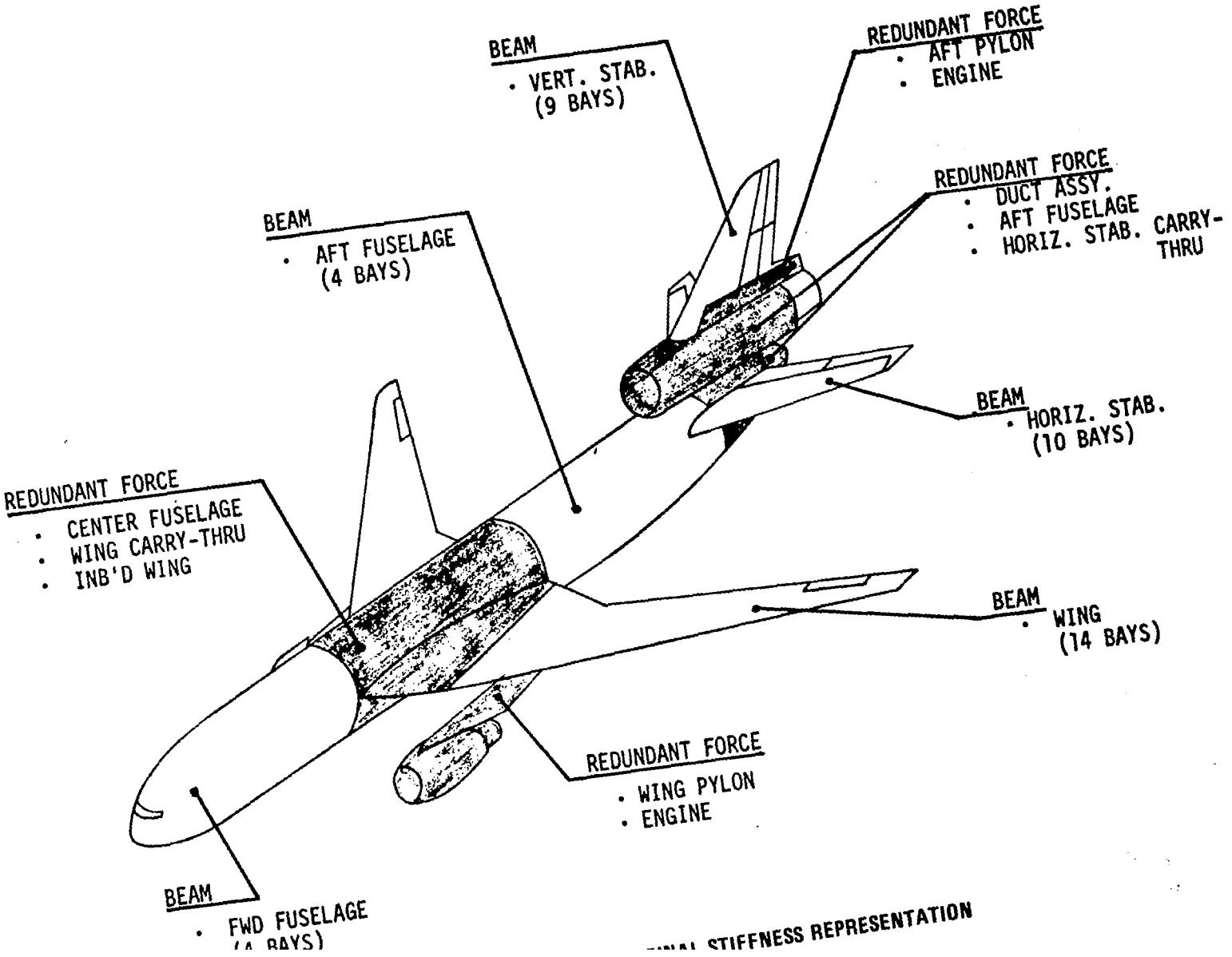

STIFFNESS REPRESENTATION

It should be noted that for this study all the vibration analyses were performed using the final structural representation. That is, the early modes were reconstructed using the respective stiffness and mass data, but with the final 50 bay structural representation. In actual practice, the earlier vibration analyses were performed using a much coarser structural representation. Therefore, the uncertainties shown for the early vibration analyses for frequencies greater than 3 or 4 hertz may be greater than these studies indicate.

As noted, the structural dynamic uncertainties were limited to those resulting from mass and stiffness variations only. In the practical consideration of structural dynamic effects, whether for the usual application to flutter or gust loads or for control-continued vehicle application, the predictability of the unsteady aerodynamic terms is as important as the predictability of the mass and stiffness dependent modes of vibration. Especially important are the unsteady aerodynamics of control surfaces which must be included in the analysis of all aircraft with highly responsive active control systems in order to assure that the required flutter speed and gust load margins are met and that flutter and excessive gust and oscillatory loads are avoided under any likely control system failure or malfunction.

Structural Dynamic Parameters Investigated

During the design phase, the airplane design data are continually changing due to configuration changes, revisions based upon test data, or refinements to existing data based upon detailed analyses. Many of these changes are minor and do not significantly affect the airplane vibration characteristics. Therefore, only those parameters which significantly impacted the airplane vibration modes were investigated. These parameters were as follows:

- Wing stiffness
- Fuselage stiffness
- Wing engine pylon stiffness
- Aft engine pylon stiffness
- Wing engine weight
- Wing engine cg location
- Aft engine weight

The chronology and relative magnitude of these parameter changes are shown in Table 6. Symmetric and antisymmetric vibration modes were calculated for both empty and full fuel conditions. These two fuel conditions result in the highest and lowest modal frequencies of the system and therefore are typical of the modal uncertainties which can be expected over the entire fuel range. For both fuel conditions the payload was held constant. These payload and fuel conditions match configurations used during the airplane ground vibration test. Thus, a direct comparison of theoretical and experimental modal vibration data was easily made which facilitated corrections to the theoretical data.

TABLE 6

DESIGN PARAMETER SUMMARY

	DESIGN PARAMETER CHANGES					
TIME ~ MON	WING STIFFNESS	FUSELAGE STIFFNESS	WING PYLON STIFFNESS	AFT PYLON STIFFNESS	WING ENG WEIGHT AND CG	AFT ENGINE WEIGHT
0	BASIC	BASIC	BASIC	BASIC	BASIC	BASIC
2	+30% BEND +13% TOR					
4			+64%			
5		−2% TORS			0.81m (32 IN.) AFT CG SHIFT	
6	+5% BEND +13% TORS			−35%		
7			+37%		24% WEIGHT INCREASE	
10	−2% BEND +6% TORS					
12	+1% BEND +1% TORS	−2% BEND −2% TORS				
14	−2% BEND −2% TORS					
16	+5% TORS					
20			+6%			
24				−32%		6% WEIGHT INCREASE
35						

NOTE: THE ABOVE CHANGES IN EACH PARAMETER ARE CUMULATIVE

Structural Dynamic Data

The results of the modal vibration uncertainty study are presented as plots of modal frequency, generalized mass and displacement versus time. The historical evolution of these parameters is shown for a selected subset of the airplane vibration modes which are important in both control system design, gust loads due to turbulence, and flutter calculation, all with or without control-configured vehicle technology. The chronology of changes to the input data is shown on each plot for easy reference. The mode names, such as first wing bending, are chosen so as to describe the predominant motion of each mode although, of course, the motion involves the entire airplane structure. Each parameter is given as a ratio of the value at a given time to the final value. The final value of each parameter is taken from a theoretical set of modes which are in agreement with ground vibration test results.

The generalized mass and deflection plots for each mode were calculated using a consistent normalization point for each particular mode. For instance, first wing bending was normalized to unit vertical deflection at the wing tip bay. The modal displacements are presented at selected stations which represent a variety of possible sensor locations which might be selected to implement various control systems. The following locations and deflections were selected:

Symmetric Analysis

1. Fuselage nose pitch angle (α)
2. Fuselage cg vertical deflection (h)
3. Wing tip vertical deflection (h)
4. Wing tip pitch angle (α)
5. Horizontal stabilizer tip vertical deflection (h)
6. Horizontal stabilizer tip pitch angle (α)

Antisymmetric Analysis

1. Fuselage nose roll angle (θ)
2. Fuselage nose yaw angle (ψ)
3. Wing tip vertical deflection (h)

4. Wing tip pitch angle (α)
5. Horizontal stabilizer tip vertical deflection (h)
6. Horizontal stabilizer tip pitch angle (α)
7. Vertical stabilizer tip lateral deflection (ℓ)
8. Vertical stabilizer tip yaw angle (ψ)

The modal data are presented in Section 3. The type of data shown for each airplane configuration is summarized in Section 3.

Discussion of Results

General. An examination of the modal frequency, generalized mass and displacement plots show, in general, that these uncertainties can be divided into two distinct phases. The first phase occurs during the early design stages, approximately 0 to 10 months, where the modal parameters exhibit large variations. These variations reflect major configuration changes such as engine weight, engine location, maximum gross weight and the introduction of stiffness constraints to satisfy dynamic conditions such as landing, gust and flutter requirements. In addition, data generated during this phase are based upon a coarse idealization of the structure.

The second phase occurs from approximately 10 to 24 months, during which time the modal parameters, in general, exhibit only small changes. This reflects the fact that the airplane configuration has been determined and all major design constraints have been introduced. Changes to the design data are minor modifications based upon additional detailed structural analyses, which produce small changes in the airplane modal characteristics.

But however detailed the analysis, uncertainties still exist. This can be seen by comparing the modal parameter values at the 24th month with the certification values. The 24th-month points represent the final predicted theoretical modes before verification by ground vibration test. The theoretical modes are a result of a highly detailed structural analysis of a fixed configuration. Therefore, the difference between the 24th month and certification values represent uncertainties in analysis techniques in idealizing the airplane stiffness and mass properties. The idealizations must reduce the continuous airplane structure to a finite number of elements, making simplification inevitable. Also, the number of elements used to represent the airplane is limited by practical computational and economic considerations.

An examination of the modal frequency, generalized mass and displacement plots does not show any discernable trend due to fuel condition or symmetry. The correlation is equally good for zero and full fuel and for symmetric and antisymmetric conditions.

Modal Frequencies. The modal frequency plots, Section 3, show that extreme variations of -30 to +84 percent may occur for some modes during the first phase. However, the majority of the modal frequencies appear to be in the ±20 percent range. During the second phase, the modal frequencies show variations of only 3 to 4 percent on the average. The final theoretical modes (24 month point) differ from the certification modes by 4 to 5 percent on the average, although maximum differences reach +13 to -20 percent for a small percentage of the modes. An average of 5 percent difference in modal frequency is extremely good correlation considering the complexity of the structure being analyzed.

Generalized Mass and Displacement. The modal generalized mass and displacement plots, Section 3, show much the same trend as do the frequency plots. However, the magnitudes of the variations are much more extreme. It appears, in general, that changes in design data produce larger variations in generalized mass and deflections than in modal frequency.

However, care must be exercised in interpreting the generalized mass and deflection data. It is true that the data show the uncertainty of each parameter as a ratio of its value at a given time to its final value. But the actual value of the parameter may be small. Therefore, seemingly large variations in its value may still be insignificant as they affect the airplane response characteristics and hence the control system design. In addition, the ratio of any particular parameter, such as fuselage nose pitch angle, varies for each mode of a given configuration. Note that the parameter ratio is greater than unity in some modes and less than unity in others in which there is usually a bias in one direction or the other.

Evaluation of Results. The importance of the structural dynamic behavior of the aircraft to the control system design depends upon the intended function of the control system and its gain/phase properties. For low frequency control systems such as conventional autopilot and yaw damper systems, the effect of the aircraft stiffness distribution on the steady aerodynamic

derivatives is of significance. For higher frequency control systems, particularly those required for gust load and flutter suppression, the stiffness and mass distributions become more significant and hence the vibration modes of the aircraft become meaningful measures of potential control system interaction. Of course, in any control loop with significant gain and phase shift in the elastic modal frequency range knowledge of the vibration characteristics of the vehicle is desirable. Use of mode shapes to determine nodal and anti-nodal points for sensor locations is desirable for passive gain stabilization procedures, but for large flexible aircraft significant shifts in node lines can occur with fuel and payload distribution changes.

The use of natural frequencies to assess the change in the vibration modes during the design cycle is a useful (but not unique) measure of potential effects on the control system design. The natural frequencies may be identified by the aircraft components which are the most directly involved in the mode and some subjective evaluation will be made by the engineer as to the significance to any given control system. For example, a low frequency fuselage bending mode may have a very direct bearing on the control system design for a high gain system and a low frequency is an indication that significant data error from forward mounted sensors may occur in turbulence conditions.

Knowledge of amplitudes at various stations on the aircraft and the generalized masses is considerably less useful. The control system designer faced with the task of designing a system for response or stability in the elastic frequency range or a system with significant gain and phase variation in this frequency range must use these data in his analyses along with the appropriate aerodynamic functions.

A review of the modal parameters variations through the design cycle presented herein indicates a reasonable convergence with time on the final design values for the modal frequencies. The generalized mass and modal deflections for various modes and locations on the aircraft, however, indicate large variations and an apparent lack of continuity. This latter is not surprising in view of the fact that during the design cycle data updates resulting from structural modifications and improved data (resulting from both quality

and idealization modifications) are generally made for one or two aircraft components at a time. For example, a shift in wing engine cg with respect to the wing may not significantly effect the basic fuselage and empennage modes but can cause large variations in generalized mass of modes involving significant engine motion. The frequency variation however will show significantly less variation.

The importance to the control system design from the above change will be insignificant in the basic low frequency autopilot design but of major significance for a flutter suppression system.

A more significant measure of the structural dynamic parameter uncertainties may be found by observing the variation of the aircraft open loop transfer function for specific control surface inputs at specific potential sensor locations. For such response analyses to be valid in the elastic frequency ranges, they must use the unsteady aerodynamic functions which more realistically represent the complex aerodynamic forces which occur in these frequency ranges.

To illustrate the above, a frequency response analyses was performed to determine if the modal data herein would correlate with the aircraft transfer functions for two points in the design cycle. The transfer functions were evaluated for 0 to 10 Hertz for a plus-or-minus 1-degree elevator oscillation using unsteady aerodynamics for Mach 0.88 and flight at 7,315 meters (24,000 feet). Table 7 shows a summary of results for two dynamic aeroelastic modes, the aircraft short-period mode and the Wing Engine Pitch/Fuselage Bending mode. The input modal displacement and generalized mass ratios and output acceleration ratios for these modes are shown for several aircraft locations. Free-free aircraft modes were used in the analysis.

It is apparent from these summary data that while the generalized mass and normalized modal displacements show large variations, the acceleration responses for the selected locations are similar and indicate relatively small variations. These response data are of significant use to the control system designer using the elevator for force generation and any of the selected location response parameters for sensor locations.

TABLE 7

RESPONSE ANALYSIS SUMMARY

SYMMETRIC MACH 0.88 ZERO FUEL 7315M (24,000 FT)

RESPONSE PARAMETER	3.23 Hz MODE INPUT MODEL DISPLACEMENT RATIO	RESPONSE ACCEL. RATIO ($\ddot{u}_{24}/\ddot{u}_c$)	
		0.45 Hz SHORT PERIOD MODE	3.23 Hz FUSELAGE BENDING MODE
FUSELAGE NOSE α	0.80	1.02	1.18
FUSELAGE CG h	3.21	1.02	1.12
WING TIP h	0.94	1.02	1.04
WING TIP α	0.44	1.03	0.85
HORIZONTAL STABILIZER h	1.00	1.02	1.27

- ABOVE RATIOS ARE FOR 24TH MONTH DATA VERSUS CERTIFICATION DATA
- (GM_{24}/GM_c) = 0.51 FOR THE 3.23 HERTZ FUSELAGE BENDING MODE

For any given aircraft structure the structural dynamic characteristics vary significantly over the normal fuel and payload range. As a matter of interest the symmetrical modal frequency variation from full fuel to zero fuel was compared to the maximum frequency variation for zero fuel over the design period from ATP to GVT. A similar comparison was made for the full fuel frequencies over the design period. These comparisons are shown in Table 8 and indicate that the modal frequencies vary with fuel loading by the same level of magnitude as the uncertainty variations and in some cases more. Payload variations, which have not been considered, would show even a larger range in the frequencies of the final design.

TABLE 8

COMPARISON OF FUEL EFFECTS TO UNCERTAINTIES EFFECT SYMMETRIC MODAL FREQUENCIES

MODE DESCRIPTION	$f_{FULL\ FUEL}$ / $f_{ZERO\ FUEL}$	UNCERTAINTIES RATIO f_{MAX}/f_{MIN}	
		ZERO FUEL	FULL FUEL
FIRST WING BENDING	0.63	1.26	1.16
WING ENGINE YAW	0.98	1.20	1.16
FUSELAGE BENDING	0.90	1.13	1.09
HORIZONTAL STABILIZER BENDING/AFT ENG PITCH	1.01	1.72	1.08
WING INNER PANEL TORSION	0.90	1.39	1.35
WING ENGINE ROLL	1.01	1.16	1.15
SECOND WING BENDING	0.71	1.30	1.09
WING FORE AND AFT BENDING	0.56	1.27	1.20
WING TORSION/ENGINE PITCH	0.94	1.13	1.17

SECTION 3
DATA

Aerodynamic, inertial, and structural data are presented in this section. The data are discussed in detail in Section 2 so that this section provides as concise a compendium as possible. The parameters are defined in the list of symbols at the beginning of this report. The equations of motion and dimensional stability derivative definitions are given in the Appendix. The data are organized as follows:

Longitudinal Aerodynamic Parameters:

Figure 11 Historical Uncertainties of C_{L_α}, C_{m_α}, C_{D_α}, $C_{L_{\dot{\alpha}}}$

Figure 12 Historical Uncertainties of $C_{m_{\dot{\alpha}}}$, $C_{D_{\dot{\alpha}}}$, C_{L_u}, C_{m_u}

Figure 13 Historical Uncertainties of C_{D_u}, C_{L_q}, C_{m_q}, $C_{L_{\delta_e}}$

Figure 14 Historical Uncertainties of $C_{m_{\delta_e}}$, $C_{D_{\delta_e}}$, C_L, C_D

Lateral-Directional Aerodynamic Parameters:

Figure 15 Historical Uncertainties of C_{y_β}, C_{n_β}, C_{ℓ_β}, C_{y_p}

Figure 16 Historical Uncertainties of C_{n_p}, C_{ℓ_p}, C_{y_r}, C_{n_r}

Figure 17 Historical Uncertainties of C_{ℓ_r}, $C_{y_{\delta_r}}$, $C_{n_{\delta_r}}$

Figure 18 Historical Uncertainties of $C_{\ell_{\delta_r}}$, $C_{y_{\delta_a}}$, $C_{n_{\delta_a}}$, $C_{\ell_{\delta_a}}$, $C_{y_{\delta_{sp}}}$, $C_{n_{\delta_{sp}}}$

Figure 19 Historical Uncertainties of $C_{\ell_{\delta_{sp}}}$

Inertial Parameters:

Figure 20 Manufacturer's Empty Weight Growth History

Figure 21 MEW Growth History - Cabin, Wing, Empennage, Forward Fuselage

Table 9 Major Weight Change Summary

Table 10 Moment of Inertia History

Figure 22 Design Weights Histories

Structural Dynamic Parameters:

Table 11 Symmetric Modal Analysis Summary

Table 12 Antisymmetric Modal Analysis Summary

Figures 23 through 26 Mode Shapes and Mode Lines

Figures 27 through 60 Evolution of Frequency Ratio (see Tables 11 and 12 for index)

Figures 61 through 90 Evolution of Generalized Mass Ratio (see Tables 11 and 12 for index)

Figures 91 through 196 Evolution of Displacement Ratio (see Tables 11 and 12 for index)

LIST OF FIGURES

LIST OF FIGURES (Contd)

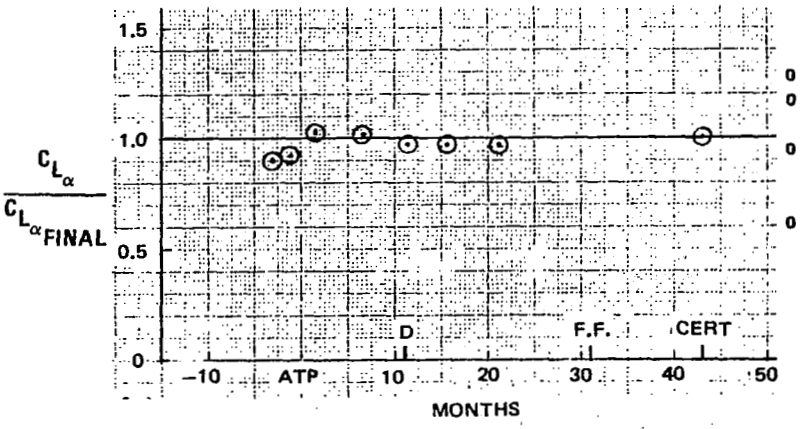

C_{L_α}

- PRIMARY AERODYNAMIC DERIVATIVE
- CONTRIBUTES TO DAMPING OF SHORT-PERIOD MODE
- ESTABLISHES LEVEL OF ACCELERATION SENSITIVITY, n/α (NUMERATOR PROPERTY OF θ/δ_e TRANSFER FUNCTION)
- FINAL VALUE VERY CAREFULLY CHECKED IN FLIGHT TEST BECAUSE OF PERFORMANCE GUARANTEES

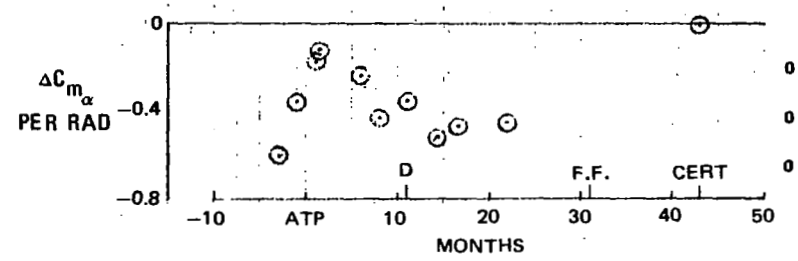

C_{m_α}

- BASIC LONGITUDINAL STABILITY DERIVATIVE
- ESTABLISHES FREQUENCY OF SHORT-PERIOD MODE
- FINAL VALUE CHECKED BY FLIGHT TEST RESULTS; NORMALLY NO ASSESSMENT OF ACCURACY MADE

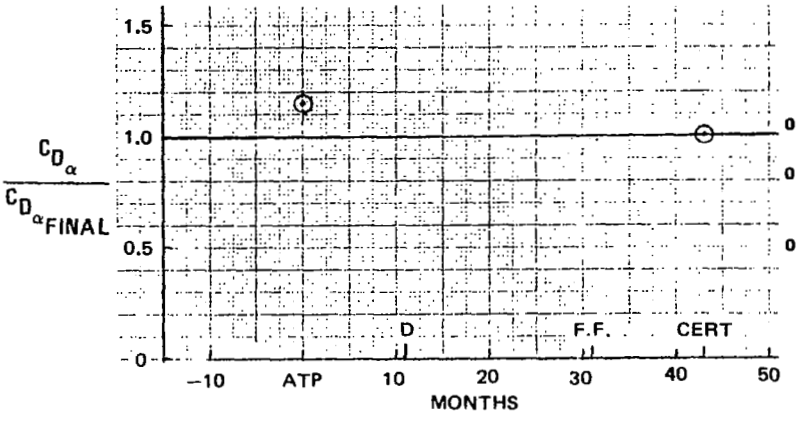

C_{D_α}

- RELATIVELY UNIMPORTANT TO CHARACTERISTIC EQUATION
- IMPORTANT IN ESTABLISHING FLIGHT-PATH STABILITY (NUMERATOR PROPERTY OF h/δ_e TRANSFER FUNCTION)
- FINAL VALUE VERY CAREFULLY CHECKED IN FLIGHT TEST BECAUSE OF PERFORMANCE GUARANTEES

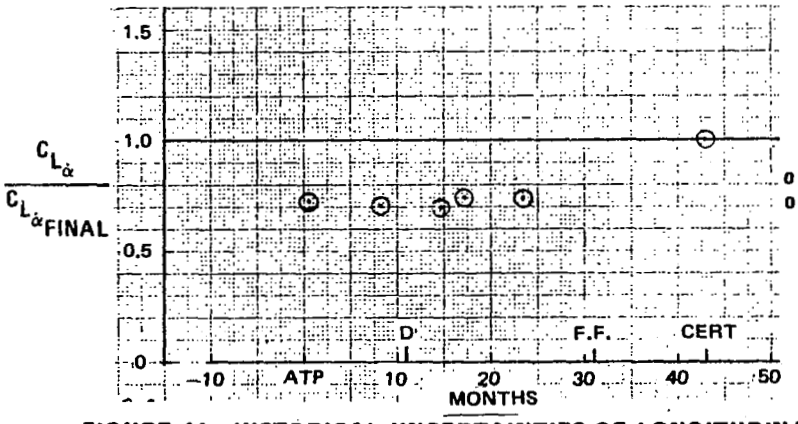

$C_{L_{\dot\alpha}}$

- SECONDARY IMPORTANCE
- FINAL VALUE NOT CHECKED IN FLIGHT TEST; IMPACT TOO SMALL

FIGURE 11. HISTORICAL UNCERTAINTIES OF LONGITUDINAL AERODYNAMIC PARAMETERS

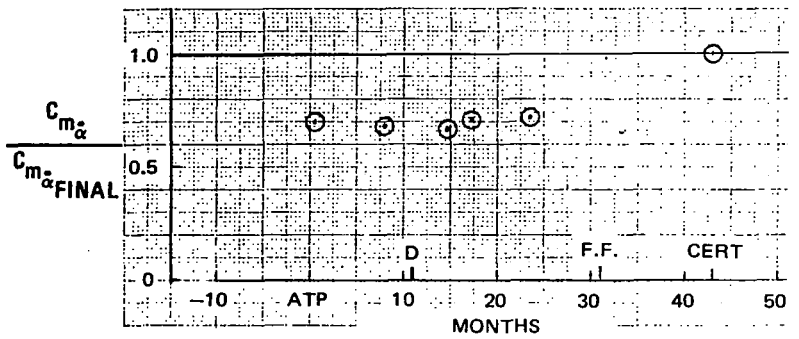

$C_{m_{\dot{\alpha}}}$

- CONTRIBUTES TO SHORT-PERIOD DAMPING
- FINAL VALUE CHECKED USING FLIGHT TEST DYNAMIC RESPONSE MATCH

$C_{D_{\dot{\alpha}}}$

NEGLIGIBLE, NOT PLOTTED

- NEGLIGIBLE
- FINAL VALUE NOT CHECKED IN FLIGHT TEST; IMPACT TOO SMALL

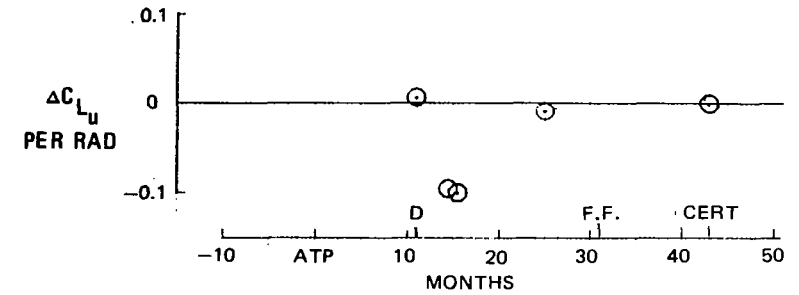

C_{L_u}

- SECONDARY EFFECT ON PHUGOID MODE
- FINAL VALUE CHECKED BY FLIGHT TEST RESULTS; NORMALLY NO ASSESSMENT OF ACCURACY MADE

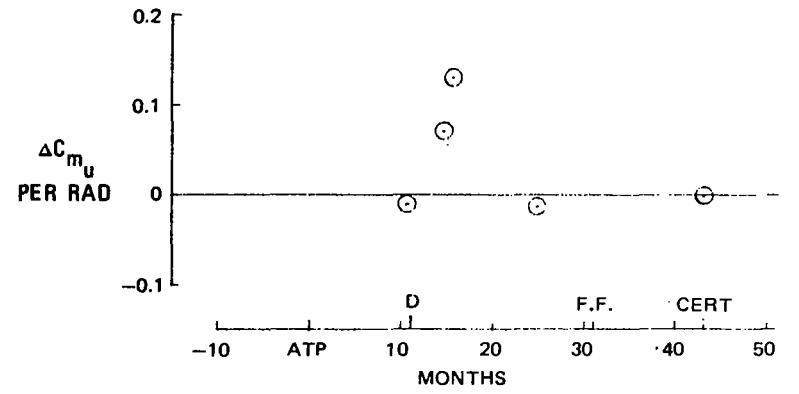

C_{m_u}

- AFFECTS PHUGOID MODE
- FINAL VALUE CHECKED BY FLIGHT TEST RESULTS; NORMALLY NO ASSESSMENT OF ACCURACY MADE

FIGURE 12. HISTORICAL UNCERTAINTIES OF LONGITUDINAL AERODYNAMIC PARAMETERS

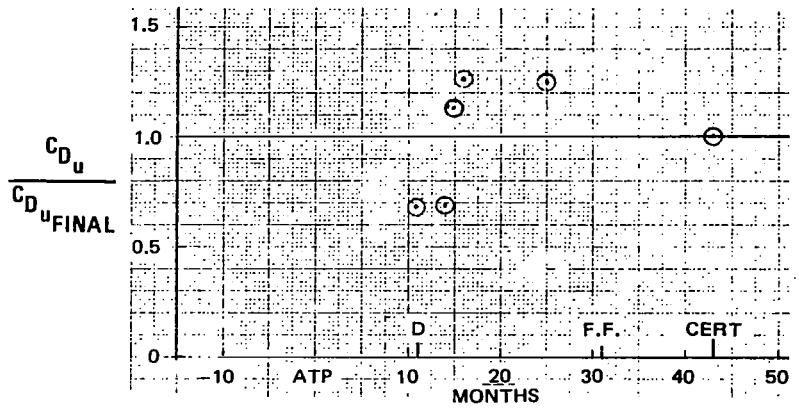

C_{D_u}

- AFFECTS PHUGOID DAMPING
- CONTRIBUTES TO FLIGHT-PATH STABILITY (NUMERATOR PROPERTY OF h/δ_e TRANSFER FUNCTION)
- FINAL VALUE VERY CAREFULLY CHECKED IN FLIGHT TEST BECAUSE OF PERFORMANCE GUARANTEES

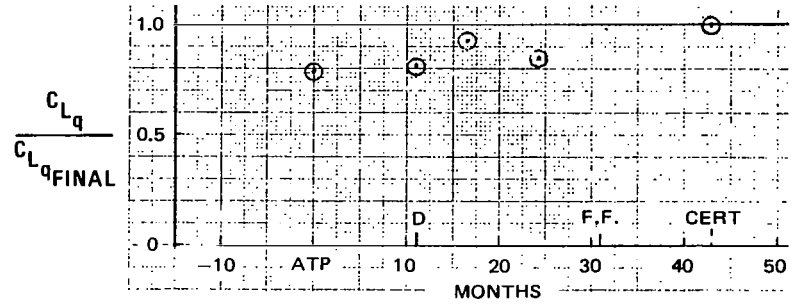

C_{L_q}

- SECONDARY EFFECT ON SHORT-PERIOD MODE
- FINAL VALUE NOT CHECKED IN FLIGHT TEST; IMPACT TOO SMALL

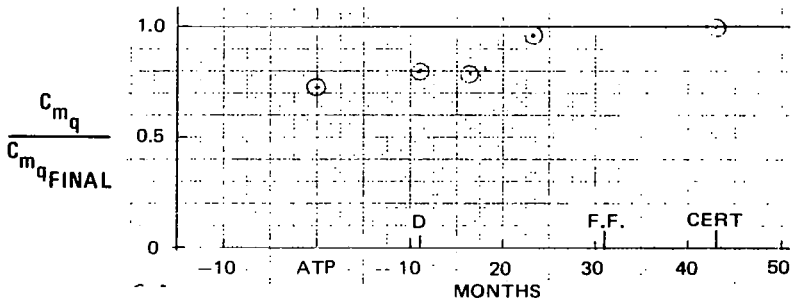

C_{m_q}

- PRIMARY PITCH DAMPING DERIVATIVE
- GREATEST EFFECT ON SHORT-PERIOD MODE
- FINAL VALUE CHECKED USING FLIGHT TEST DYNAMIC RESPONSE MATCHING

C_{D_q}

NEGLIGIBLE, NOT PLOTTED

- NEGLIGIBLE
- FINAL VALUE NOT CHECKED IN FLIGHT TEST; IMPACT TOO SMALL

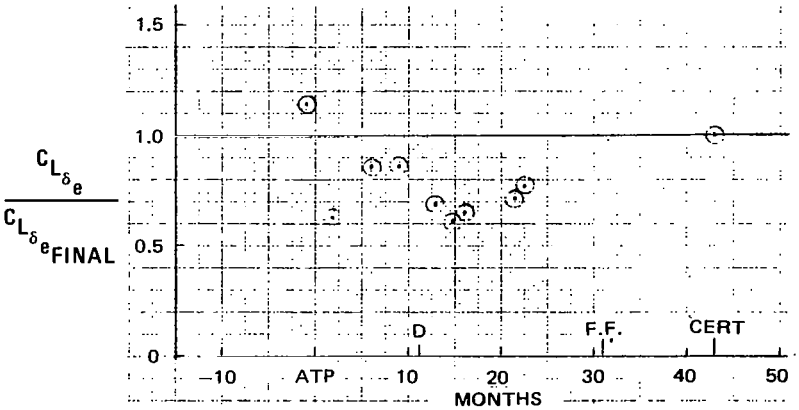

$C_{L_{\delta_e}}$

- SECONDARY IMPORTANCE FOR CONVENTIONAL AIRCRAFT
- FINAL VALUE CHECKED BY FLIGHT TEST RESULTS; NORMALLY NO ASSESSMENT OF ACCURACY MADE

FIGURE 13. HISTORICAL UNCERTAINTIES OF LONGITUDINAL AERODYNAMIC PARAMETERS

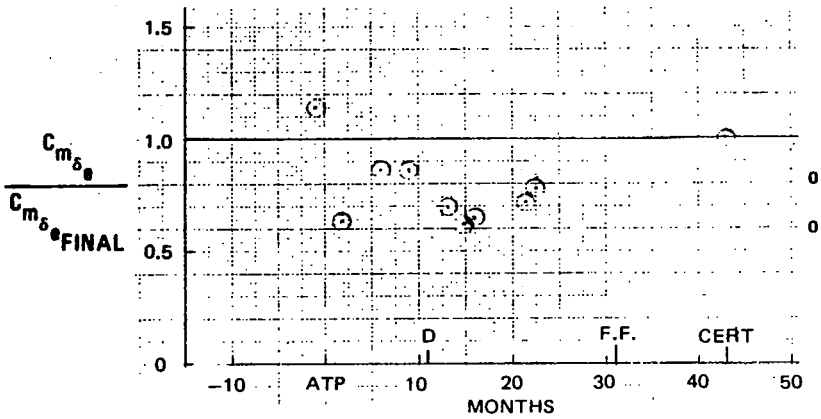

$C_{m_{\delta_e}}$

- PRIMARY PITCH CONTROL DERIVATIVE
- FINAL VALUE CHECKED BY FLIGHT TEST RESULTS; NORMALLY NO ASSESSMENT OF ACCURACY MADE

ESTIMATED ACCURACY: ±4 PERCENT

$C_{D_{\delta_e}}$

NEGLIGIBLE, NOT PLOTTED

- USUALLY NEGLIGIBLE
- FINAL VALUE NOT CHECKED IN FLIGHT TEST; IMPACT TOO SMALL

C_L

NOT PLOTTED

- PRIMARY FLIGHT CONDITION PARAMETER
- AFFECTS PHUGOID MODE
- AFFECTS FLIGHT-PATH STABILITY (NUMERATOR PROPERTY OF h/δ_e TRANSFER FUNCTION)
- FINAL VALUE VERY CAREFULLY CHECKED IN FLIGHT TEST BECAUSE OF PERFORMANCE GUARANTEES

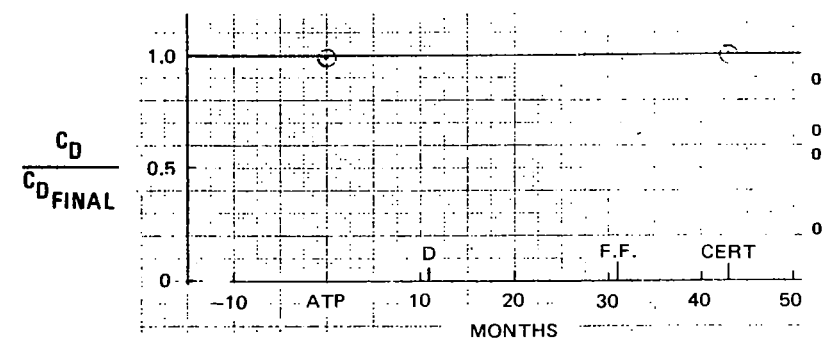

C_D

- PRIMARY PERFORMANCE PARAMETER
- AFFECTS PHUGOID MODE DAMPING
- AFFECTS FLIGHT-PATH STABILITY (NUMERATOR PROPERTY OF h/δ_e TRANSFER FUNCTION)
- FINAL VALUE VERY CAREFULLY CHECKED IN FLIGHT TEST BECAUSE OF PERFORMANCE GUARANTEES

ESTIMATED ACCURACY: ±2 PERCENT

FIGURE 14. HISTORICAL UNCERTAINTIES OF LONGITUDINAL AERODYNAMIC PARAMETERS

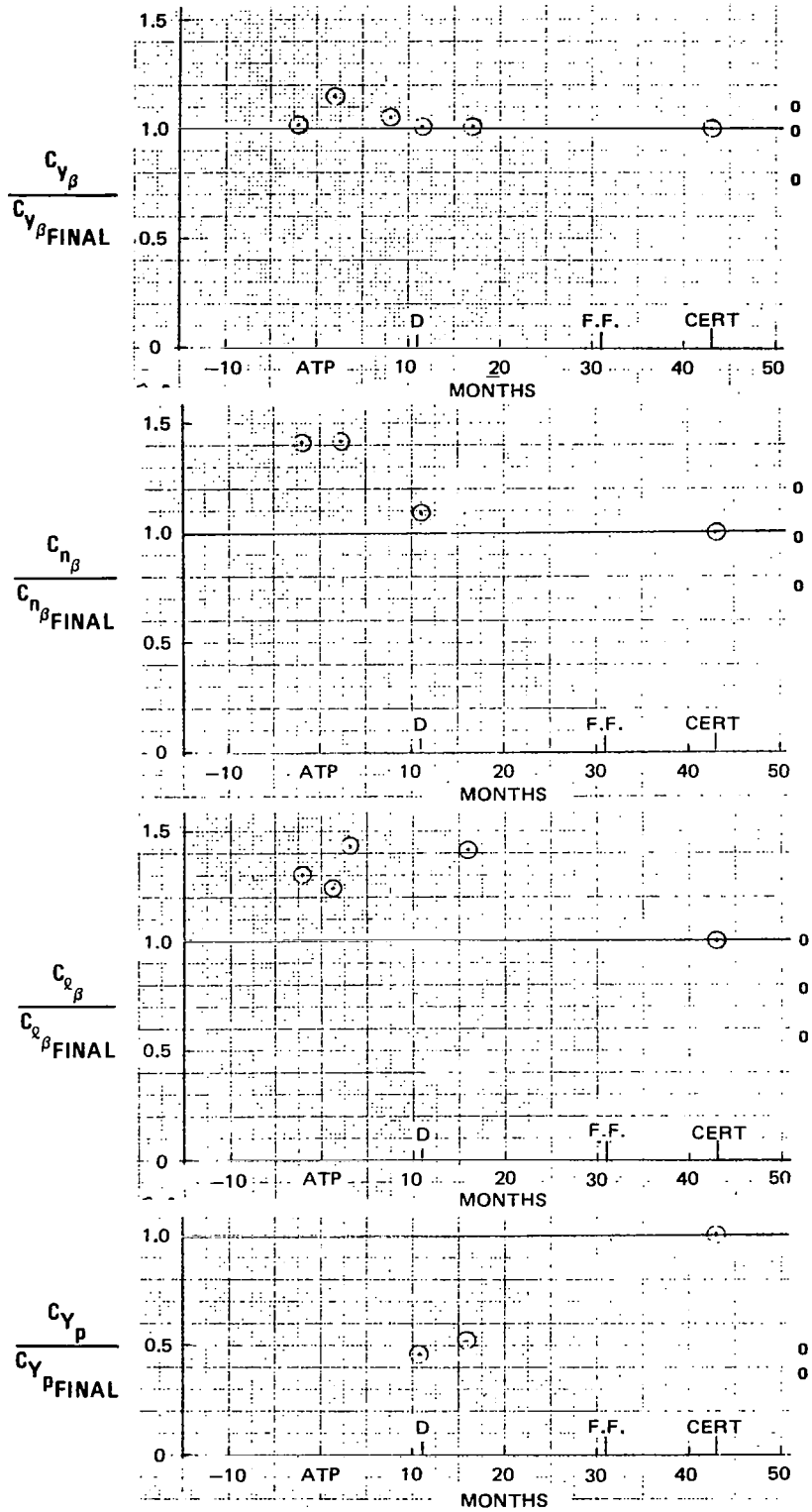

C_{Y_β}

- MODERATE IMPORTANCE
- CONTRIBUTES TO DUTCH ROLL DAMPING
- FINAL VALUE CHECKED BY FLIGHT TEST RESULTS; NORMALLY NO ASSESSMENT OF ACCURACY MADE

C_{n_β}

- PRIMARY DIRECTIONAL STABILITY PARAMETER
- AFFECTS BOTH DUTCH ROLL AND SPIRAL MODES
- FINAL VALUE CHECKED BY FLIGHT TEST RESULTS; NORMALLY NO ASSESSMENT OF ACCURACY MADE

C_{ℓ_β}

- PRIMARY LATERAL STABILITY PARAMETER
- AFFECTS BOTH DUTCH ROLL AND SPIRAL MODES
- FINAL VALUE CHECKED BY FLIGHT TEST RESULTS; NORMALLY NO ASSESSMENT OF ACCURACY MADE

C_{Y_p}

- NEGLIGIBLE IN MANY CASES
- FINAL VALUE NOT CHECKED IN FLIGHT TEST; IMPACT TOO SMALL

FIGURE 15. HISTORICAL UNCERTAINTIES OF LATERAL-DIRECTIONAL AERODYNAMIC PARAMETERS

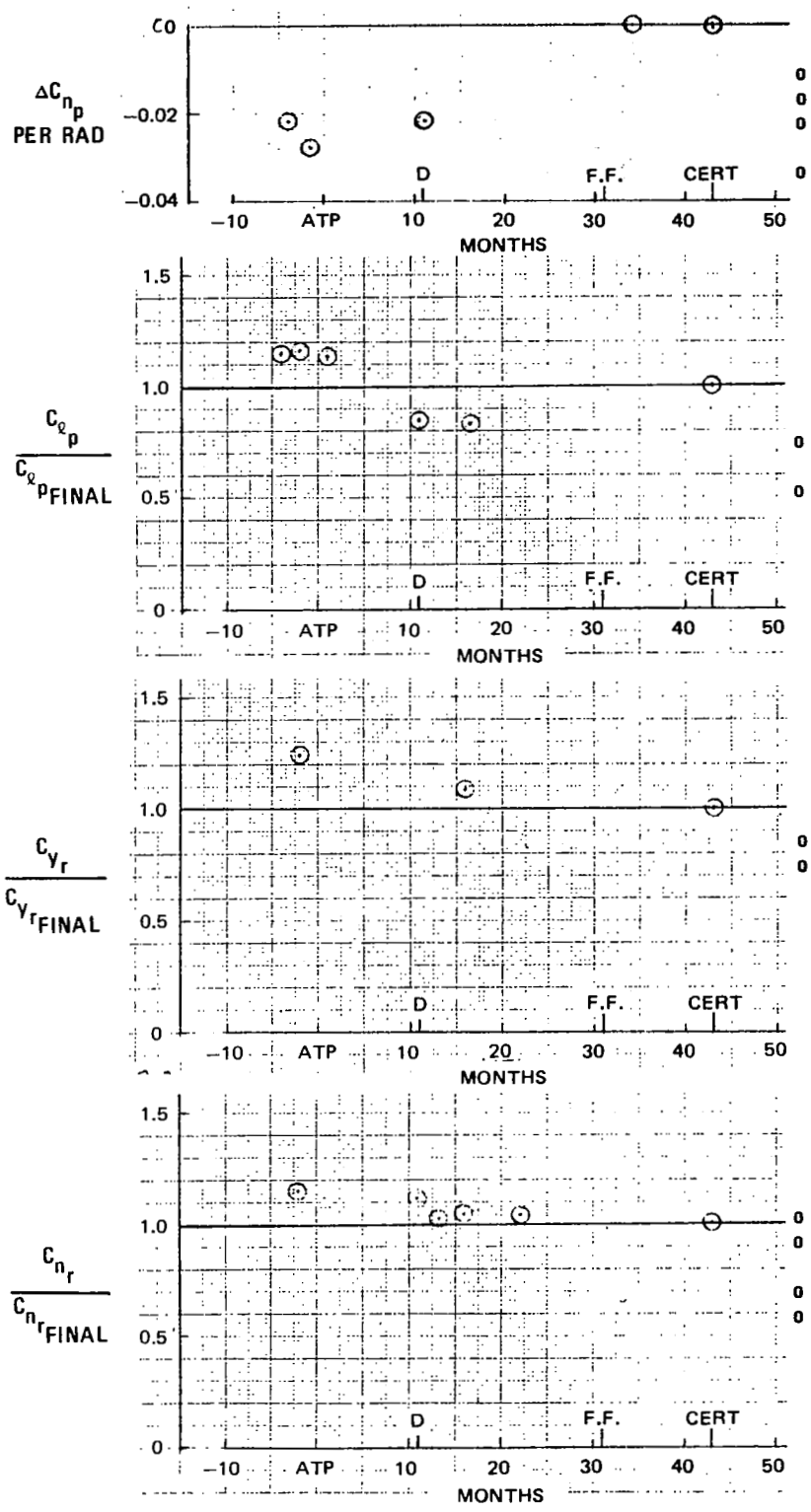

C_{n_p}

- SECONDARY IMPORTANCE
- AFFECTS DUTCH ROLL DAMPING
- AFFECTS TURN COORDINATION CHARACTERISTICS
- FINAL VALUE NOT CHECKED IN FLIGHT TEST; IMPACT TOO SMALL

C_{ℓ_p}

- BASIC ROLL DAMPING DERIVATIVE
- FINAL VALUE CHECKED USING FLIGHT TEST DYNAMIC RESPONSE MATCHING

C_{y_r}

- NEGLIGIBLE IN MANY CASES
- FINAL VALUE NOT CHECKED IN FLIGHT TEST; IMPACT TOO SMALL

C_{n_r}

- BASIC YAW DAMPING DERIVATIVE
- IMPORTANT TO DUTCH ROLL DAMPING
- ALSO AFFECTS SPIRAL MODE
- FINAL VALUE CHECKED USING FLIGHT TEST DYNAMIC RESPONSE MATCHING

FIGURE 16. HISTORICAL UNCERTAINTIES OF LATERAL-DIRECTIONAL AERODYNAMIC PARAMETERS

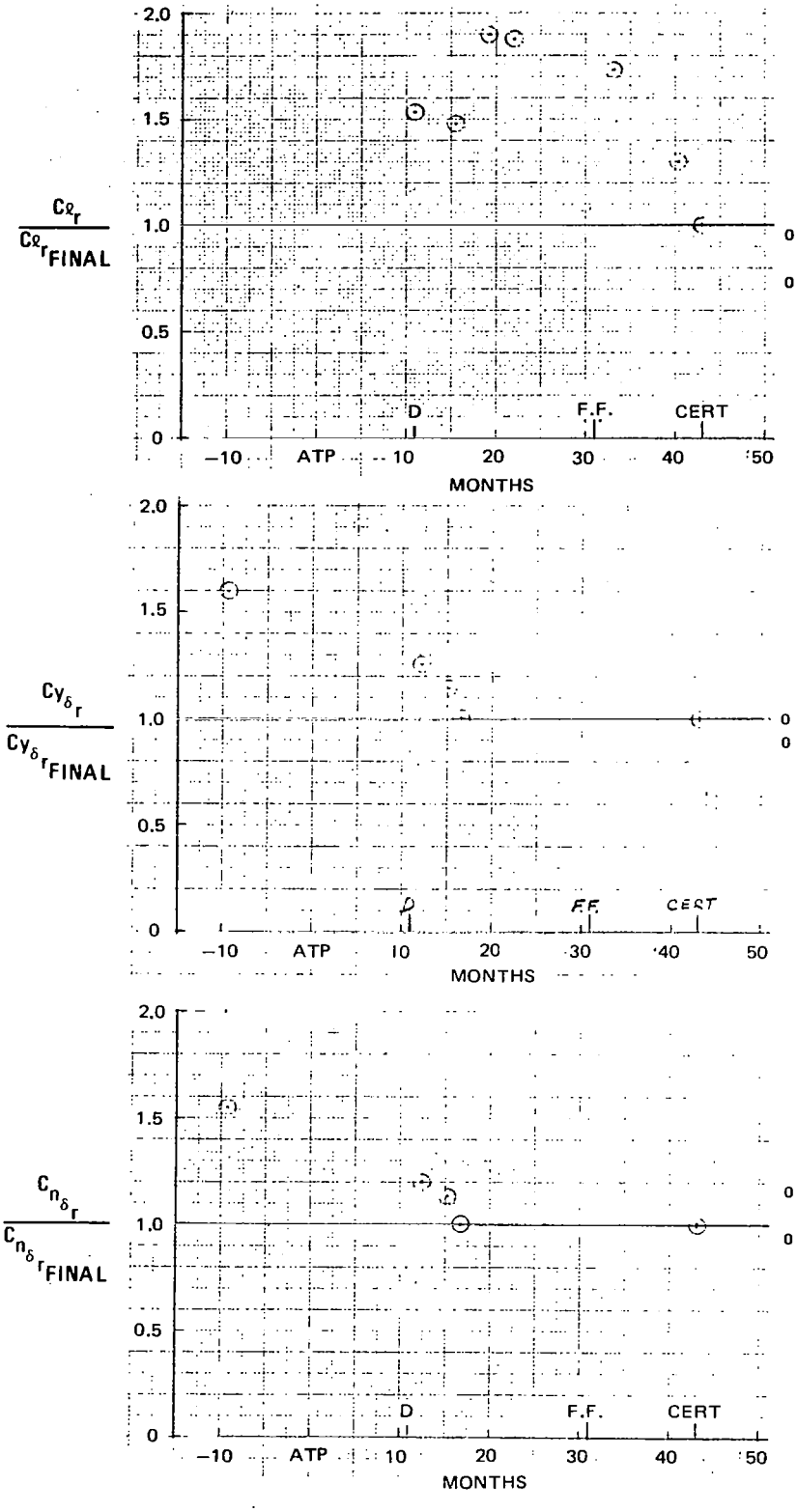

C_{ℓ_r}

- MODERATE IMPORTANCE TO SPIRAL MODE
- FINAL VALUE CHECKED USING FLIGHT TEST DYNAMIC RESPONSE MATCHING

$C_{y_{\delta_r}}$

- SECONDARY CONTROL DERIVATIVE
- FINAL VALUE NOT CHECKED IN FLIGHT TEST; IMPACT TOO SMALL

$C_{n_{\delta_r}}$

- PRIMARY DIRECTIONAL CONTROL DERIVATIVE
- FINAL VALUE CHECKED BY FLIGHT TEST RESULTS; NORMALLY NO ASSESSMENT OF ACCURACY MADE

FIGURE 17. HISTORICAL UNCERTAINTIES OF LATERAL-DIRECTIONAL AERODYNAMIC PARAMETERS

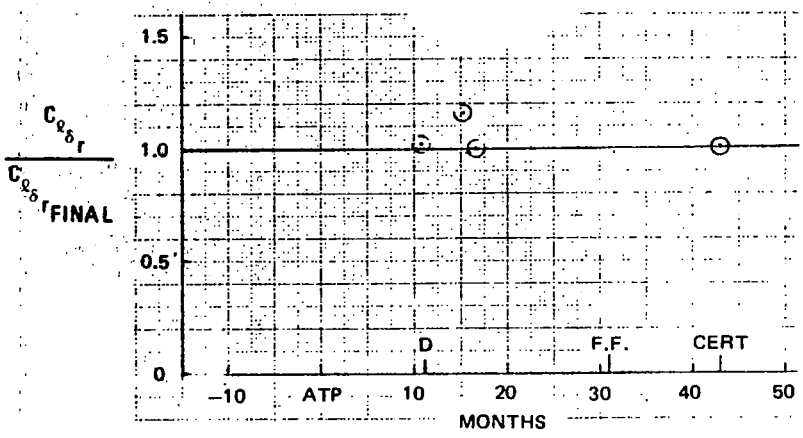

$C_{\ell_{\delta_r}}$

- SECONDARY CONTROL DERIVATIVE
- FINAL VALUE NOT CHECKED IN FLIGHT TEST; IMPACT TOO SMALL

$C_{Y_{\delta_a}}$

NEGLIGIBLE, NOT PLOTTED

- NEGLIGIBLE IN MANY CASES
- FINAL VALUE NOT CHECKED IN FLIGHT TEST; IMPACT TOO SMALL

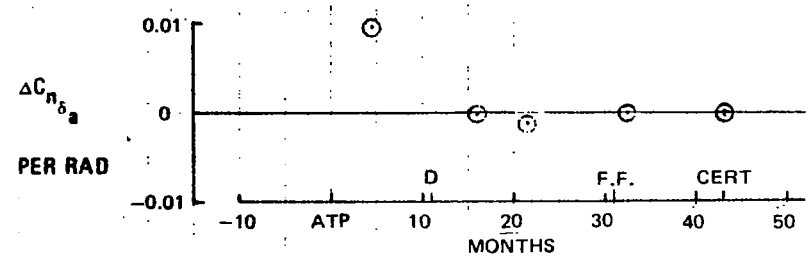

$C_{n_{\delta_a}}$

- SECONDARY CONTROL DERIVATIVE
- AFFECTS TURN COORDINATION CHARACTERISTICS
- FINAL VALUE NOT CHECKED IN FLIGHT TEST; IMPACT TOO SMALL

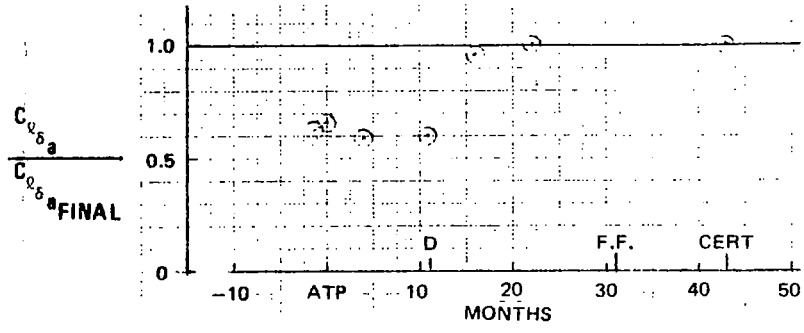

$C_{\ell_{\delta_a}}$

- PRIMARY LATERAL CONTROL DERIVATIVE
- FINAL VALUE CHECKED BY FLIGHT TEST RESULTS; NORMALLY NO ASSESSMENT OF ACCURACY MADE

$C_{Y_{\delta_{sp}}}$

NEGLIGIBLE, NOT PLOTTED

- NEGLIGIBLE IN MANY CASES
- FINAL VALUE NOT CHECKED IN FLIGHT TEST; IMPACT TOO SMALL

FIGURE 18. HISTORICAL UNCERTAINTIES OF LATERAL-DIRECTIONAL AERODYNAMIC PARAMETERS

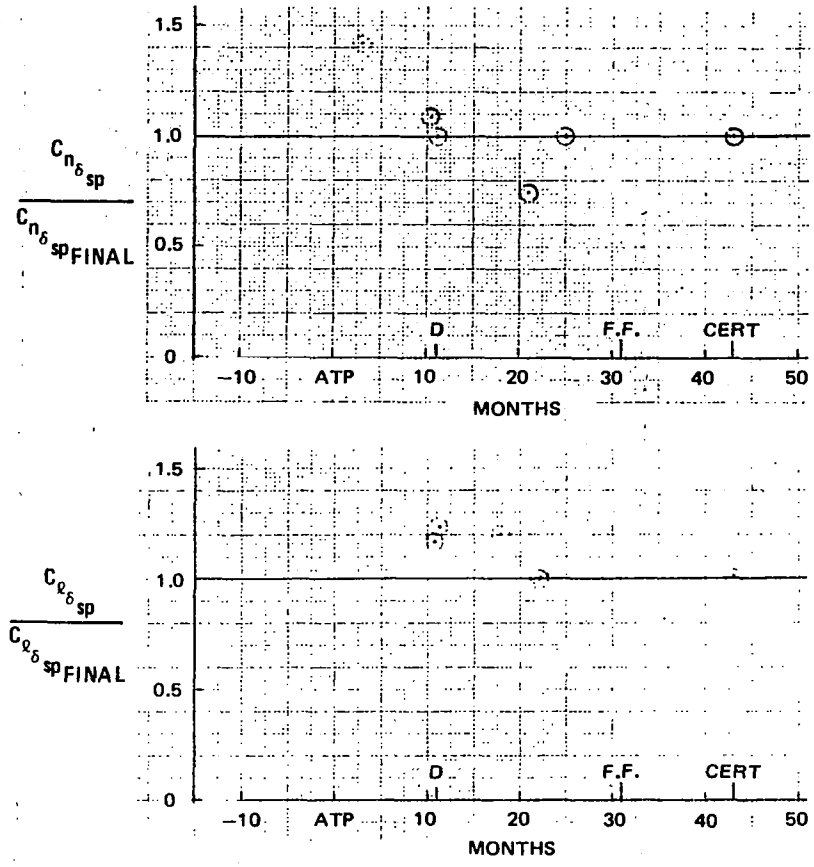

FIGURE 19. HISTORICAL UNCERTAINTIES OF LATERAL-DIRECTIONAL AERODYNAMIC PARAMETERS

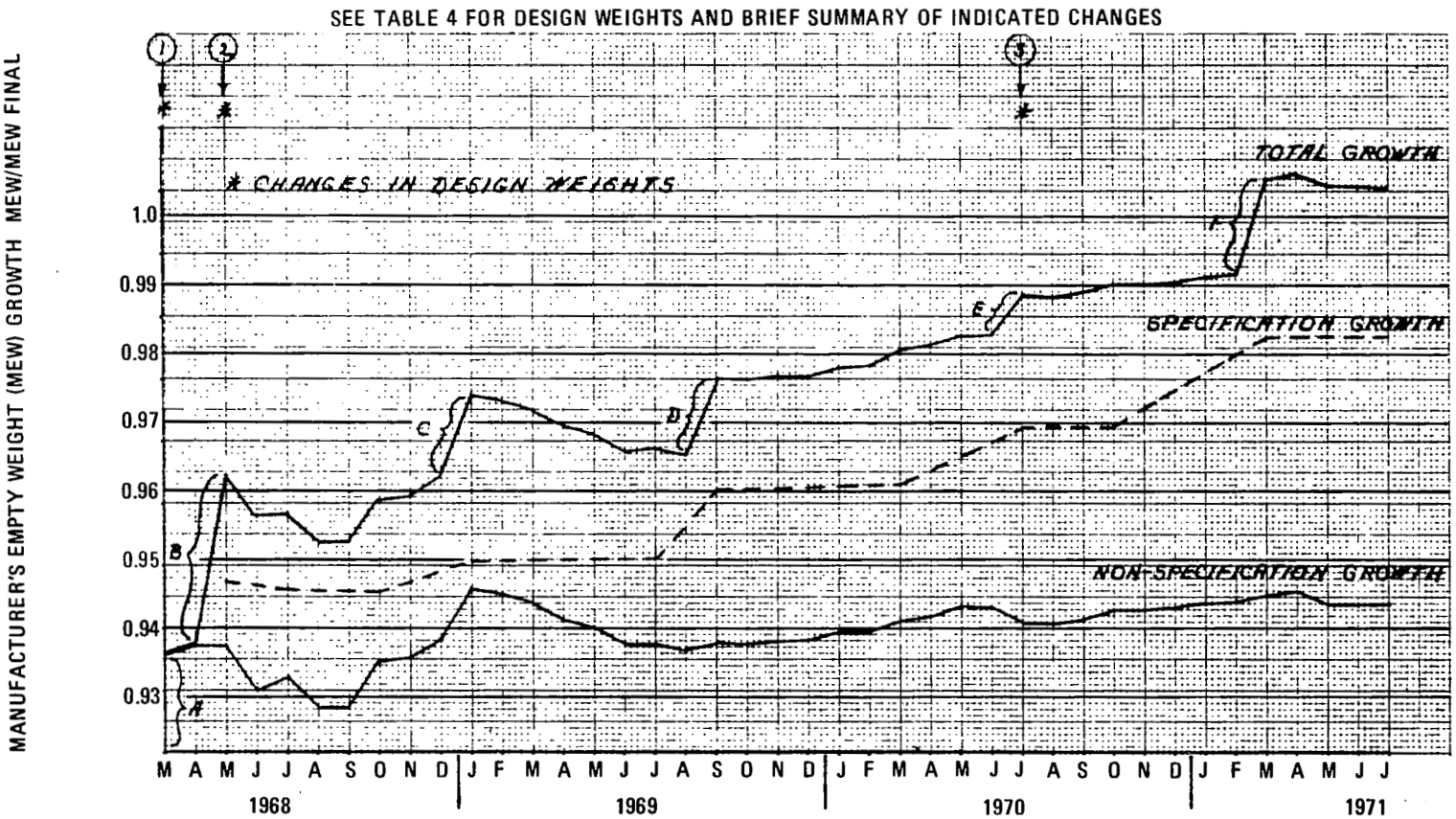

FIGURE 20. MANUFACTURER'S EMPTY WEIGHT GROWTH HISTORY

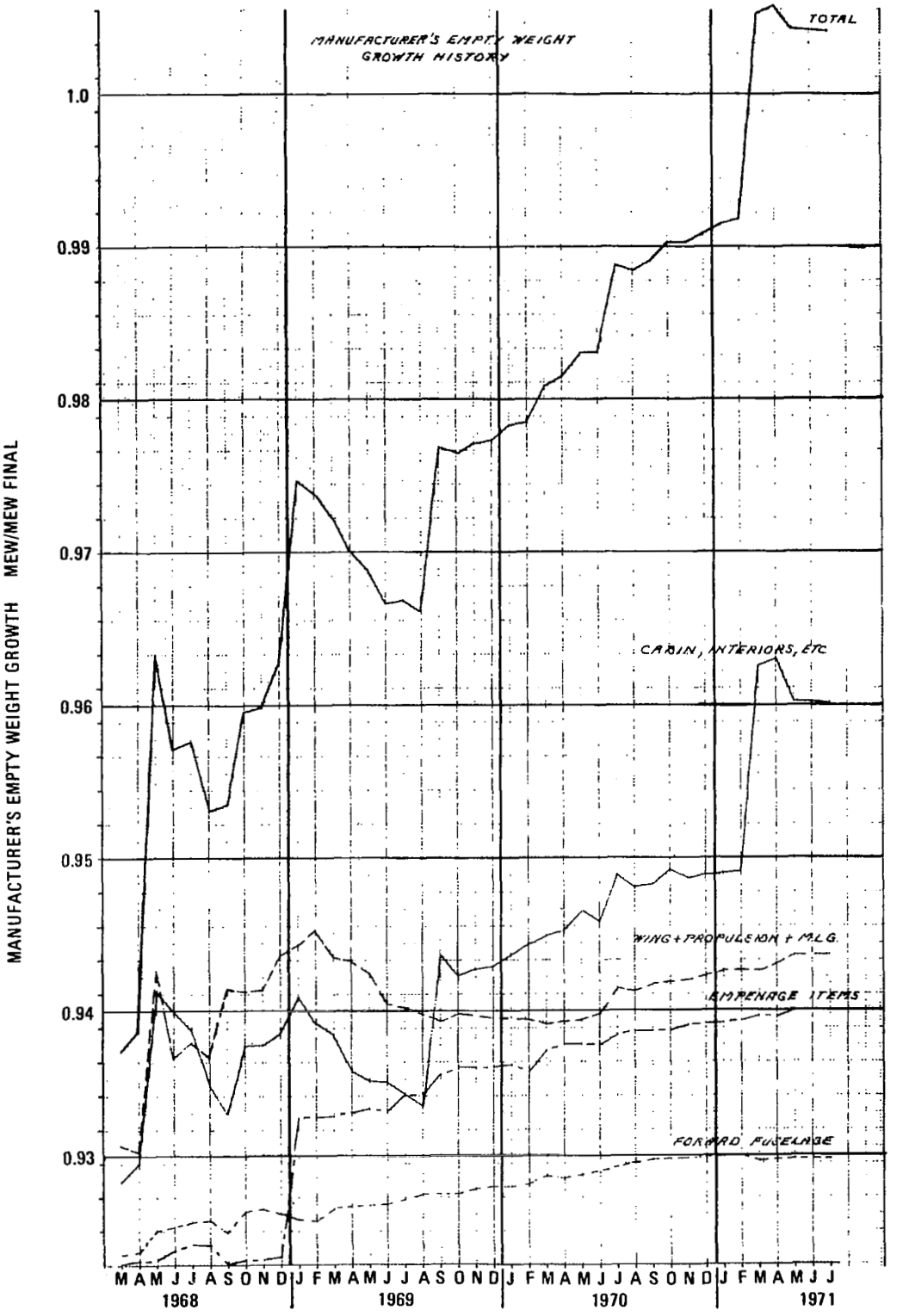

FIGURE 21. MANUFACTURER'S EMPTY WEIGHT GROWTH HISTORY

TABLE 9

MAJOR WEIGHT CHANGE SUMMARY

(see Figure 6)

A. Revised estimate for wing bending material, increased allowance for insulation and interior panels plus miscellaneous changes.

B. Increased engine weight, revised estimate for wing and landing gear to provide for an increase in takeoff gross weight plus miscellaneous changes.

C. Interior design changes, 0.102m (4-inch) fuselage stretch, addition of aft engine maintenance platform plus revised estimates for fuselage, wing and tail.

D. Customer requested interior changes plus revised estimates for miscellaneous structural and subsystem items.

E. Increased engine weight, revised estimate for wing and landing gear to provide for an increase in takeoff gross weight plus miscellaneous changes.

F. Incorporated more representative weights for galleys and passenger seats.

TABLE 10

MOMENT OF INERTIA HISTORY

Assumed Growth	Inertia Value at Program Start / Final Inertia Value
1. Manufacturers Empty Weight (MEW) Growth of 8.8 percent	
$I_X/I_{X\ Final}$	0.95
$I_Y/I_{Y\ Final}$	0.92
$I_Z/I_{Z\ Final}$	0.93
2. Maximum Takeoff Gross Weight (MTOGW) Growth of 11 percent and Constant Fuel:	
$I_X/I_{X\ Final}$	0.96
$I_Y/I_{Y\ Final}$	0.88
$I_Z/I_{Z\ Final}$	0.92
3. Maximum Takeoff Gross Weight (MTOGW) Growth of 11 percent and Constant Payload:	
$I_X/I_{X\ Final}$	0.85
$I_Y/I_{Y\ Final}$	0.93
$I_Z/I_{Z\ Final}$	0.89

Final values are those calculated at first flight (31 months after program initiation). The product of inertia (I_{XZ}) does not change significantly.

(a) MAXIMUM TAKEOFF GROSS WEIGHT

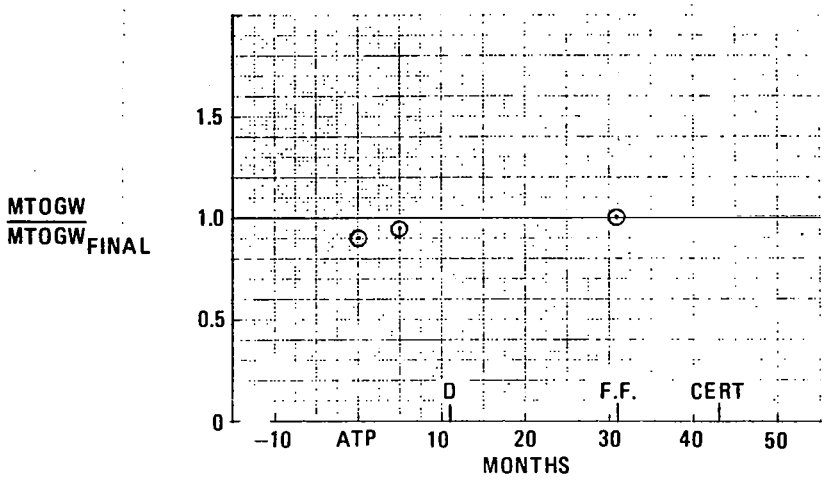

(b) MAXIMUM LANDING WEIGHT

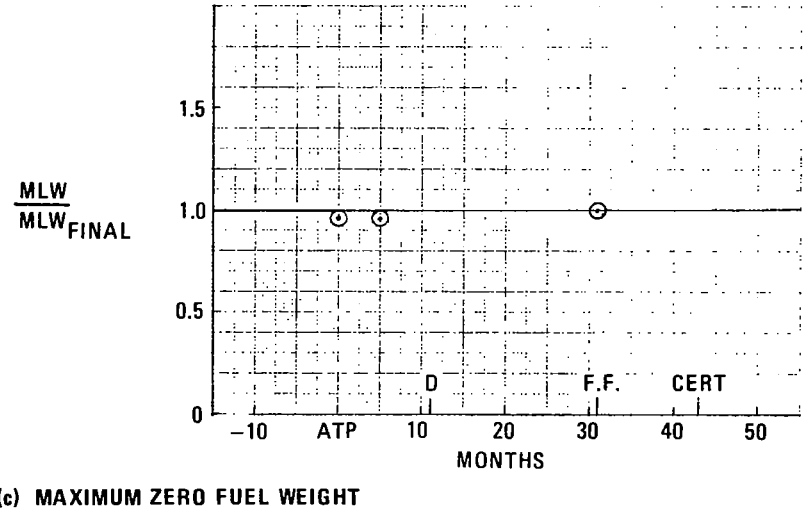

(c) MAXIMUM ZERO FUEL WEIGHT

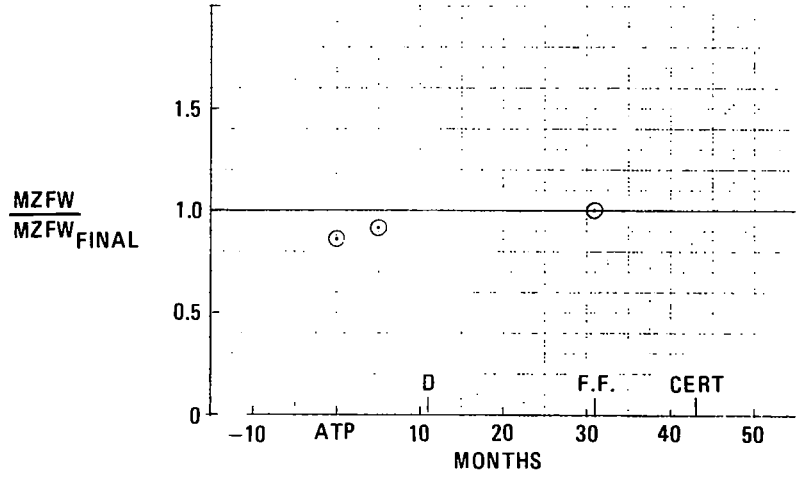

FIGURE 22. DESIGN WEIGHT HISTORIES

CR-2887

TABLE 11

SYMMETRIC MODAL ANALYSES SUMMARY

MODE DESCRIPTION	FIGURE NUMBER OF TIME HISTORY					
	ZERO FUEL			FULL FUEL		
	FREQ	GEN MASS	DEFL	FREQ	GEN MASS	DEFL
FIRST WING BENDING	27	61	91-96	36	69	115-120
WING ENGINE YAW	28	62	–	37	70	–
WING ENGINE PITCH/ FUSELAGE BENDING	29	63	97-102	38	71	121-126
HORIZONTAL STABILIZER BENDING/ AFT ENGINE PITCH	30	64	–	39	72	–
WING INNER PANEL TORSION	31	65	103-108	40	73	127-131
WING ENGINE ROLL	32	–	–	43	–	–
SECOND WING BENDING	33	66	109-114	42	75	132-135
WING FORE AND AFT BENDING	34	67	–	41	74	–
WING TORSION/ENGINE PITCH	35	68	–	45	–	–
THIRD WING BENDING/ AFT ENGINE PITCH	–	–	–	44	76	–

TABLE 12

ANTISYMMETRIC MODAL ANALYSES SUMMARY

MODE DESCRIPTION	FIGURE NUMBER OF TIME HISTORY					
	ZERO FUEL			FULL FUEL		
	FREQ	GEN MASS	DEFL	FREQ	GEN MASS	DEFL
WING ENGINE YAW	46	77	–	55	–	–
FIRST WING BENDING	47	78	136-143	56	86	166-173
AFT ENGINE YAW	48	79	–	–	87	–
HORIZONTAL STABILIZER BENDING	49	80	144-149	57	88	174-180
VERTICAL STABILIZER BENDING	50	81	150-157	59	89	189-196
AFT FUSELAGE TORSION/ WING ENGINE PITCH	51	82	158-165	58	–	181-188
AFT FUSELAGE LATERAL BENDING	52	83	–	–	–	–
SECOND WING BENDING	53	84	–	60	90	–
SECOND VERTICAL STABILIZER BENDING	54	85	–	–	–	–

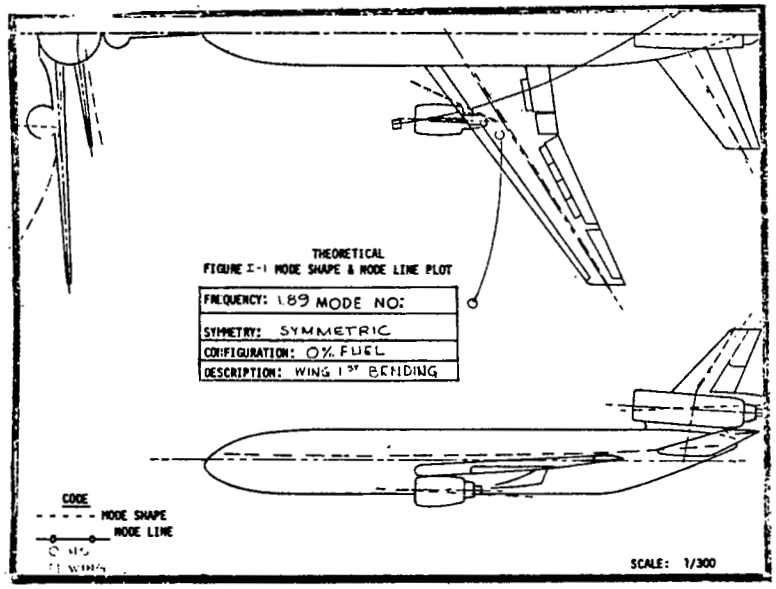

FIGURE 23. MODE SHAPES AND MODE LINES

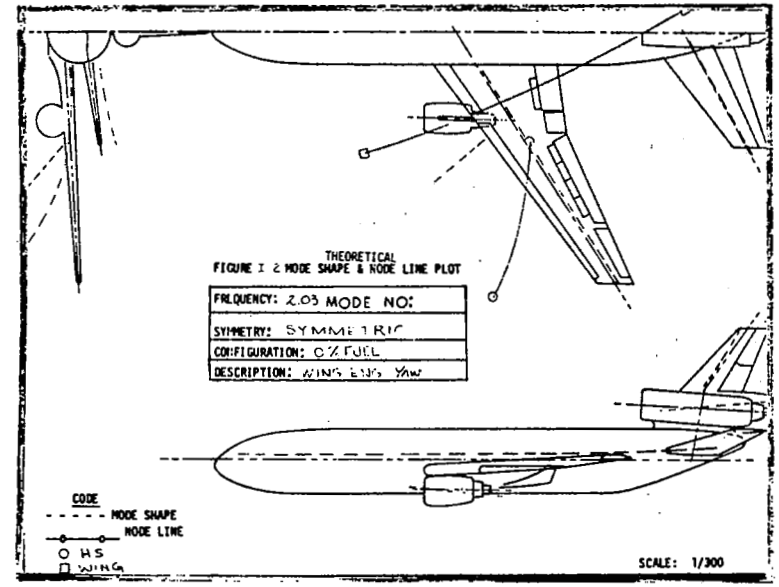

FIGURE 24. MODE SHAPES AND MODE LINES

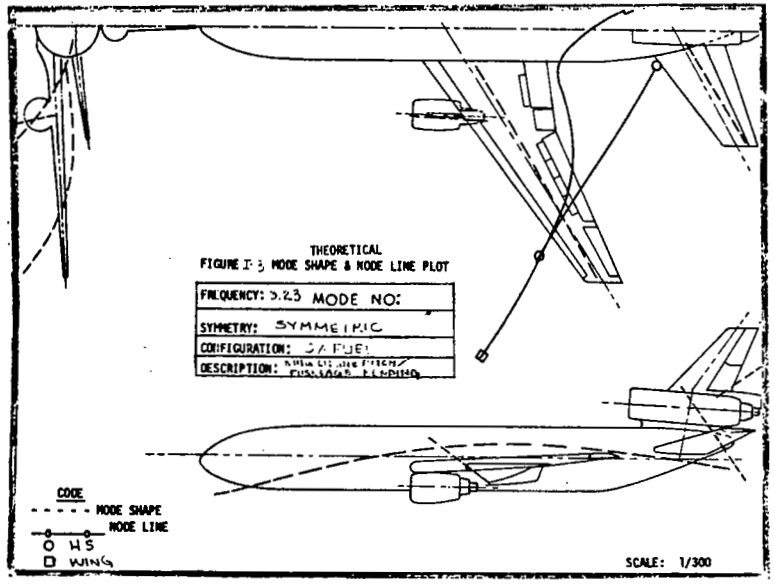

FIGURE 25. MODE SHAPES AND MODE LINES

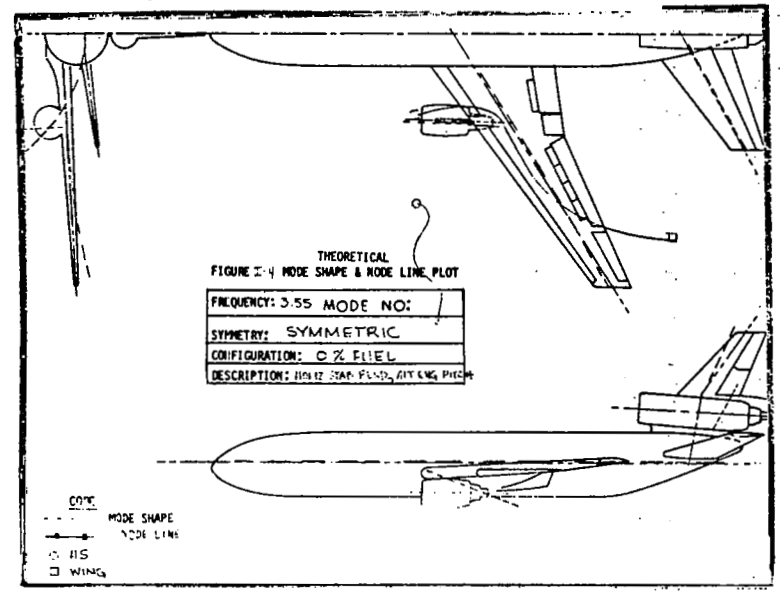

FIGURE 26. MODE SHAPES AND MODE LINES

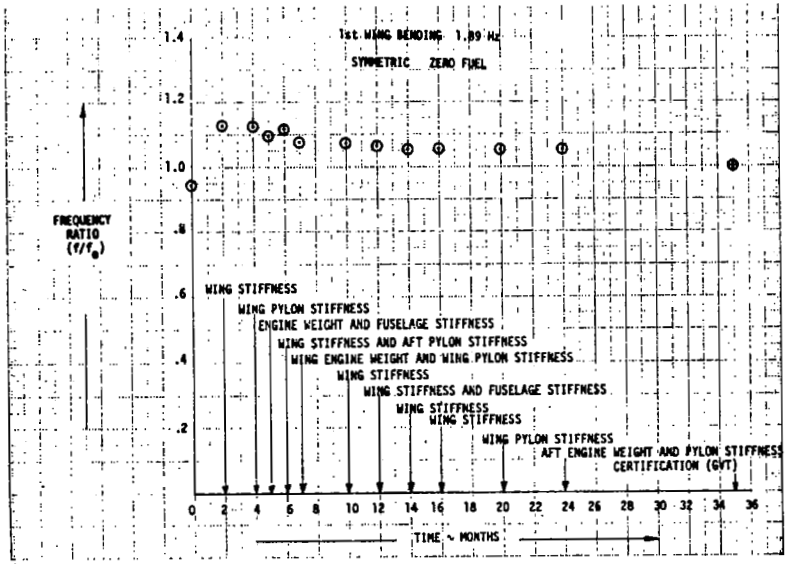

FIGURE 27. EVOLUTION OF FREQUENCY RATIO

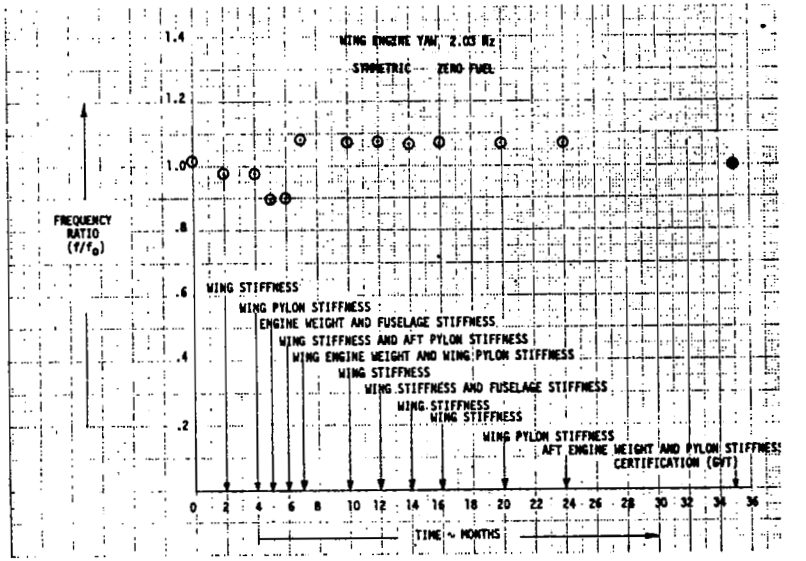

FIGURE 28. EVOLUTION OF FREQUENCY RATIO

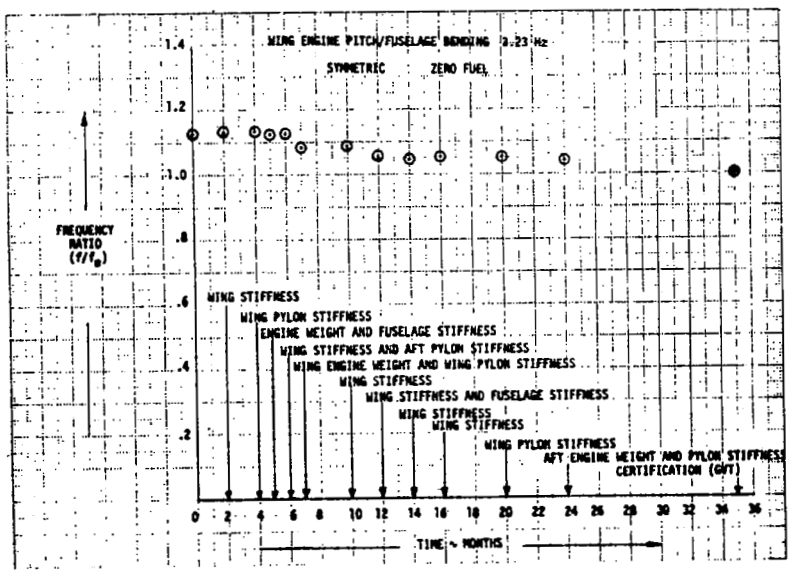

FIGURE 29. EVOLUTION OF FREQUENCY RATIO

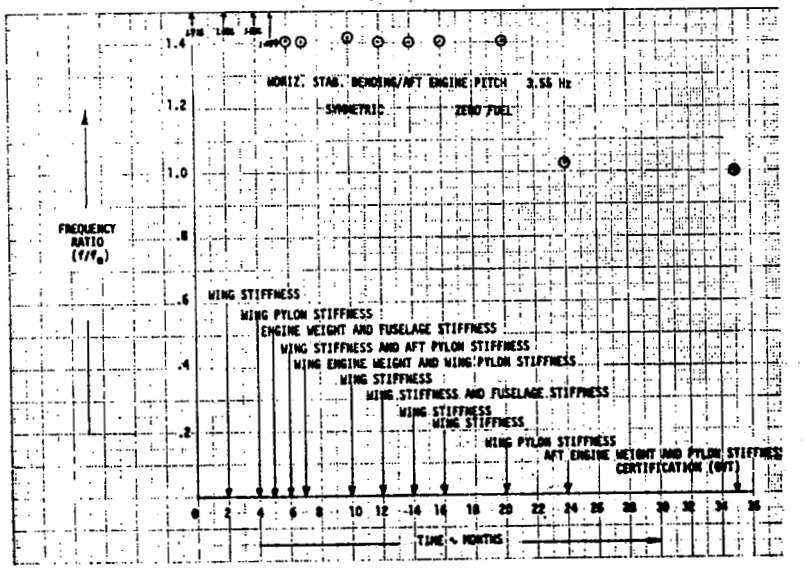

FIGURE 30. EVOLUTION OF FREQUENCY RATIO

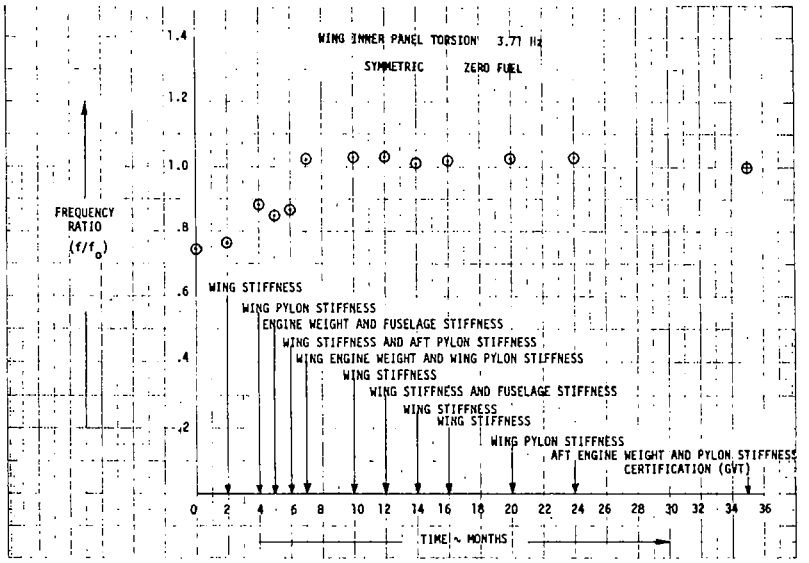

FIGURE 31. EVOLUTION OF FREQUENCY RATIO

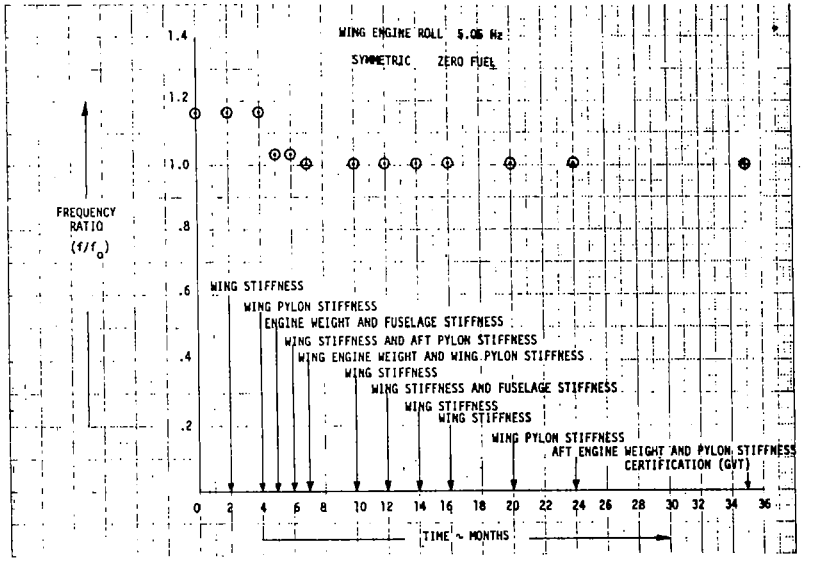

FIGURE 32. EVOLUTION OF FREQUENCY RATIO

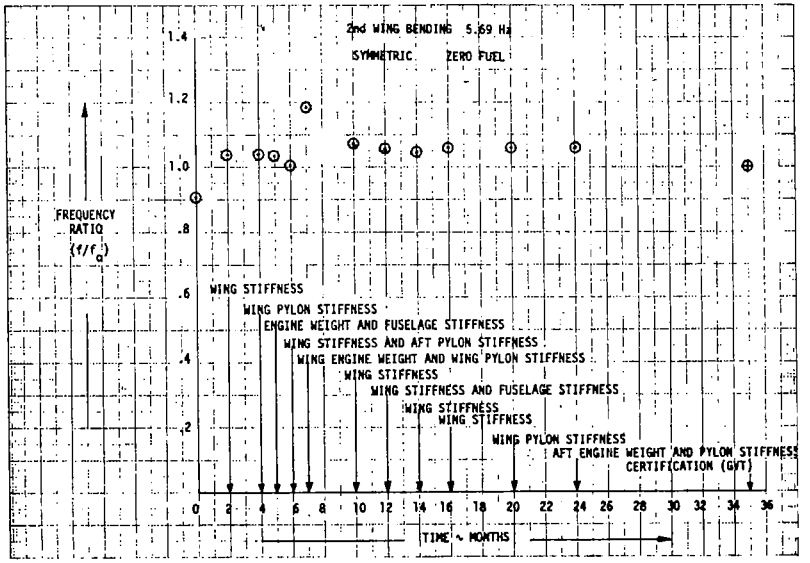

FIGURE 33. EVOLUTION OF FREQUENCY RATIO

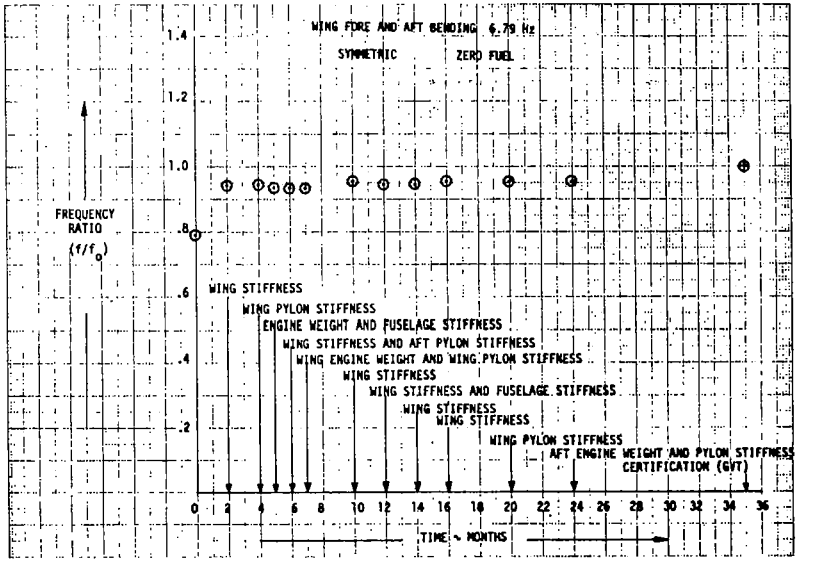

FIGURE 34. EVOLUTION OF FREQUENCY RATIO

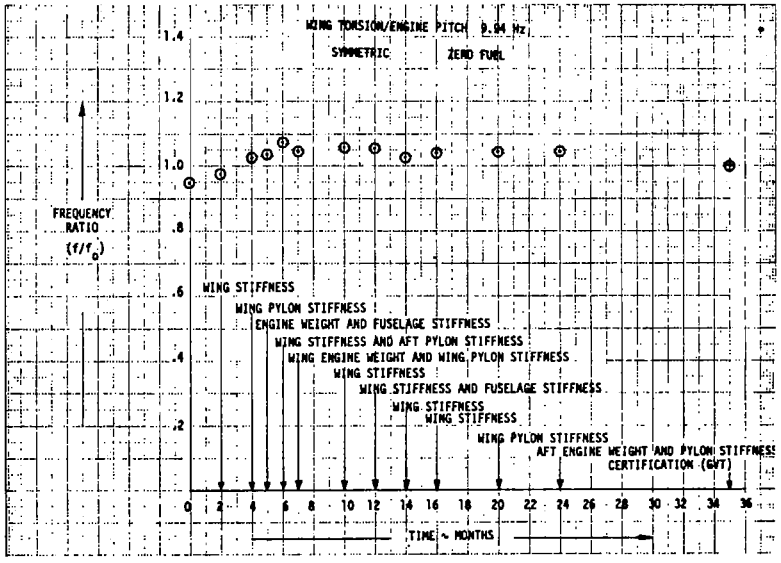

FIGURE 35. EVOLUTION OF FREQUENCY RATIO

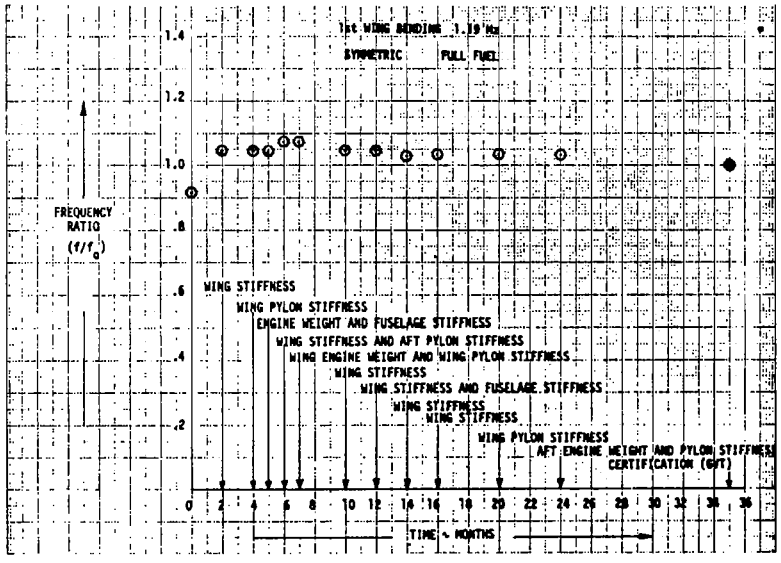

FIGURE 36. EVOLUTION OF FREQUENCY RATIO

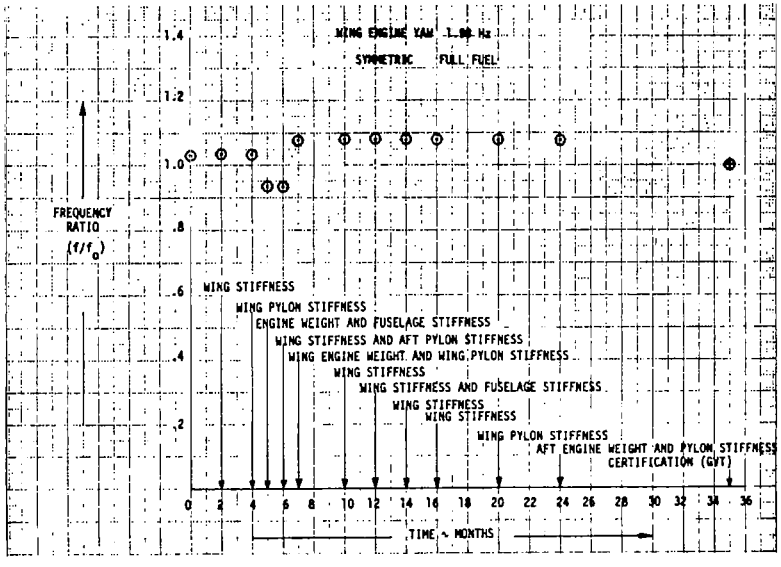

FIGURE 37. EVOLUTION OF FREQUENCY RATIO

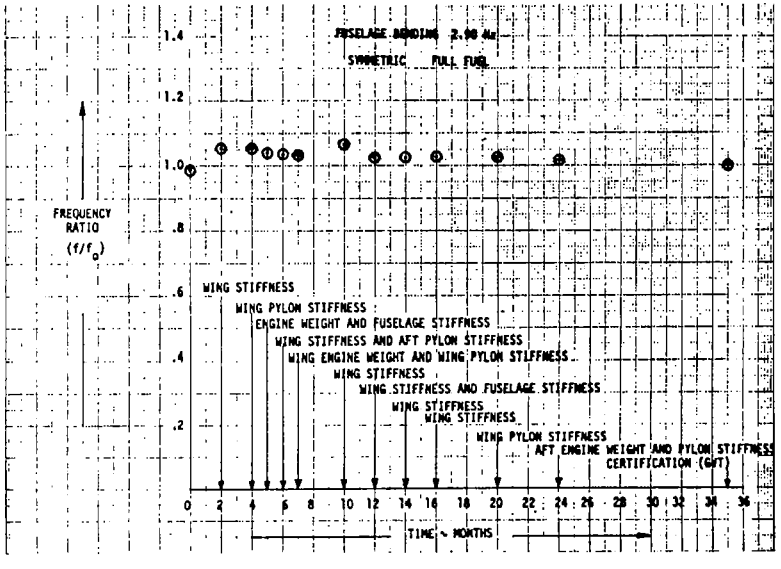

FIGURE 38. EVOLUTION OF FREQUENCY RATIO

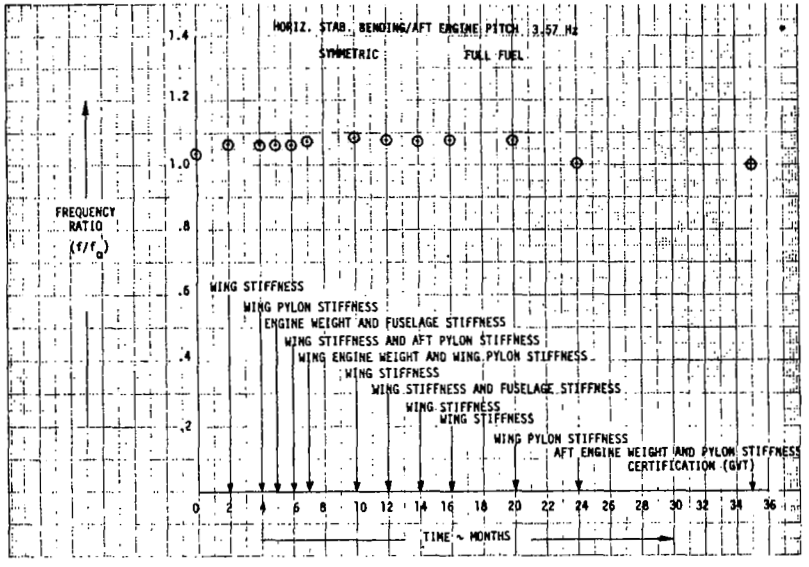

FIGURE 39. EVOLUTION OF FREQUENCY RATIO

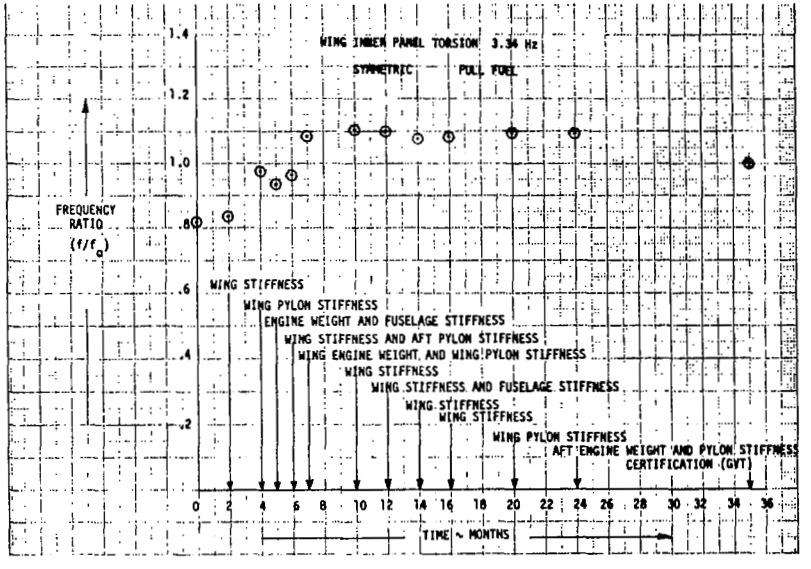

FIGURE 40. EVOLUTION OF FREQUENCY RATIO

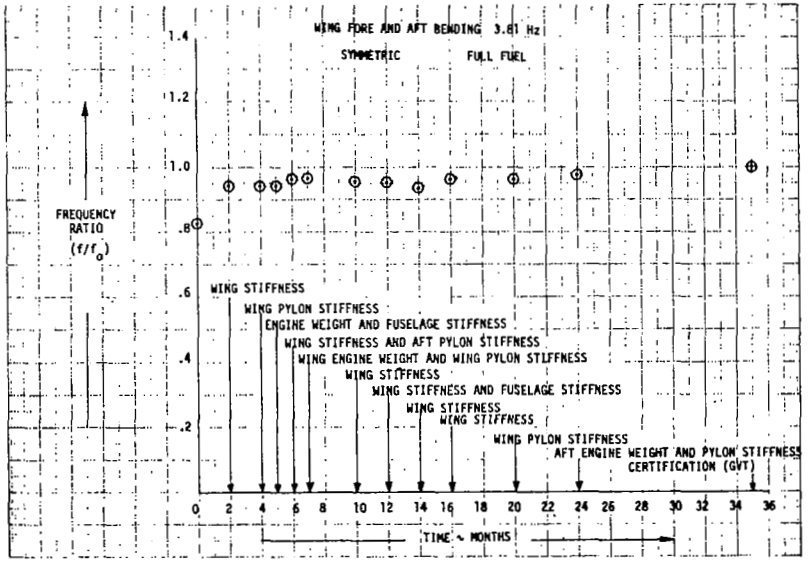

FIGURE 41. EVOLUTION OF FREQUENCY RATIO

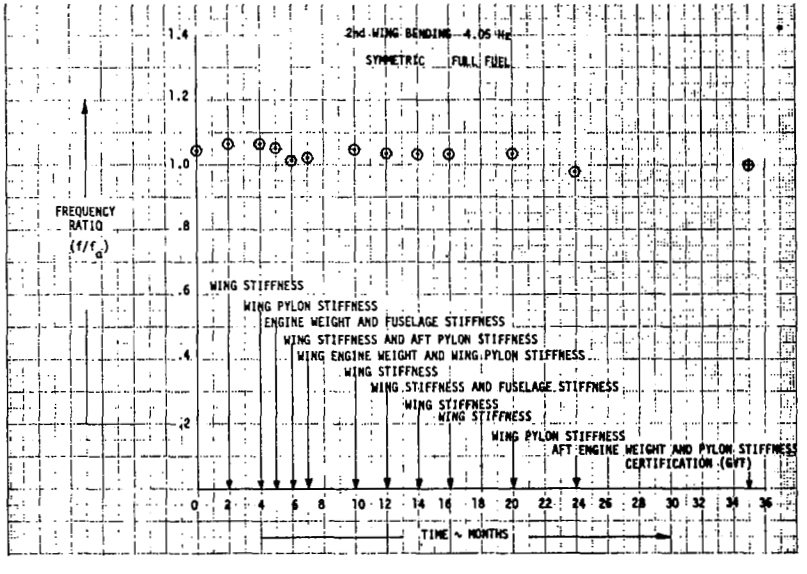

FIGURE 42. EVOLUTION OF FREQUENCY RATIO

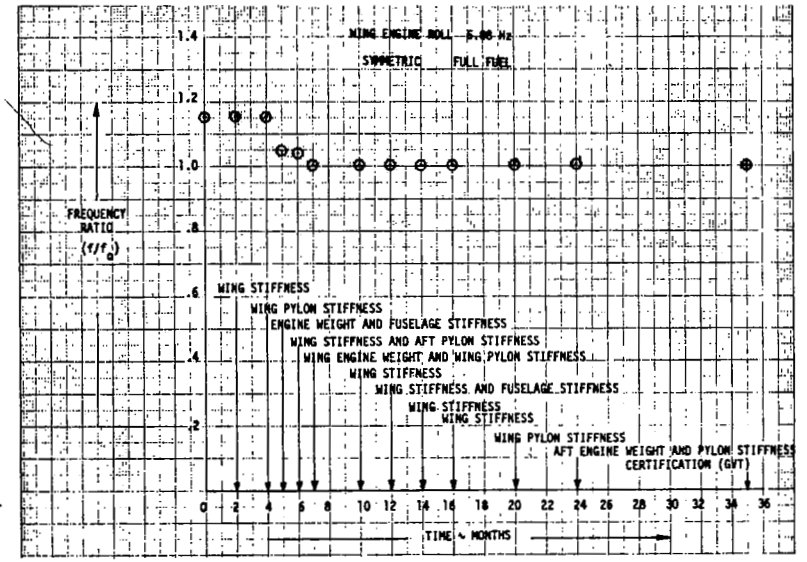

FIGURE 43. EVOLUTION OF FREQUENCY RATIO

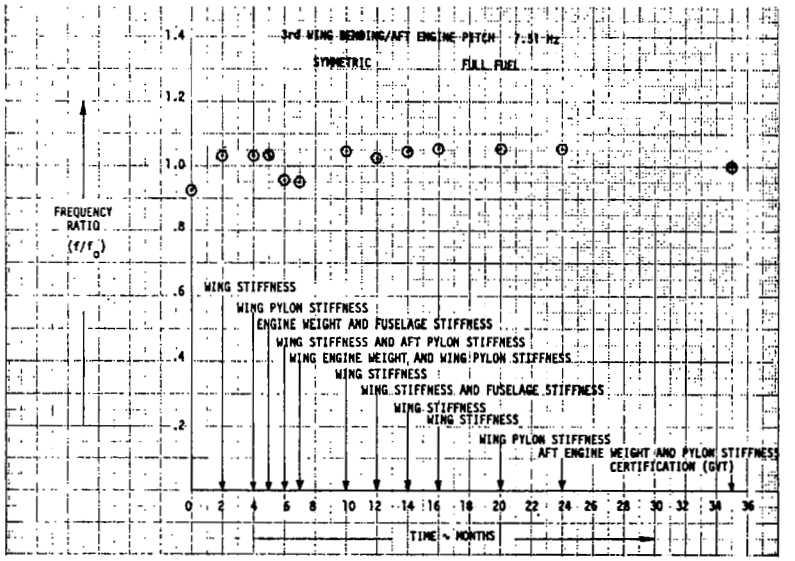

FIGURE 44. EVOLUTION OF FREQUENCY RATIO

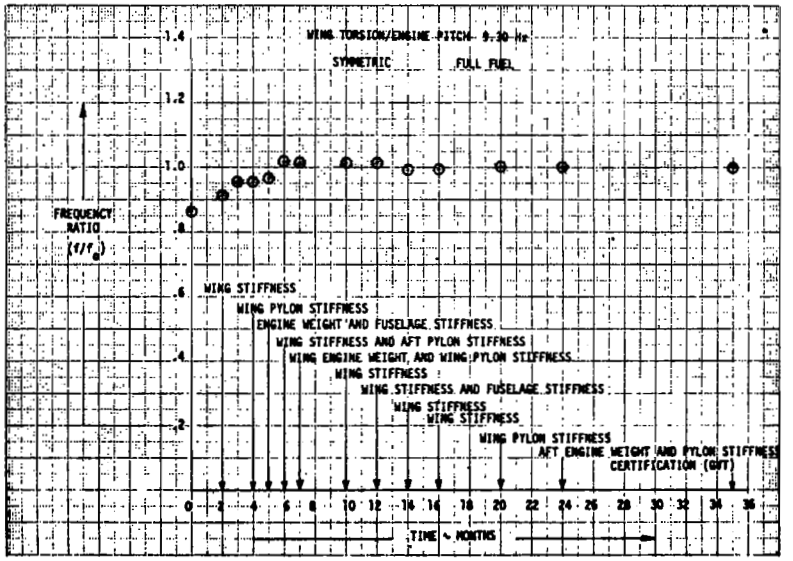

FIGURE 45. EVOLUTION OF FREQUENCY RATIO

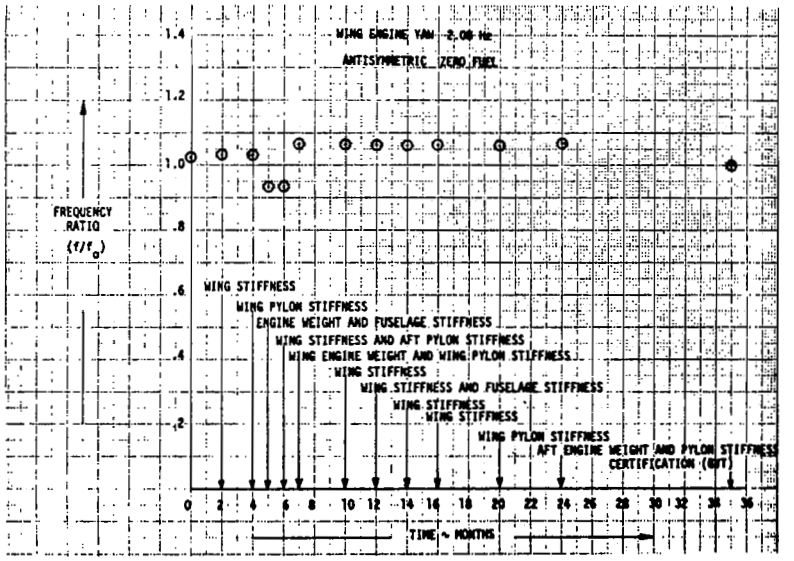

FIGURE 46. EVOLUTION OF FREQUENCY RATIO

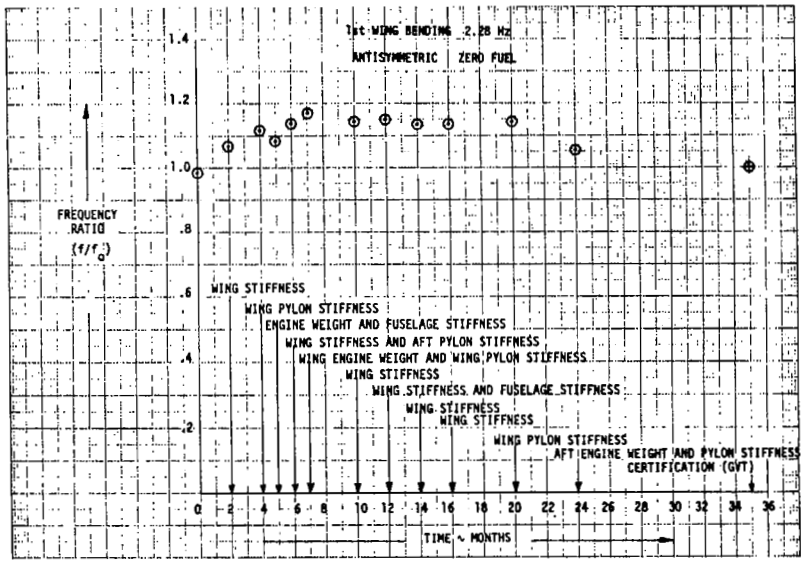

FIGURE 47. EVOLUTION OF FREQUENCY RATIO

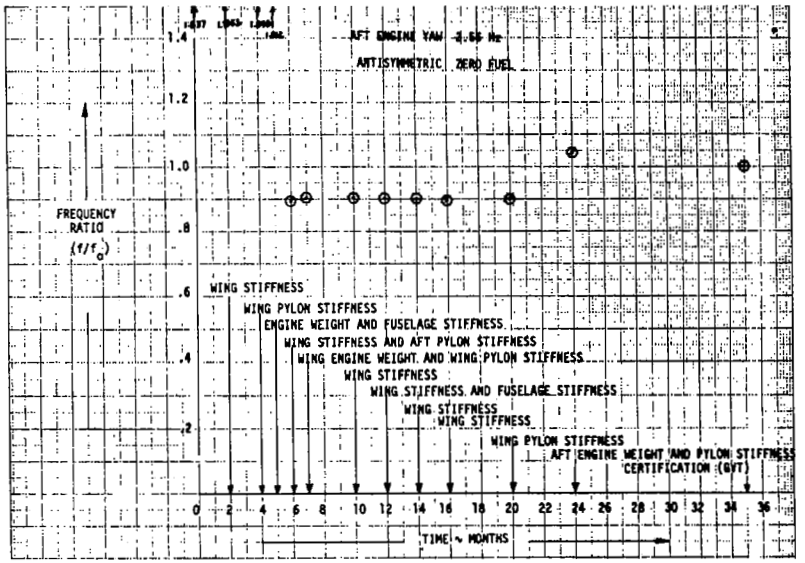

FIGURE 48. EVOLUTION OF FREQUENCY RATIO

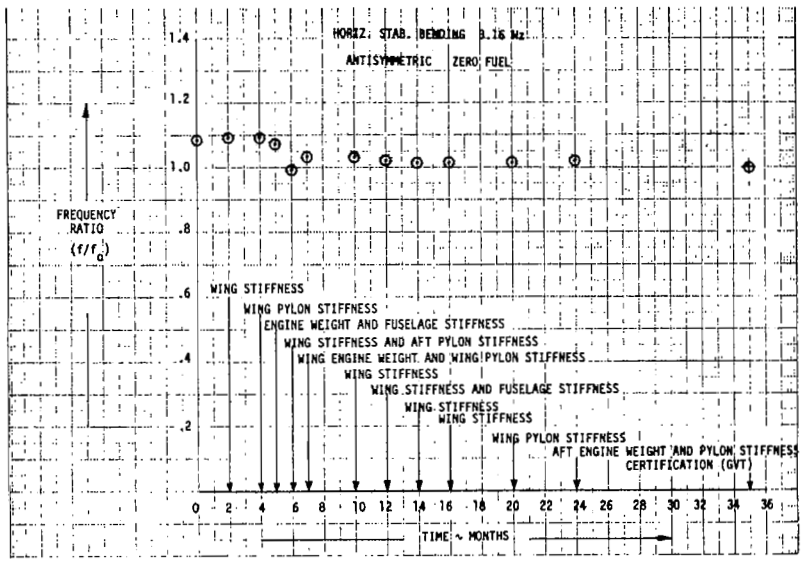

FIGURE 49. EVOLUTION OF FREQUENCY RATIO

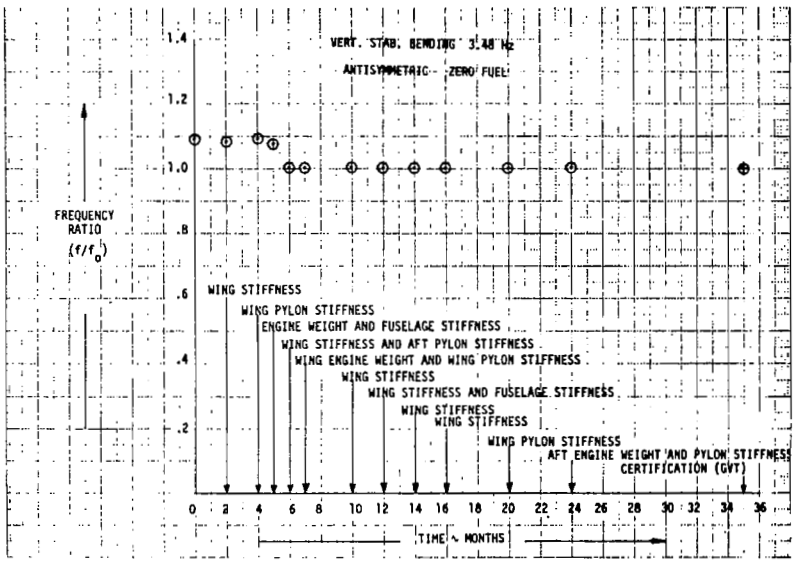

FIGURE 50. EVOLUTION OF FREQUENCY RATIO

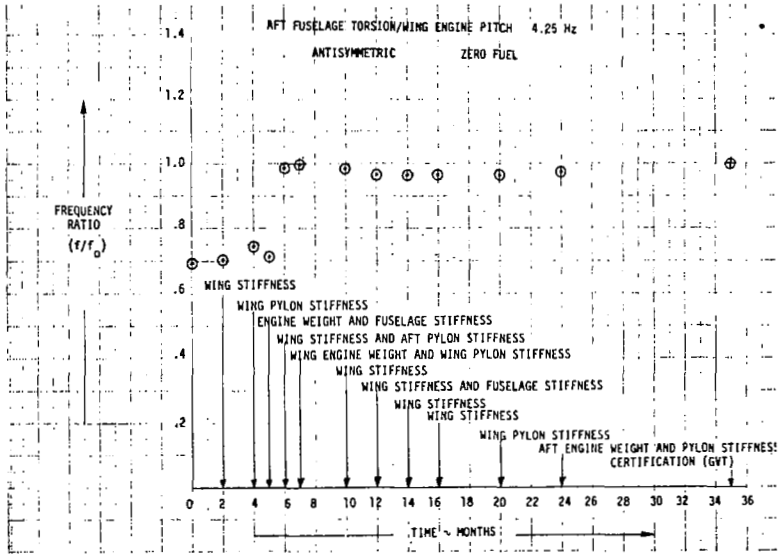

FIGURE 51. EVOLUTION OF FREQUENCY RATIO

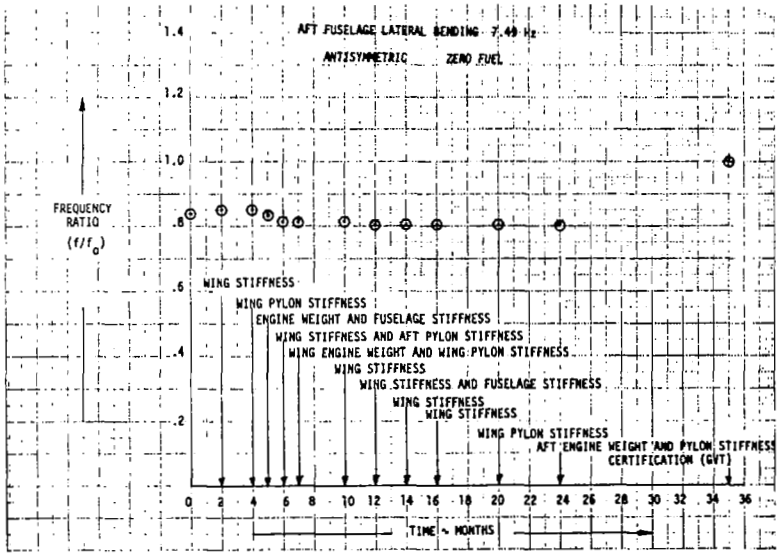

FIGURE 52. EVOLUTION OF FREQUENCY RATIO

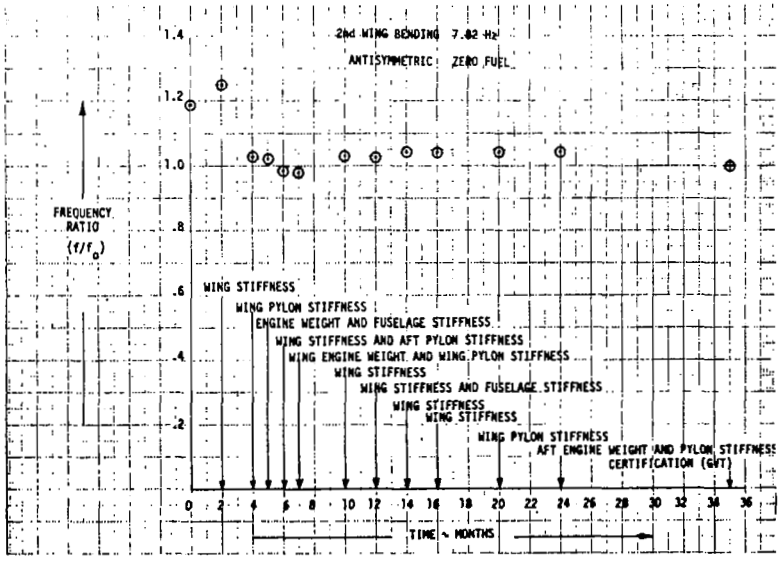

FIGURE 53. EVOLUTION OF FREQUENCY RATIO

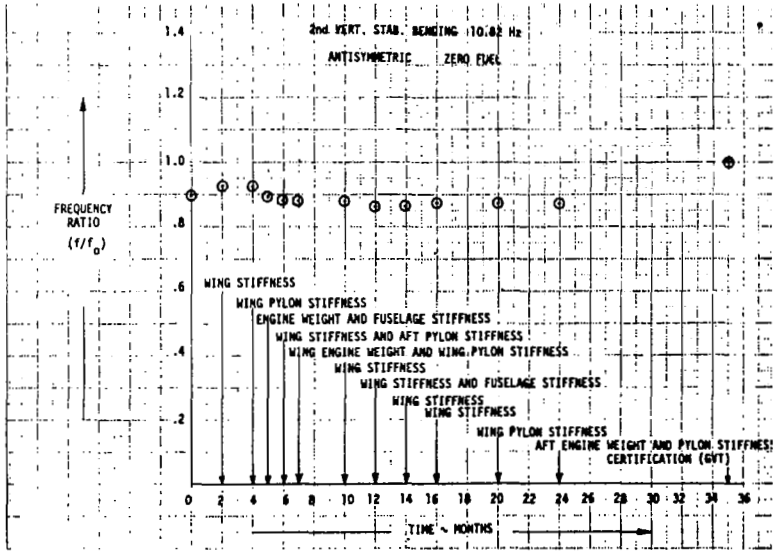

FIGURE 54. EVOLUTION OF FREQUENCY RATIO

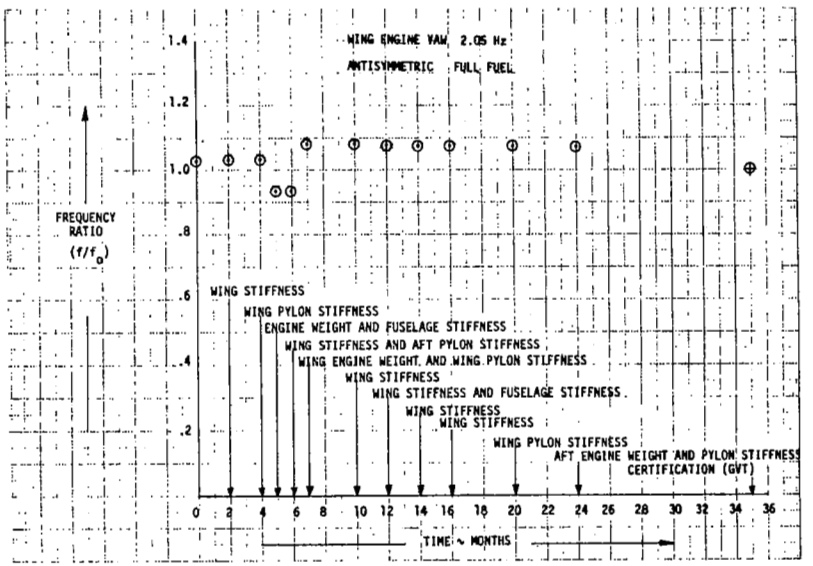

FIGURE 55. EVOLUTION OF FREQUENCY RATIO

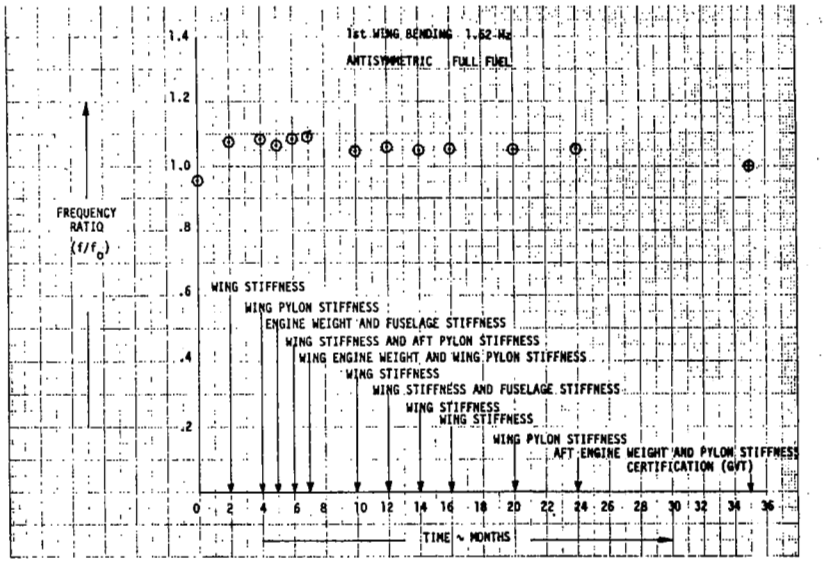

FIGURE 56. EVOLUTION OF FREQUENCY RATIO

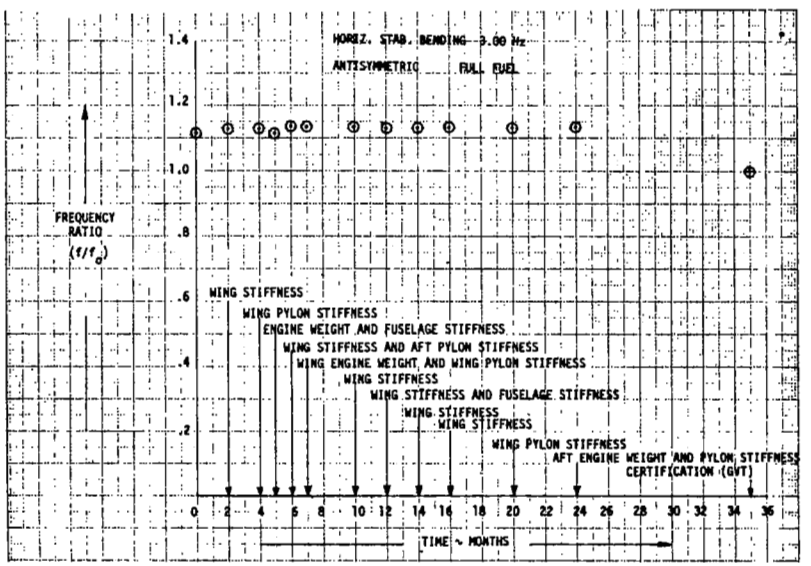

FIGURE 57. EVOLUTION OF FREQUENCY RATIO

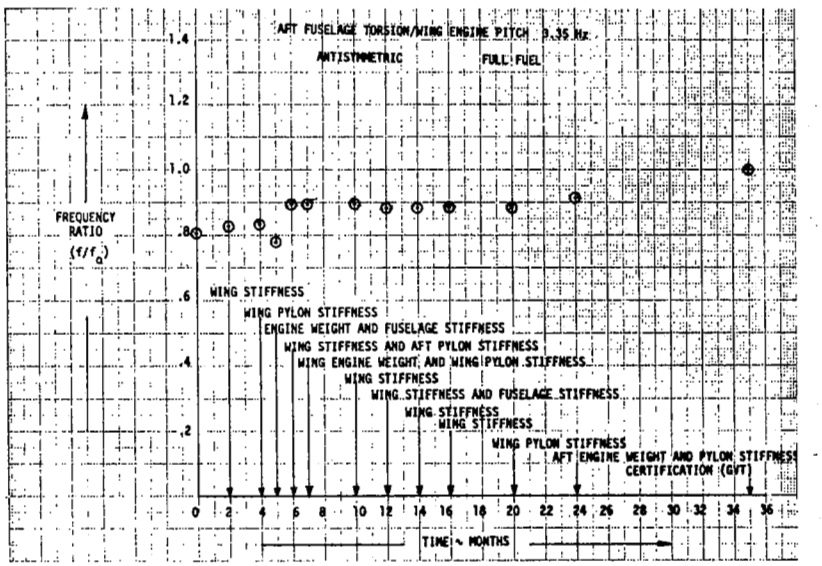

FIGURE 58. EVOLUTION OF FREQUENCY RATIO

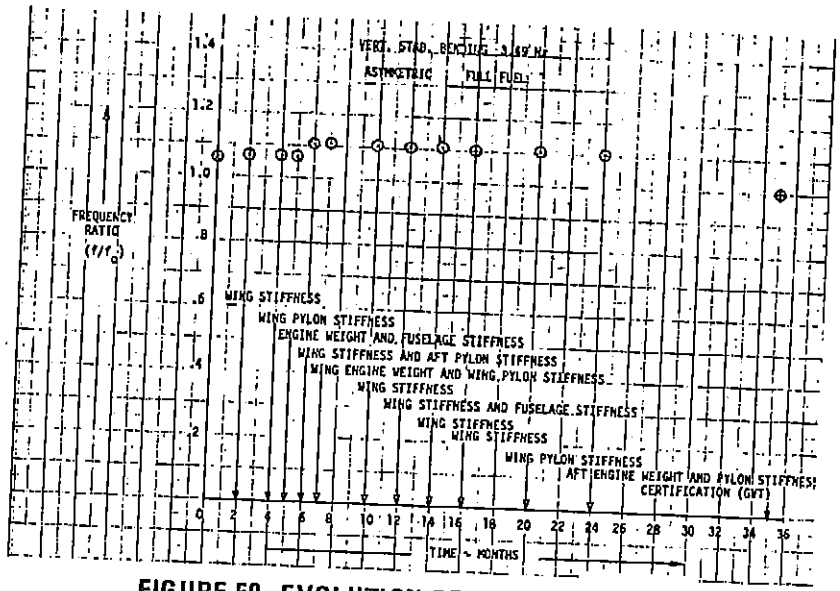

FIGURE 59. EVOLUTION OF FREQUENCY RATIO

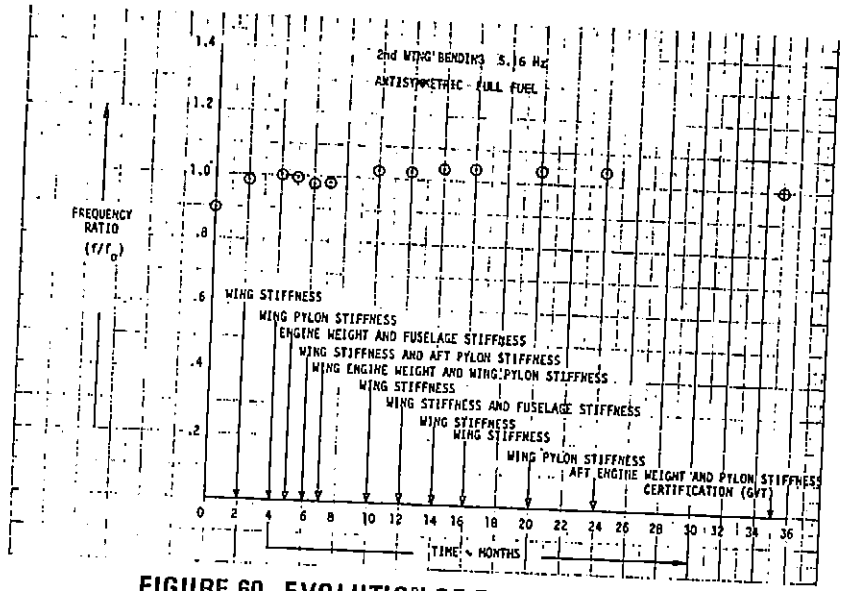

FIGURE 60. EVOLUTION OF FREQUENCY RATIO

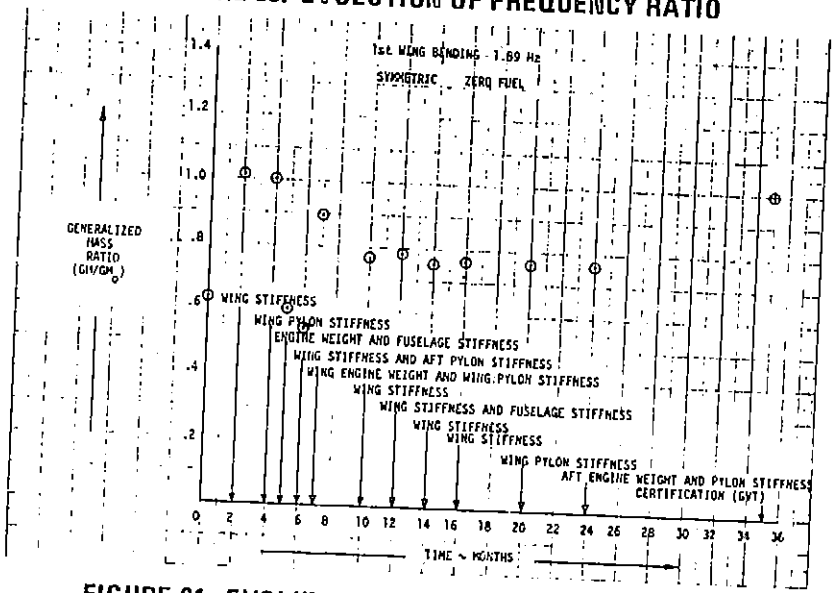

FIGURE 61. EVOLUTION OF GENERALIZED MASS RATIO

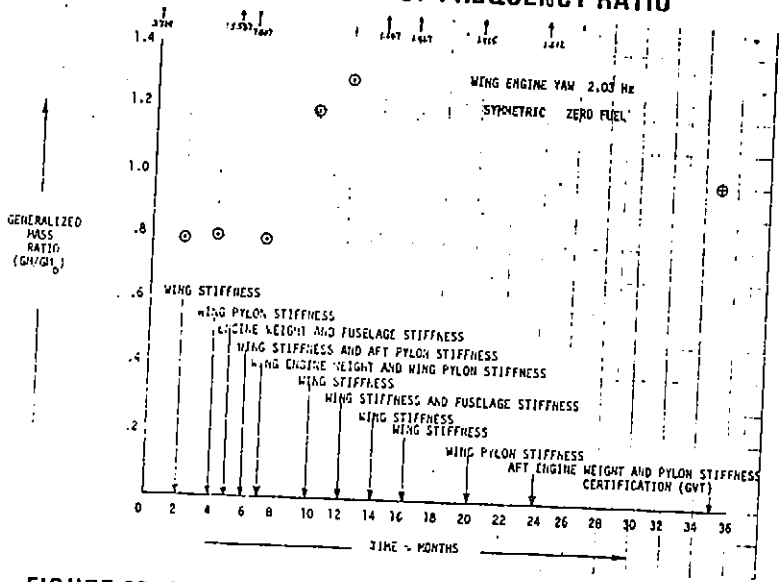

FIGURE 62. EVOLUTION OF GENERALIZED MASS RATIO

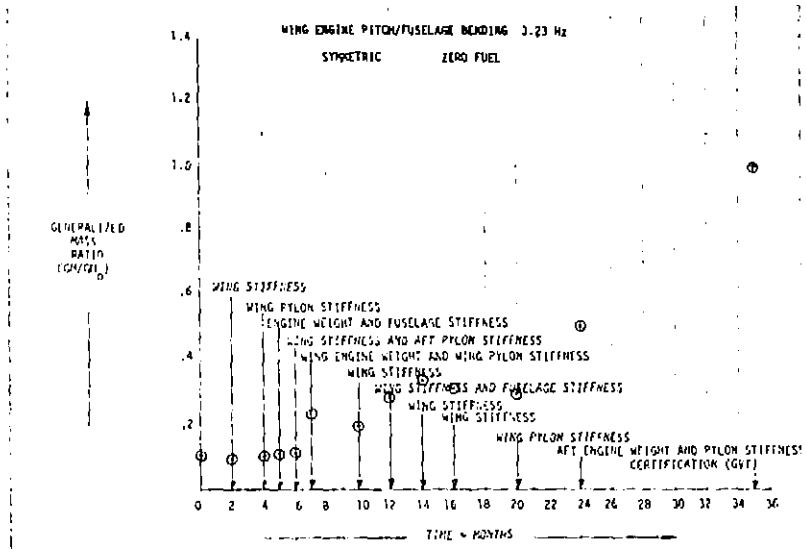

FIGURE 63. EVOLUTION OF GENERALIZED MASS RATIO

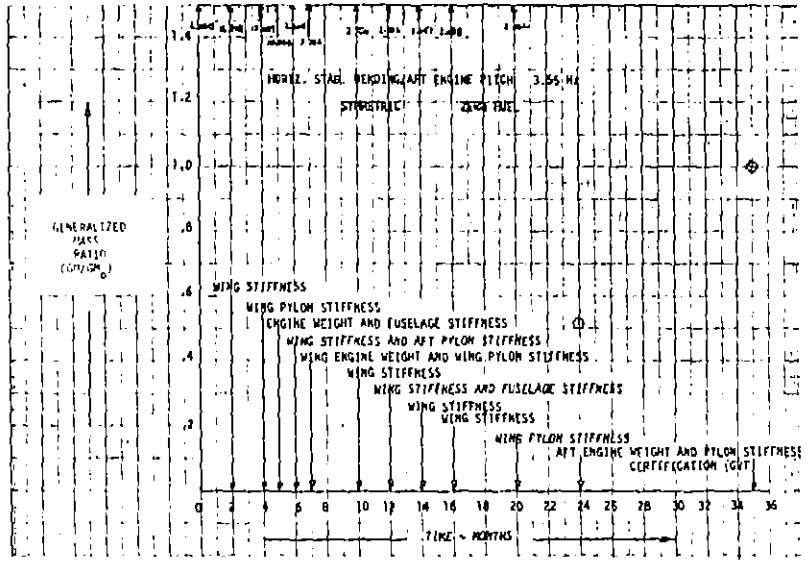

FIGURE 64. EVOLUTION OF GENERALIZED MASS RATIO

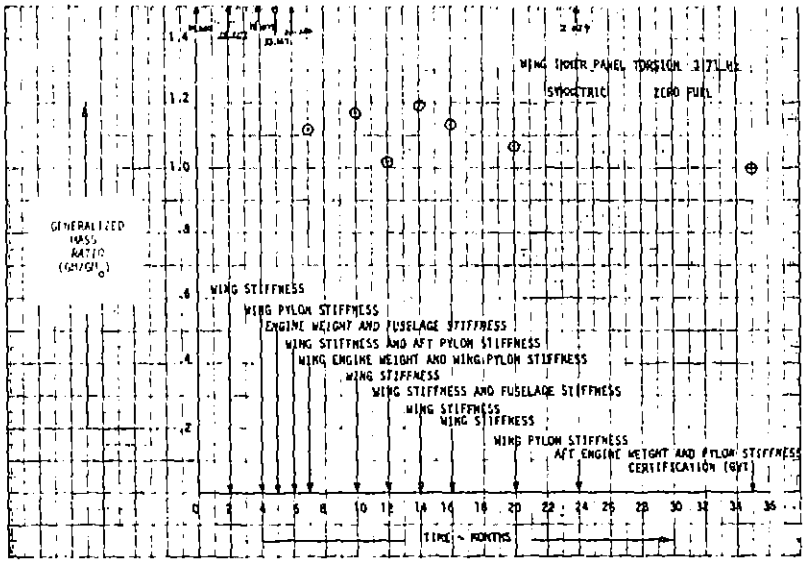

FIGURE 65. EVOLUTION OF GENERALIZED MASS RATIO

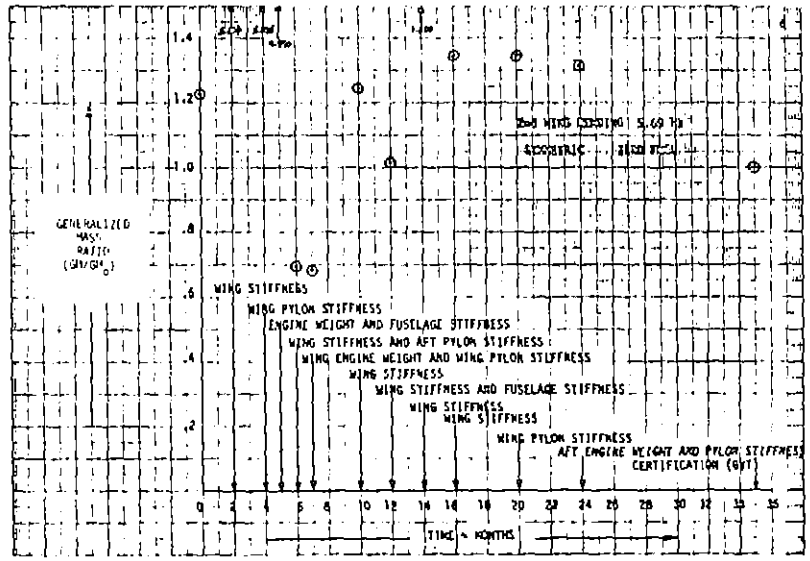

FIGURE 66. EVOLUTION OF GENERALIZED MASS RATIO

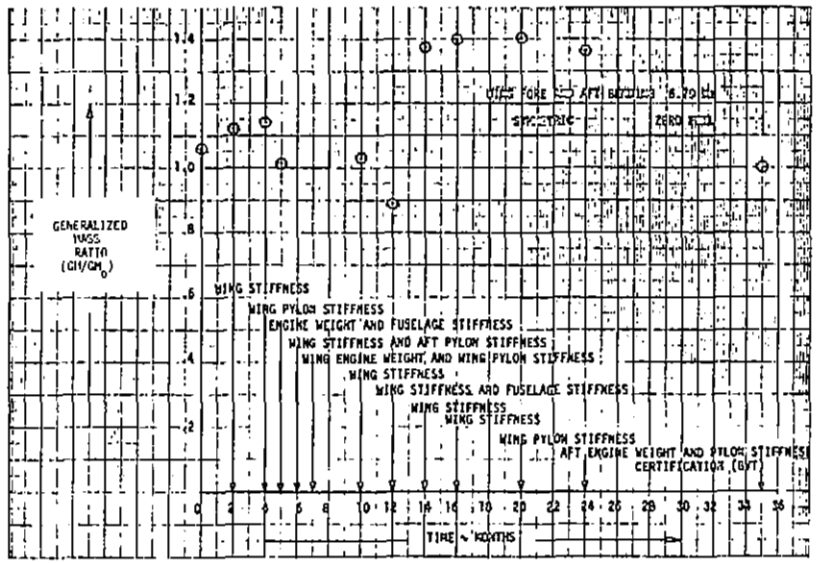

FIGURE 67. EVOLUTION OF GENERALIZED MASS RATIO

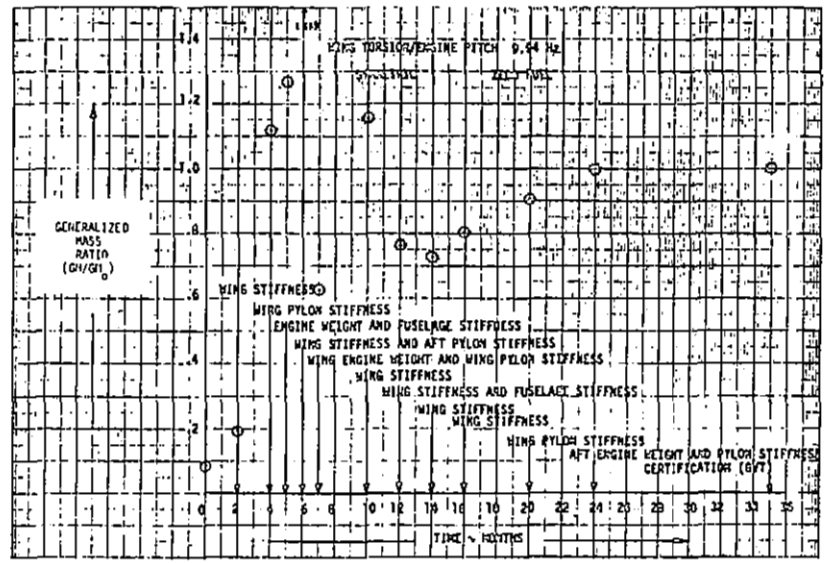

FIGURE 68. EVOLUTION OF GENERALIZED MASS RATIO

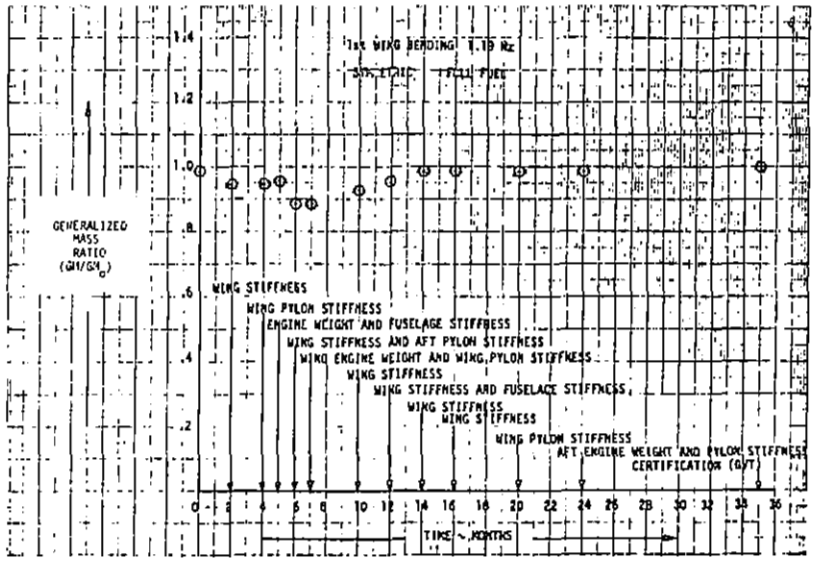

FIGURE 69. EVOLUTION OF GENERALIZED MASS RATIO

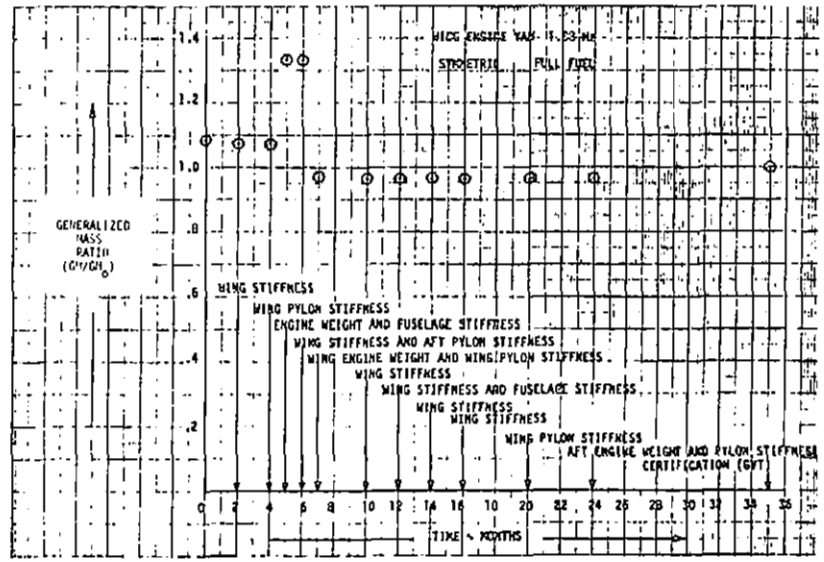

FIGURE 70. EVOLUTION OF GENERALIZED MASS RATIO

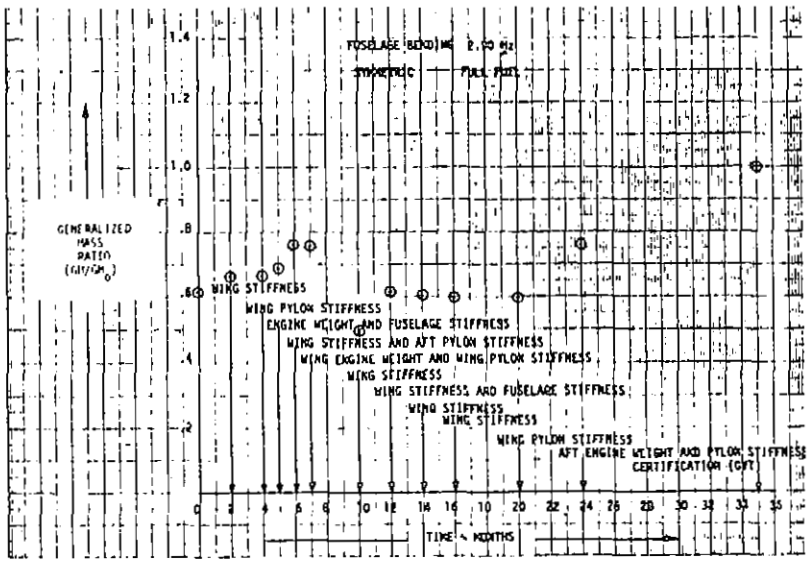

FIGURE 71. EVOLUTION OF GENERALIZED MASS RATIO

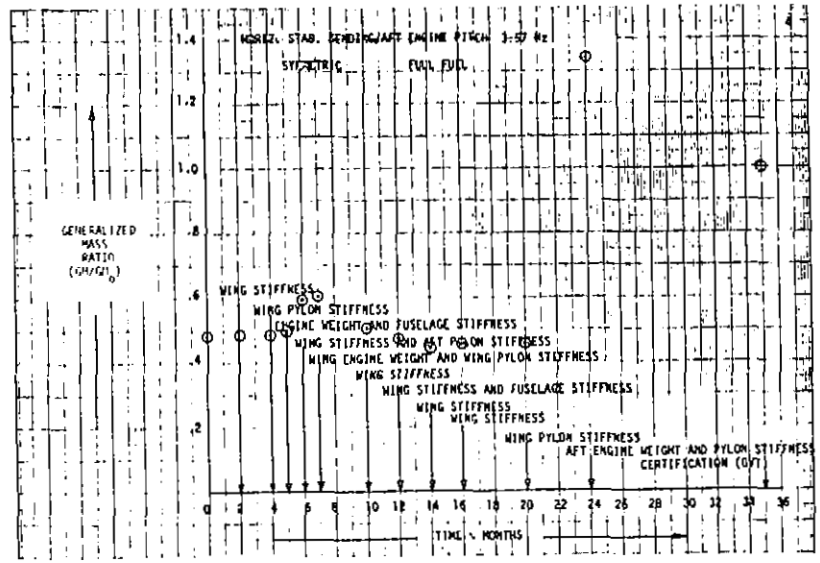

FIGURE 72. EVOLUTION OF GENERALIZED MASS RATIO

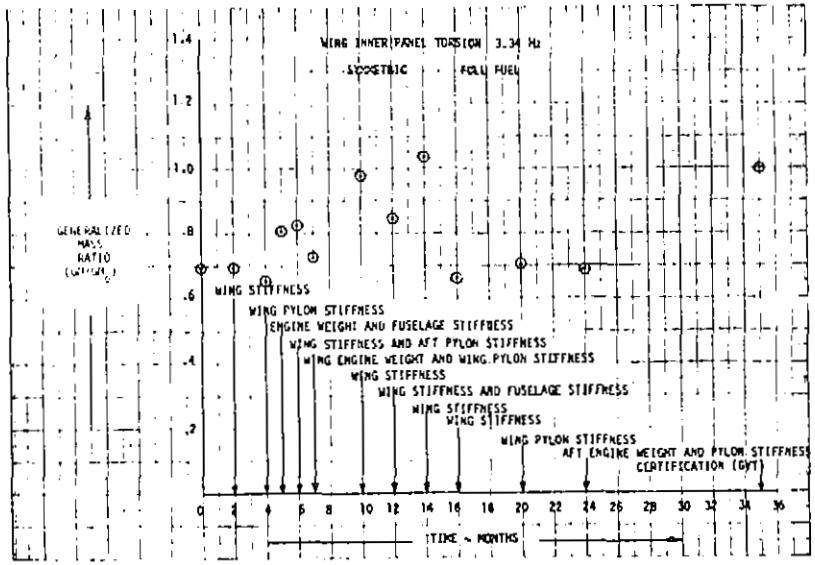

FIGURE 73. EVOLUTION OF GENERALIZED MASS RATIO

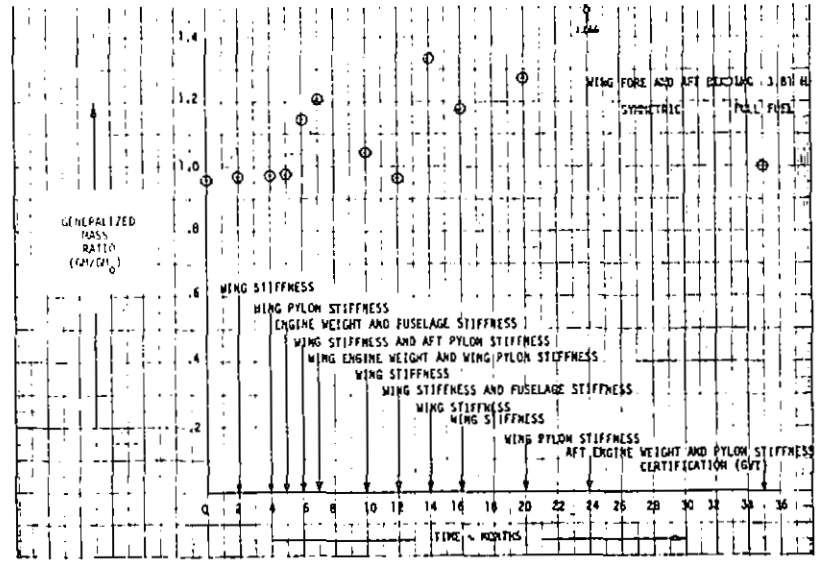

FIGURE 74. EVOLUTION OF GENERALIZED MASS RATIO

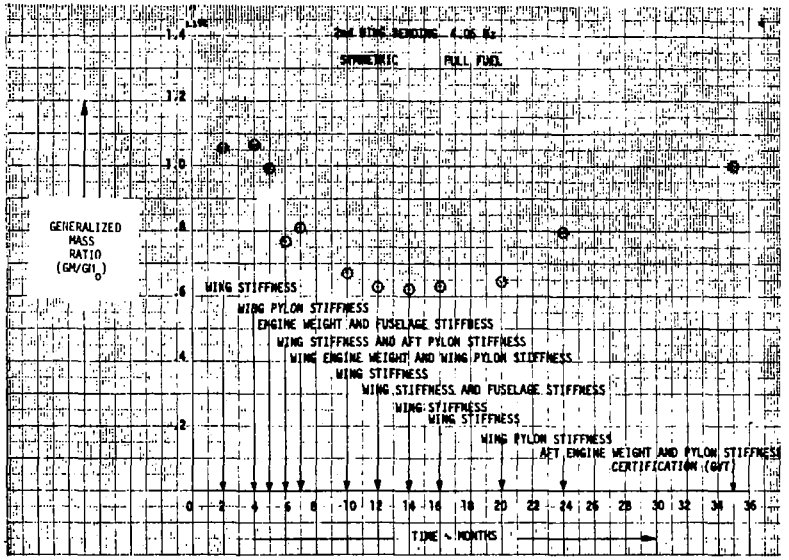

FIGURE 75. EVOLUTION OF GENERALIZED MASS RATIO

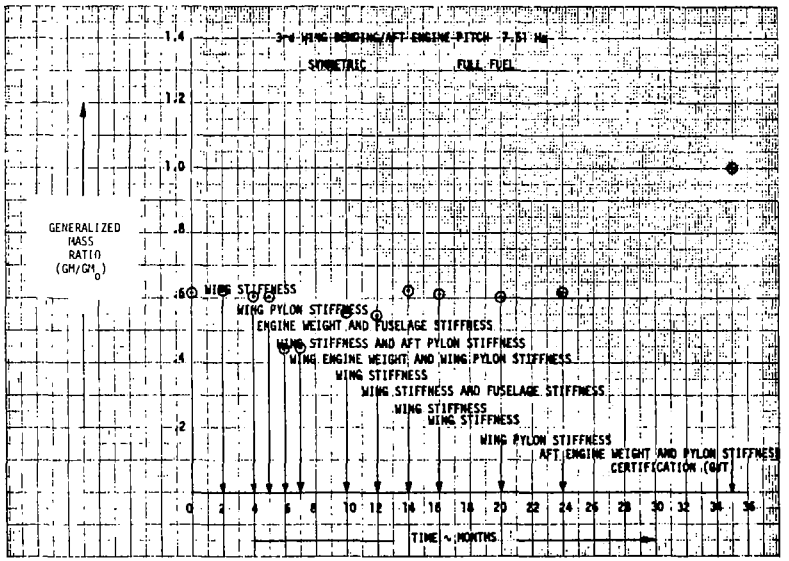

FIGURE 76. EVOLUTION OF GENERALIZED MASS RATIO

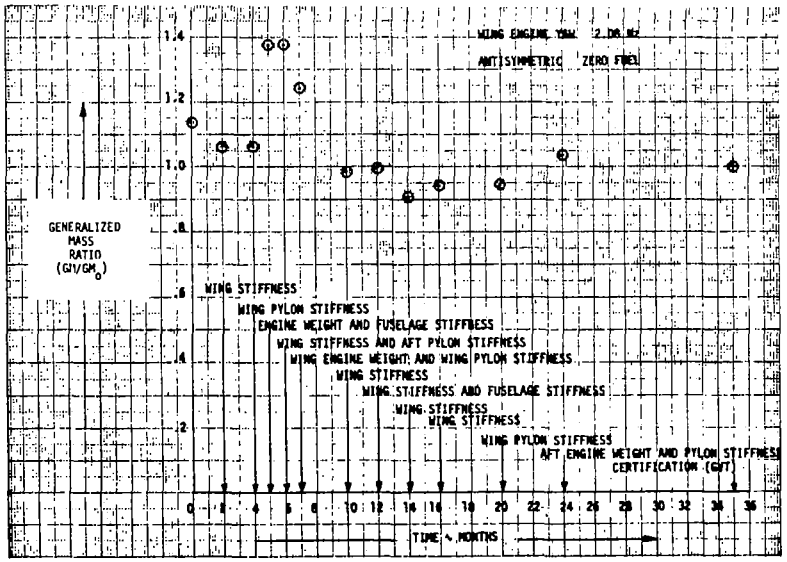

FIGURE 77. EVOLUTION OF GENERALIZED MASS RATIO

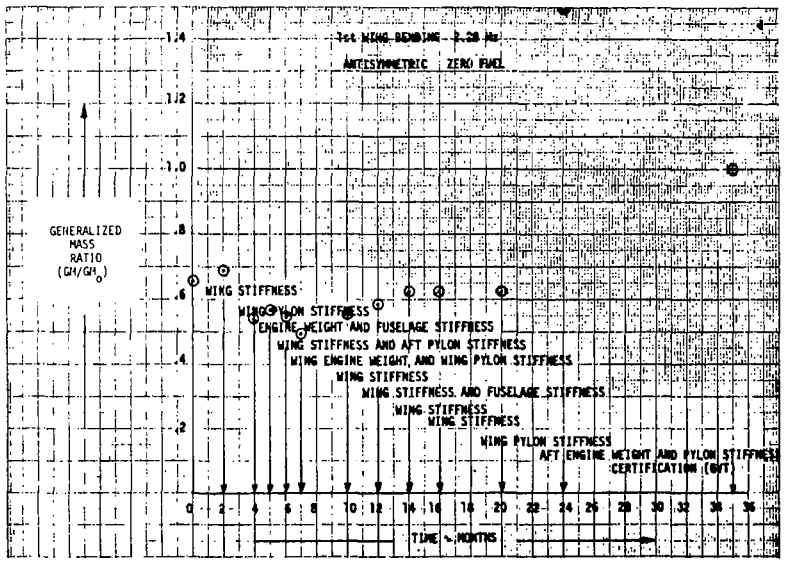

FIGURE 78. EVOLUTION OF GENERALIZED MASS RATIO

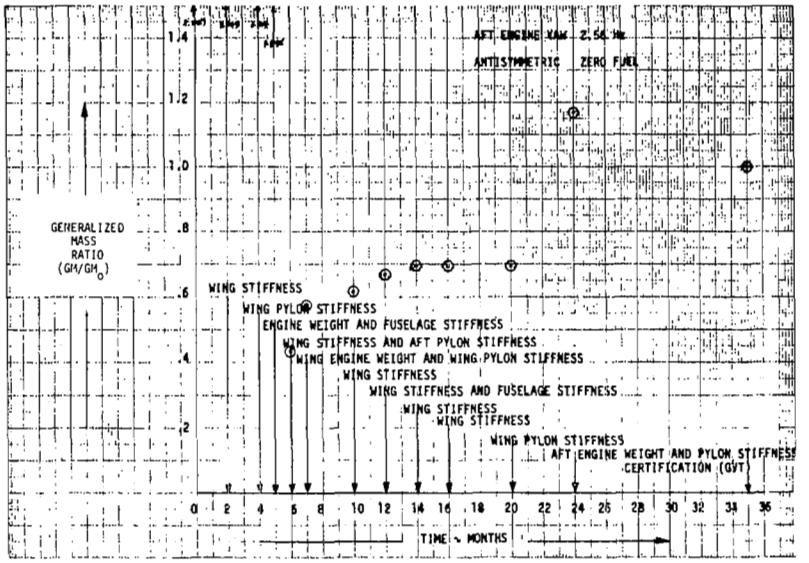

FIGURE 79. EVOLUTION OF GENERALIZED MASS RATIO

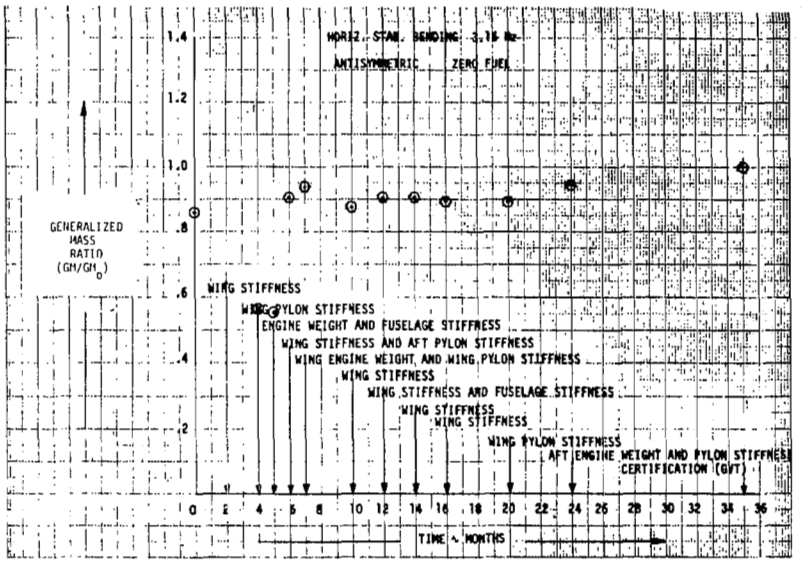

FIGURE 80. EVOLUTION OF GENERALIZED MASS RATIO

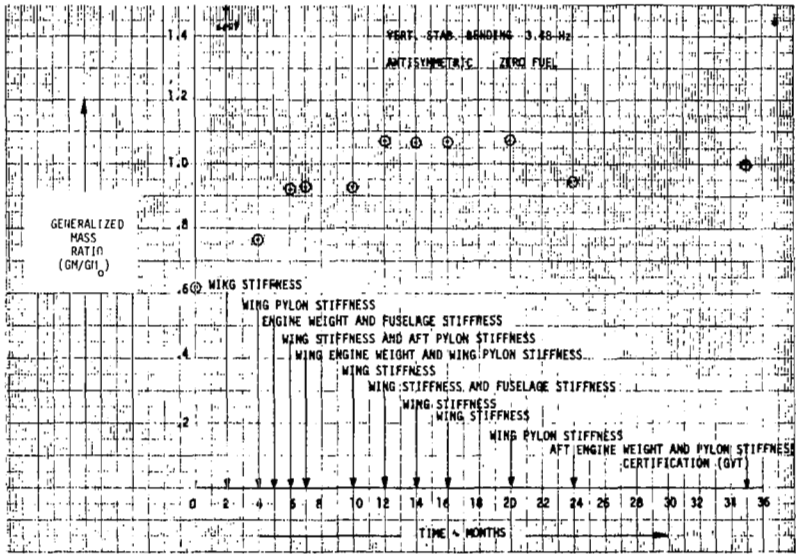

FIGURE 81. EVOLUTION OF GENERALIZED MASS RATIO

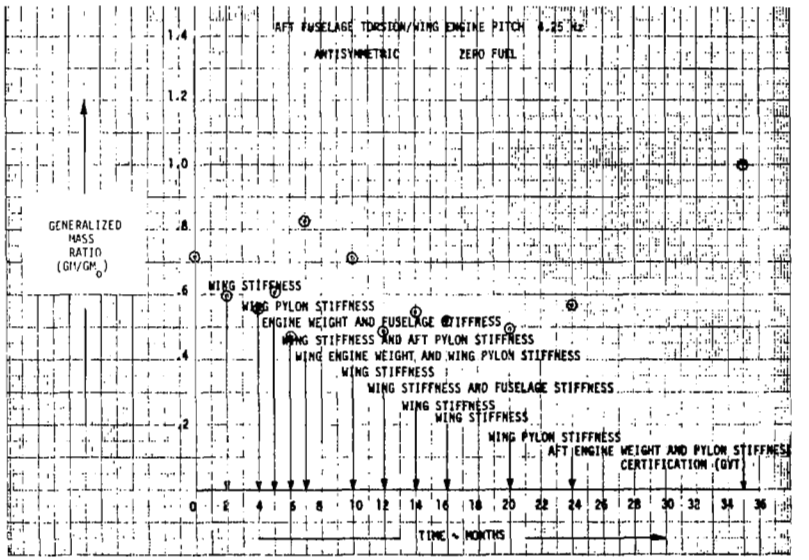

FIGURE 82. EVOLUTION OF GENERALIZED MASS RATIO

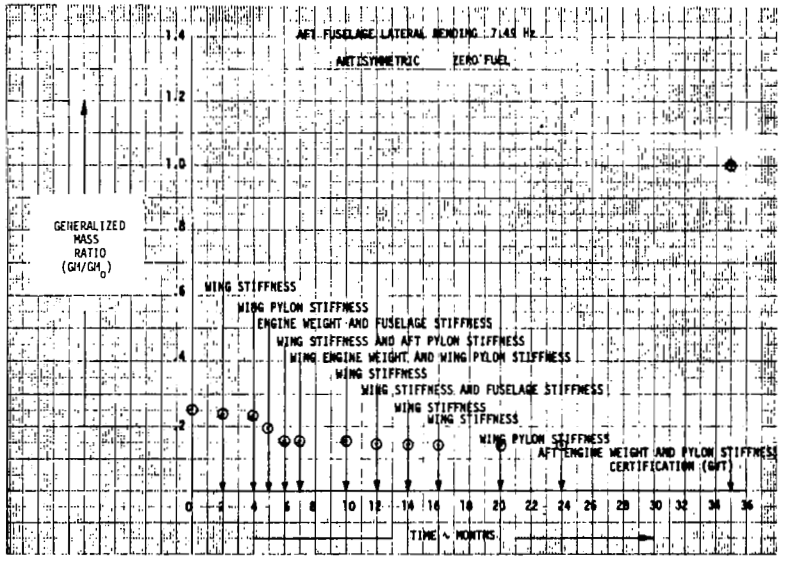

FIGURE 83. EVOLUTION OF GENERALIZED MASS RATIO

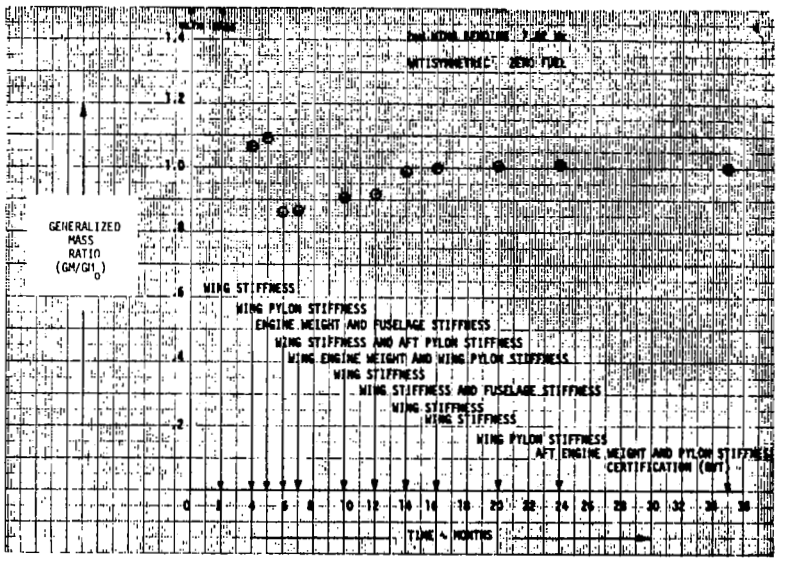

FIGURE 84. EVOLUTION OF GENERALIZED MASS RATIO

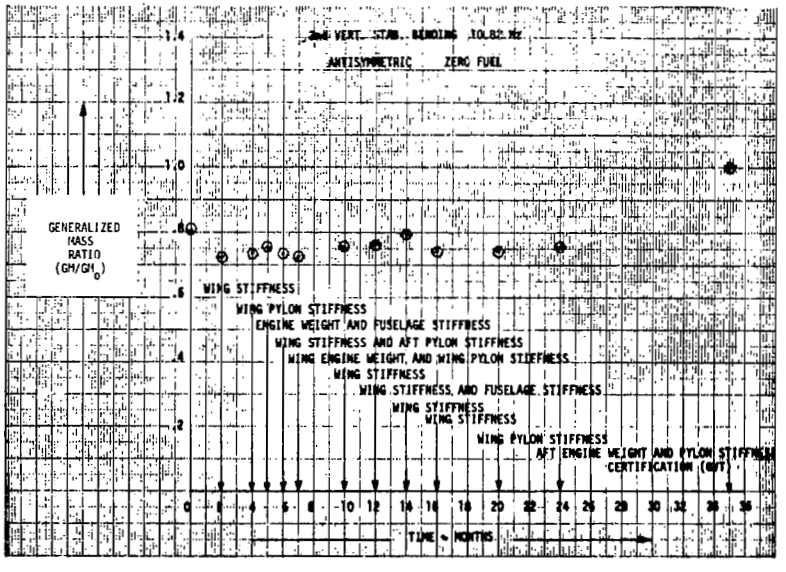

FIGURE 85. EVOLUTION OF GENERALIZED MASS RATIO

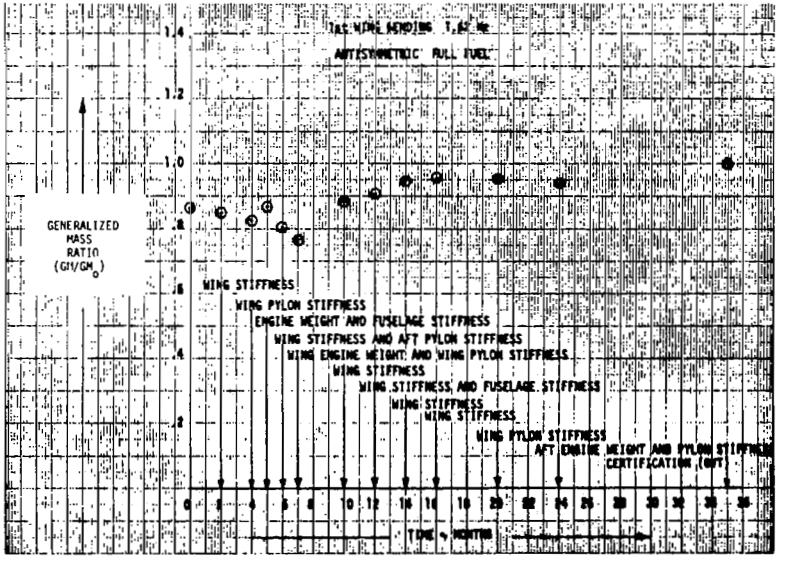

FIGURE 86. EVOLUTION OF GENERALIZED MASS RATIO

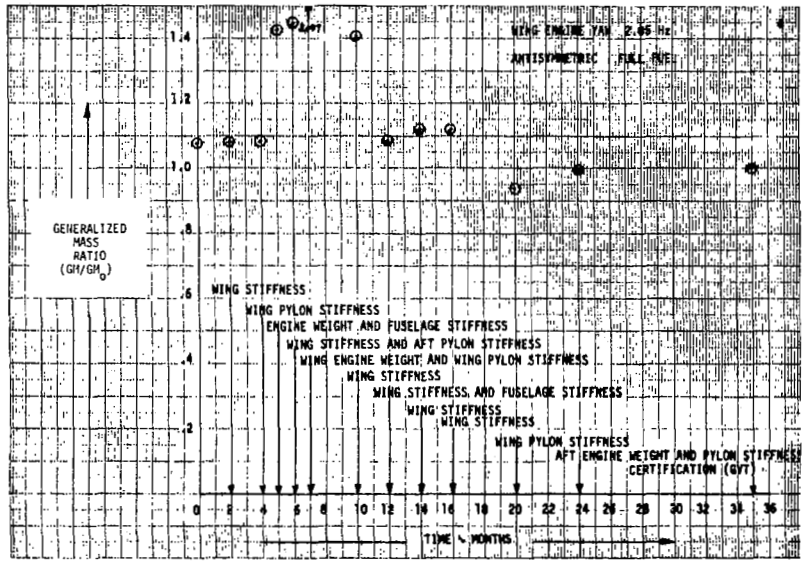

FIGURE 87. EVOLUTION OF GENERALIZED MASS RATIO

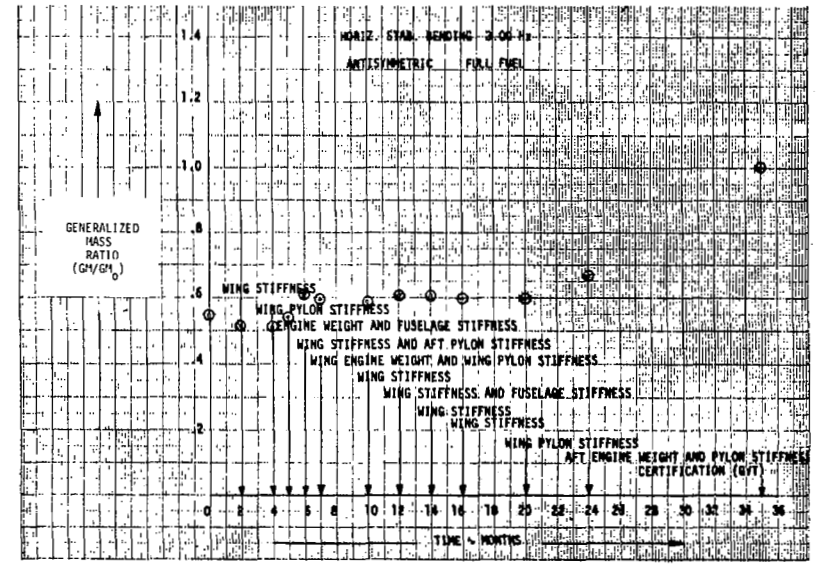

FIGURE 88. EVOLUTION OF GENERALIZED MASS RATIO

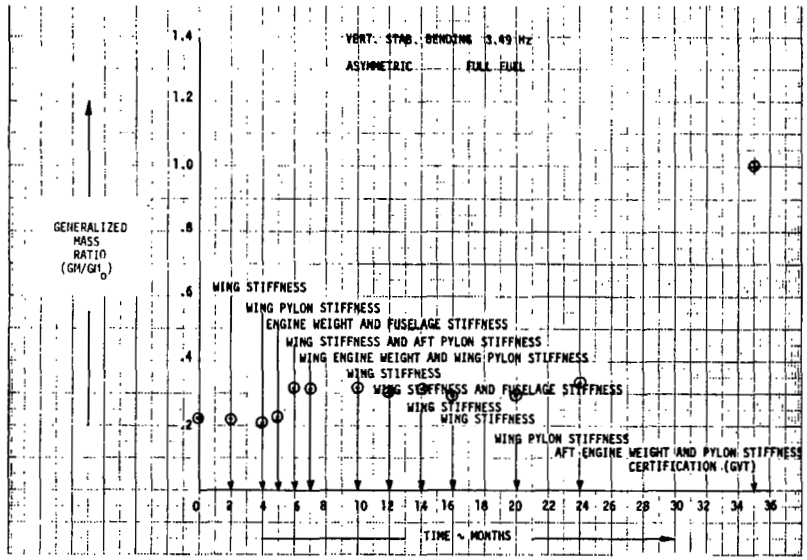

FIGURE 89. EVOLUTION OF GENERALIZED MASS RATIO

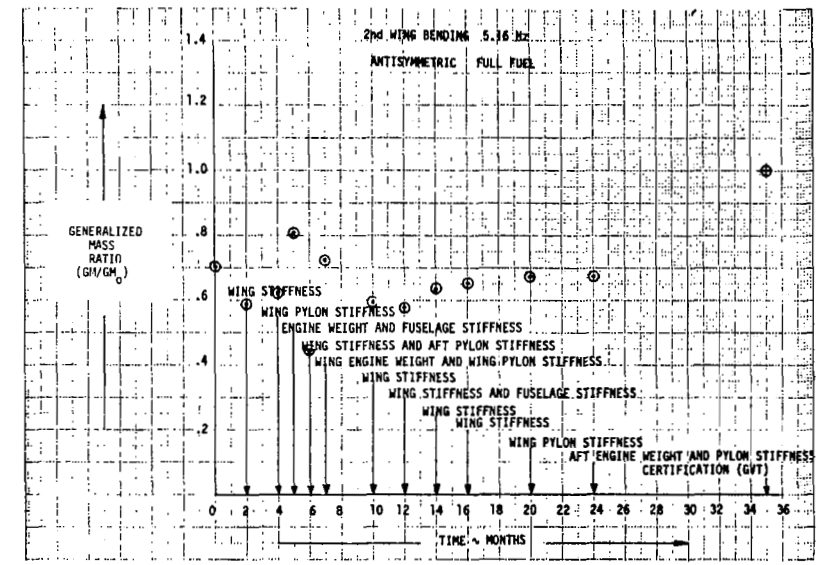

FIGURE 90. EVOLUTION OF GENERALIZED MASS RATIO

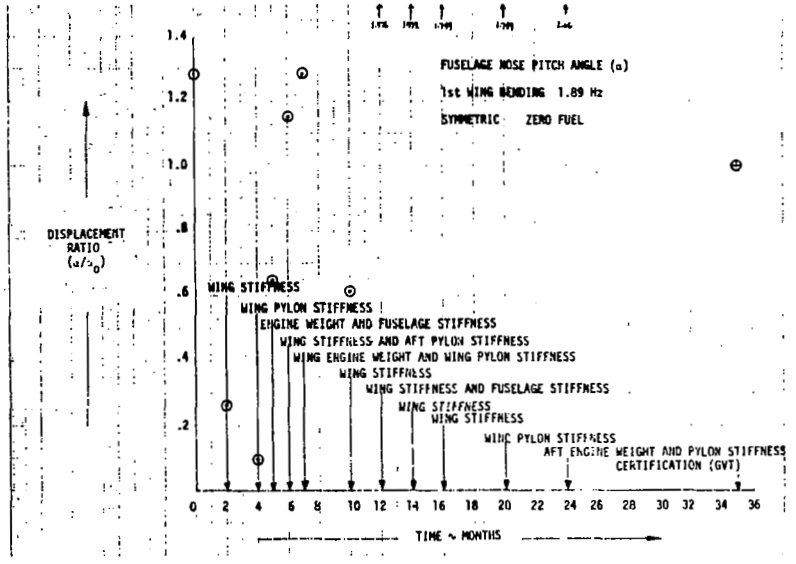

FIGURE 91. EVOLUTION OF DISPLACEMENT RATIO α

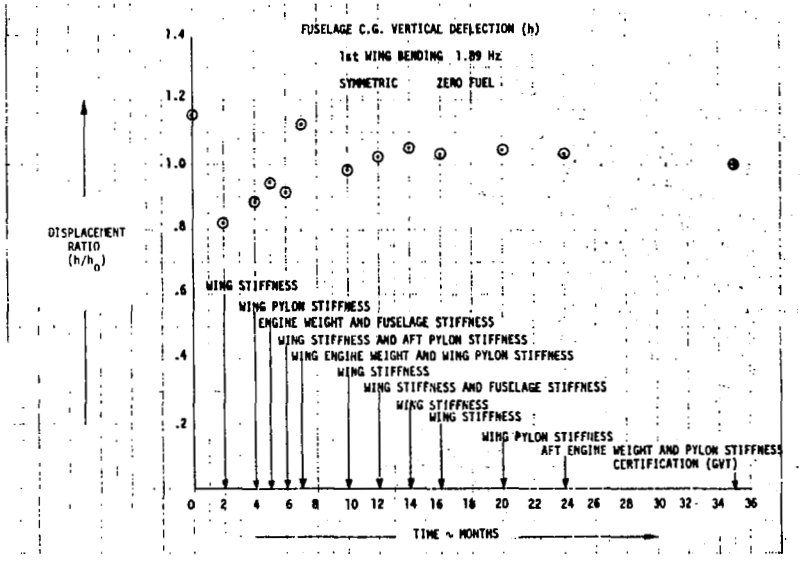

FIGURE 92. EVOLUTION OF DISPLACEMENT RATIO h

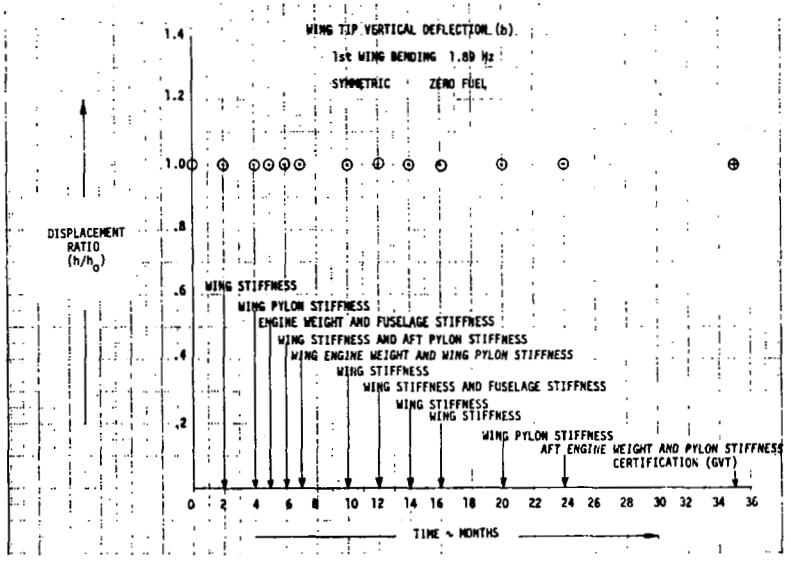

FIGURE 93. EVOLUTION OF DISPLACEMENT RATIO h

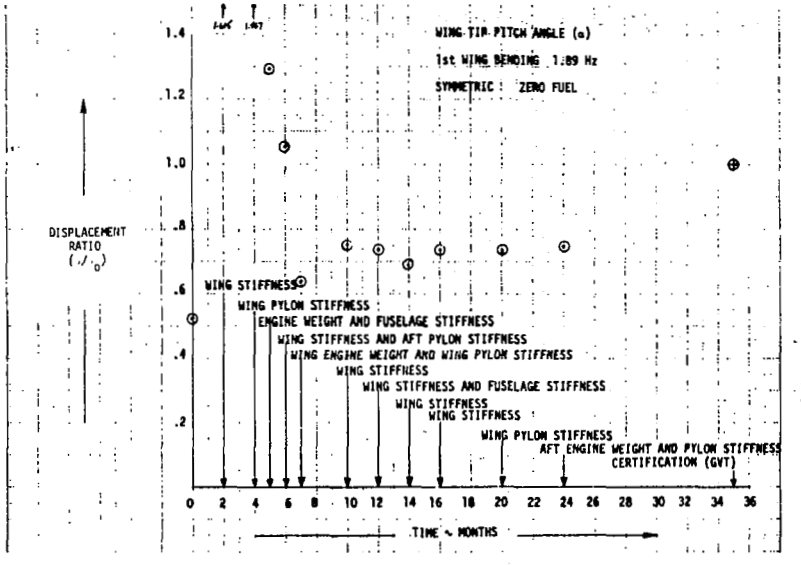

FIGURE 94. EVOLUTION OF DISPLACEMENT RATIO α

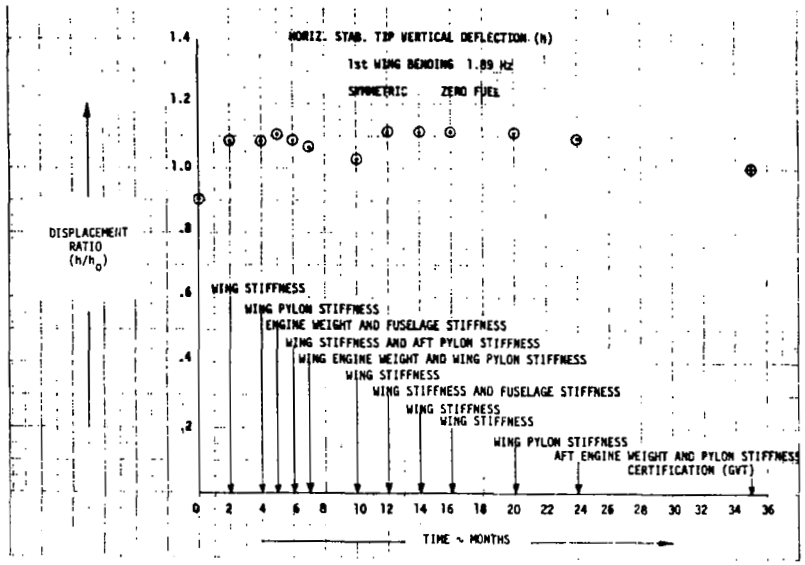

FIGURE 95. EVOLUTION OF DISPLACEMENT RATIO h

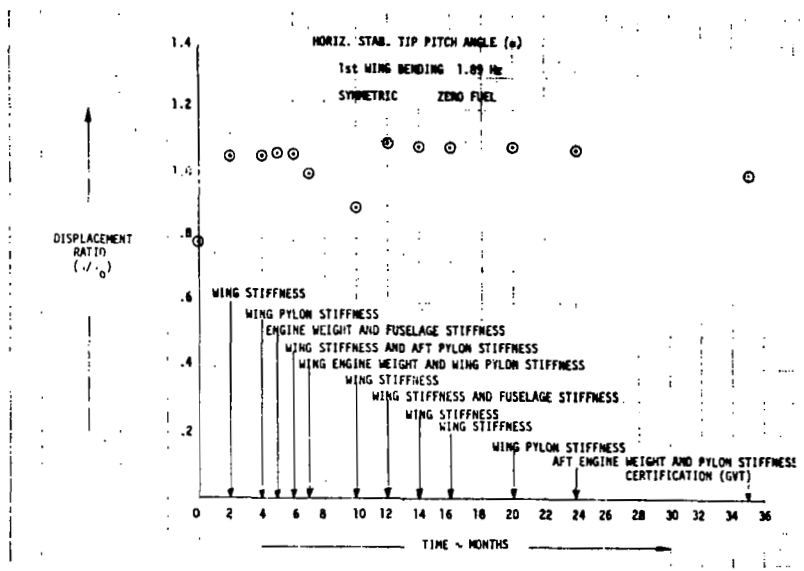

FIGURE 96. EVOLUTION OF DISPLACEMENT RATIO α

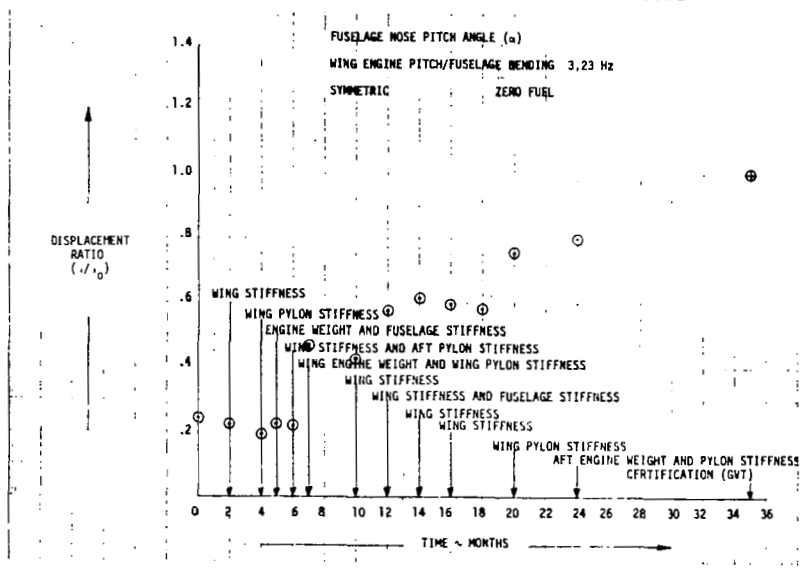

FIGURE 97. EVOLUTION OF DISPLACEMENT RATIO α

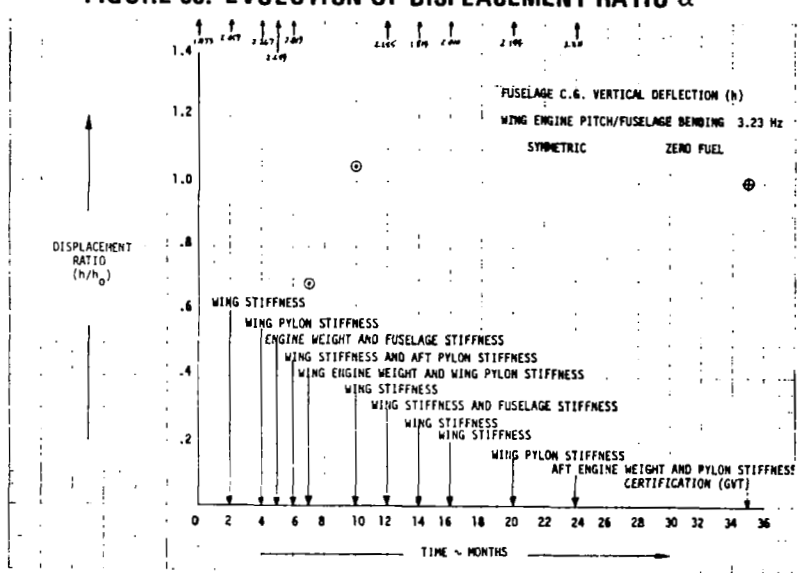

FIGURE 98. EVOLUTION OF DISPLACEMENT RATIO h

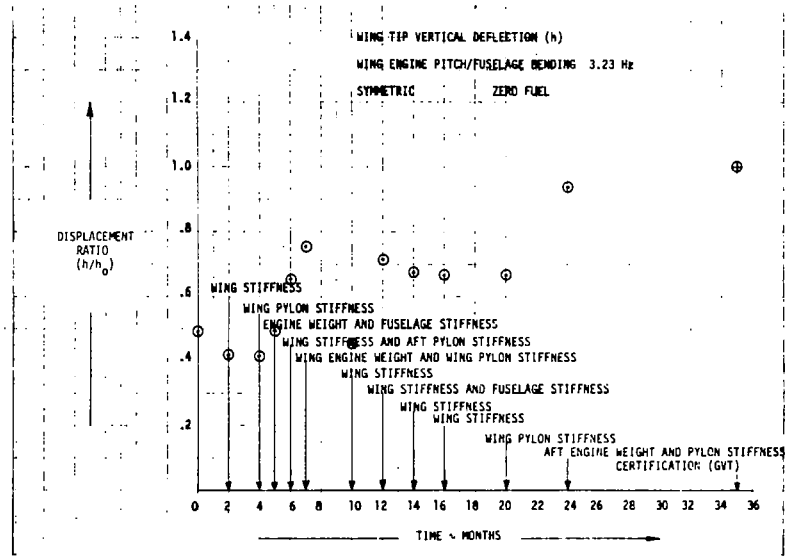

FIGURE 99. EVOLUTION OF DISPLACEMENT RATIO h

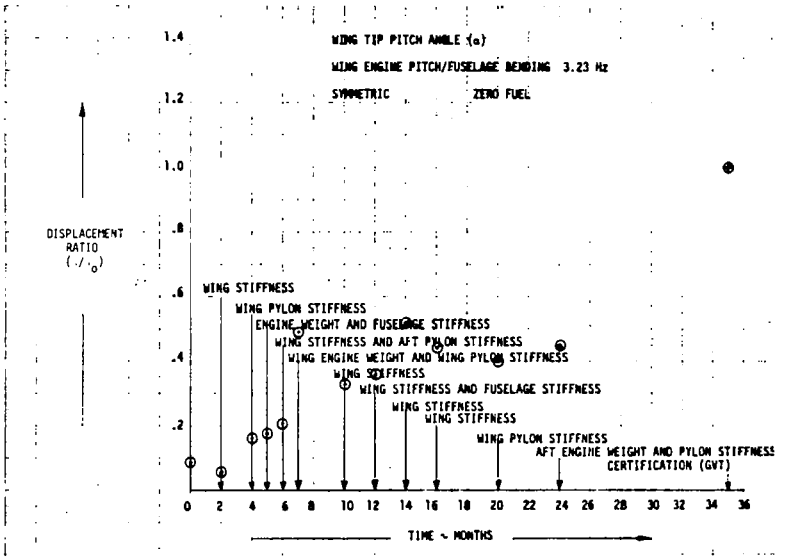

FIGURE 100. EVOLUTION OF DISPLACEMENT RATIO α

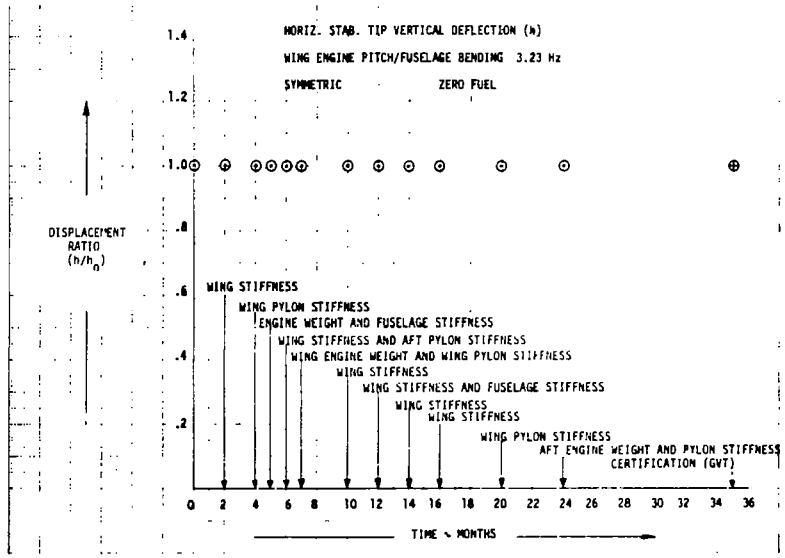

FIGURE 101. EVOLUTION OF DISPLACEMENT RATIO h

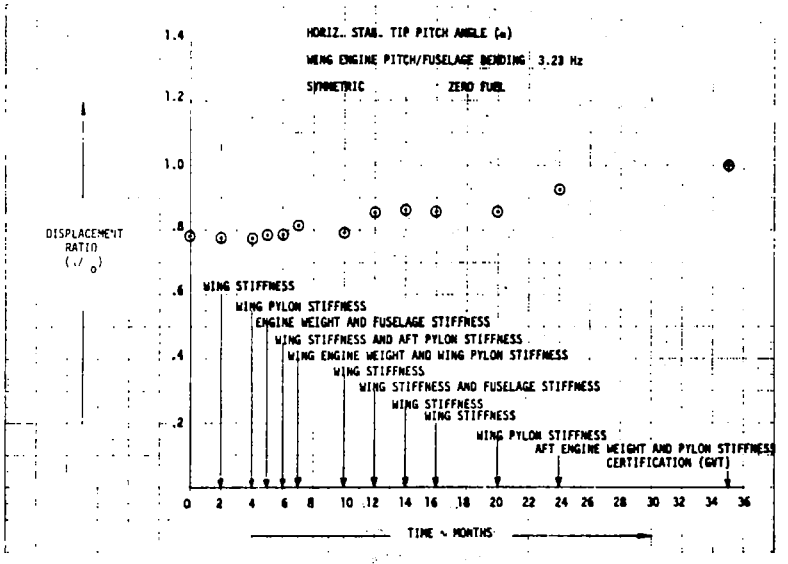

FIGURE 102. EVOLUTION OF DISPLACEMENT RATIO α

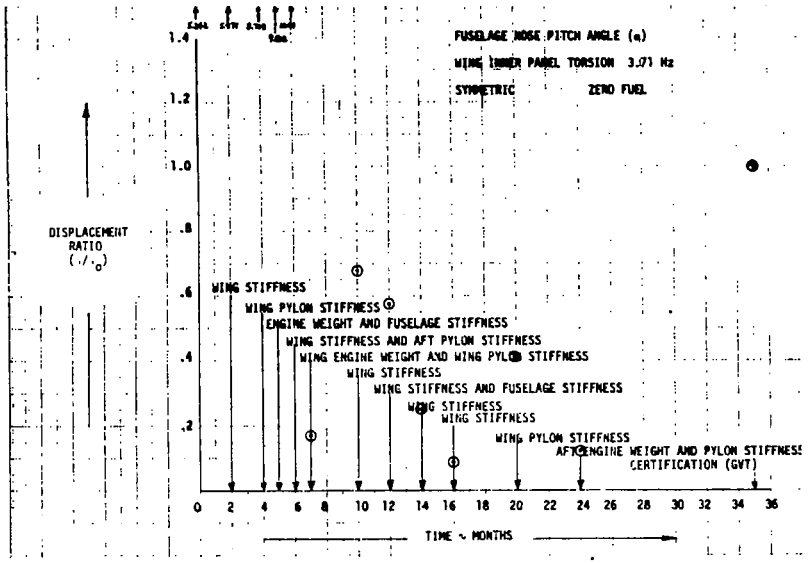

FIGURE 103. EVOLUTION OF DISPLACEMENT RATIO α

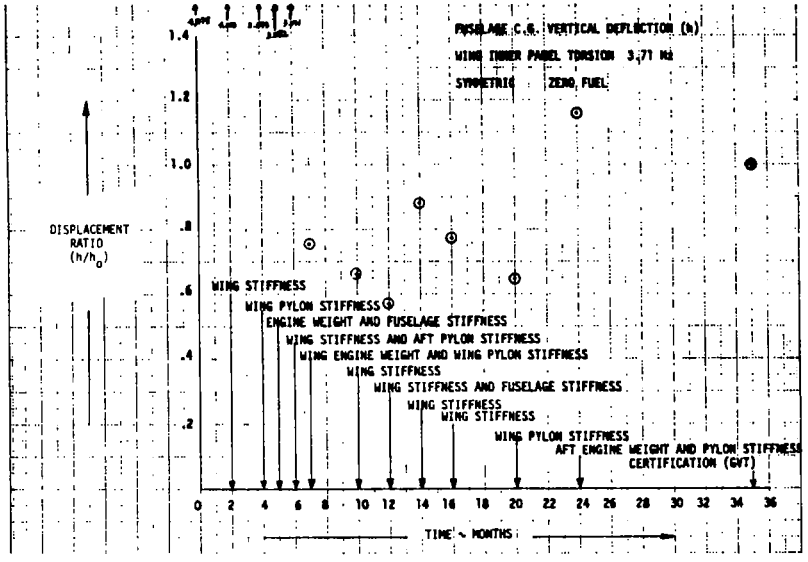

FIGURE 104. EVOLUTION OF DISPLACEMENT RATIO h

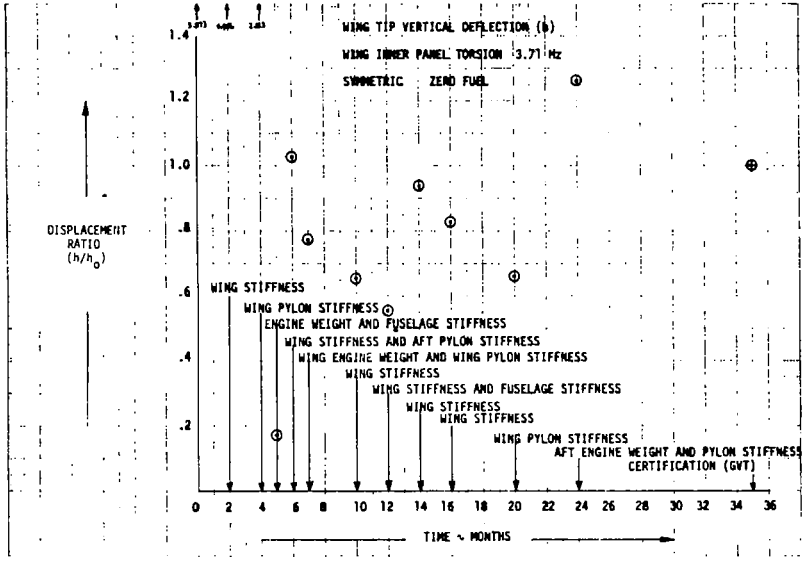

FIGURE 105. EVOLUTION OF DISPLACEMENT RATIO h

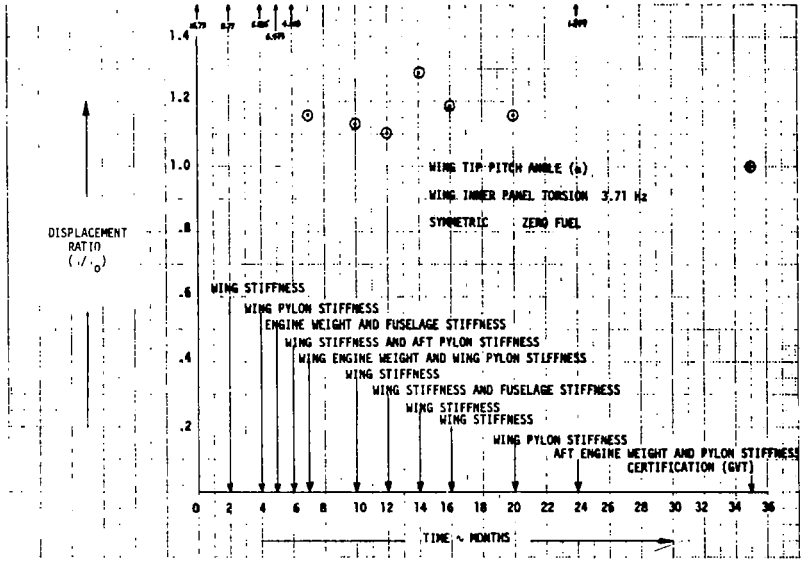

FIGURE 106. EVOLUTION OF DISPLACEMENT RATIO α

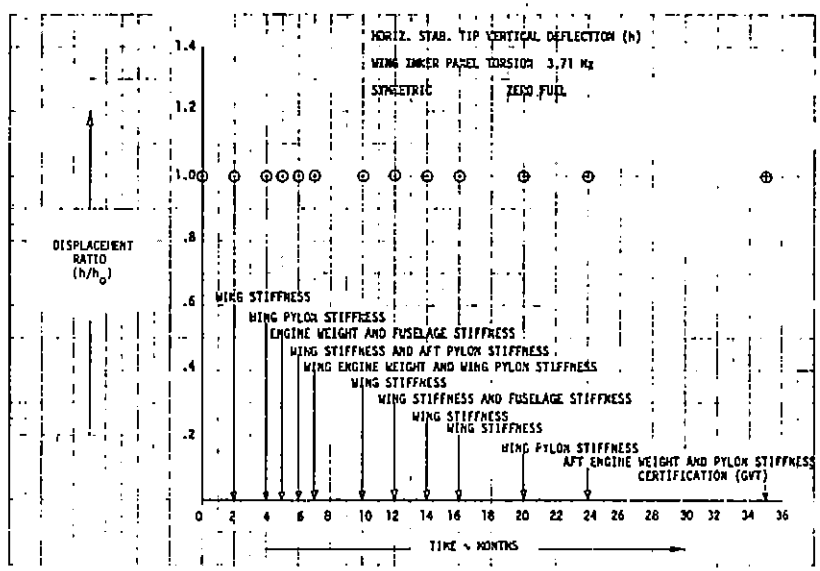

FIGURE 107. EVOLUTION OF DISPLACEMENT RATIO h

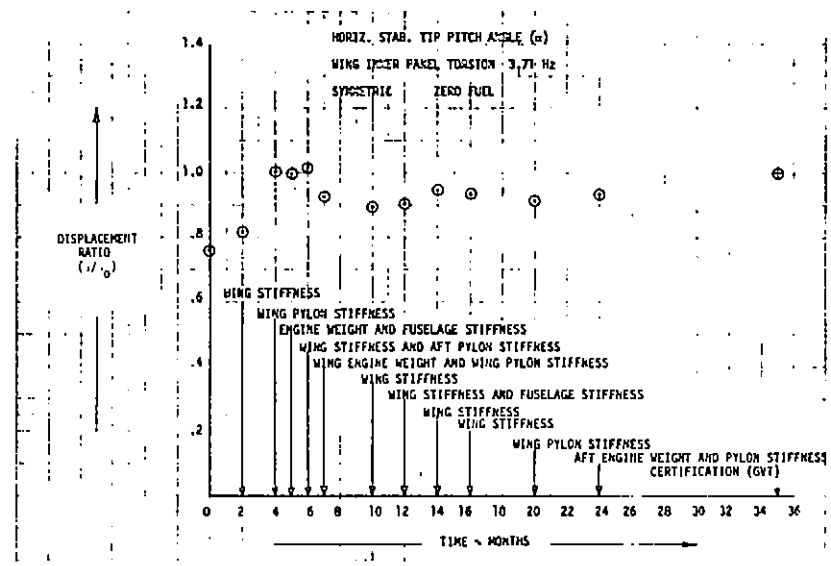

FIGURE 108. EVOLUTION OF DISPLACEMENT RATIO α

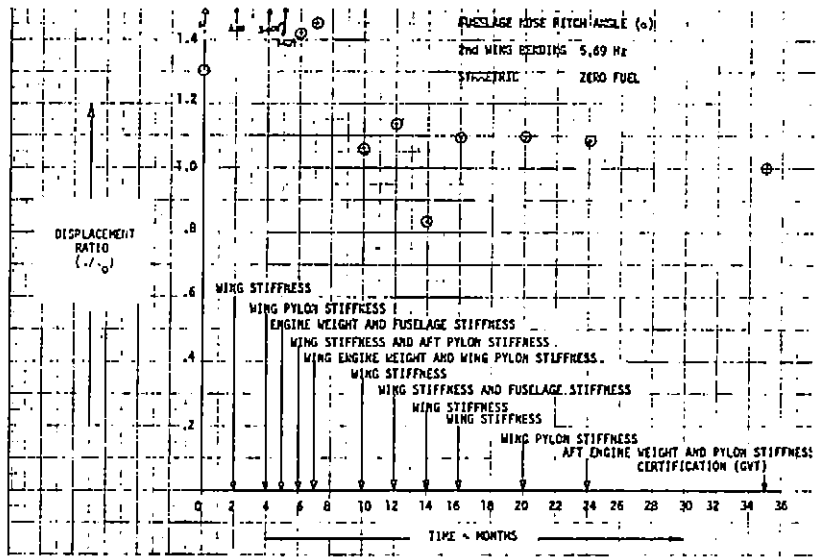

FIGURE 109. EVOLUTION OF DISPLACEMENT RATIO α

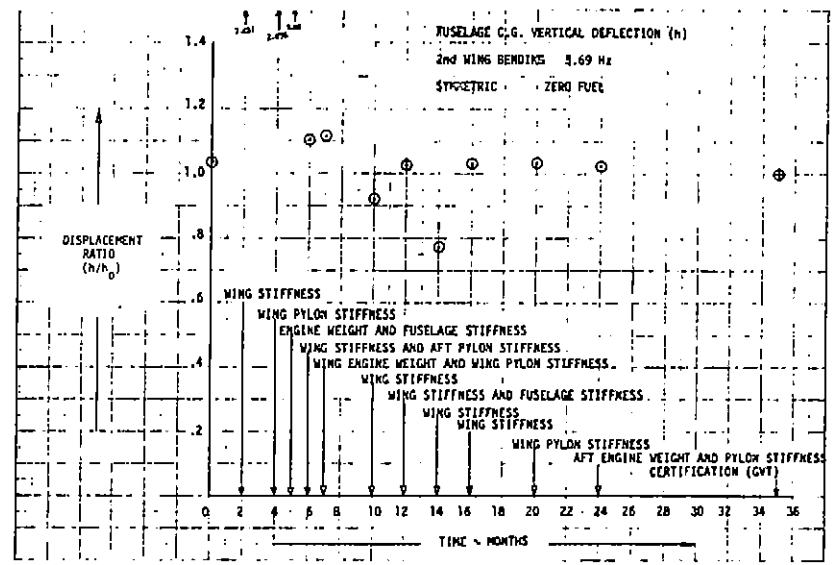

FIGURE 110. EVOLUTION OF DISPLACEMENT RATIO h

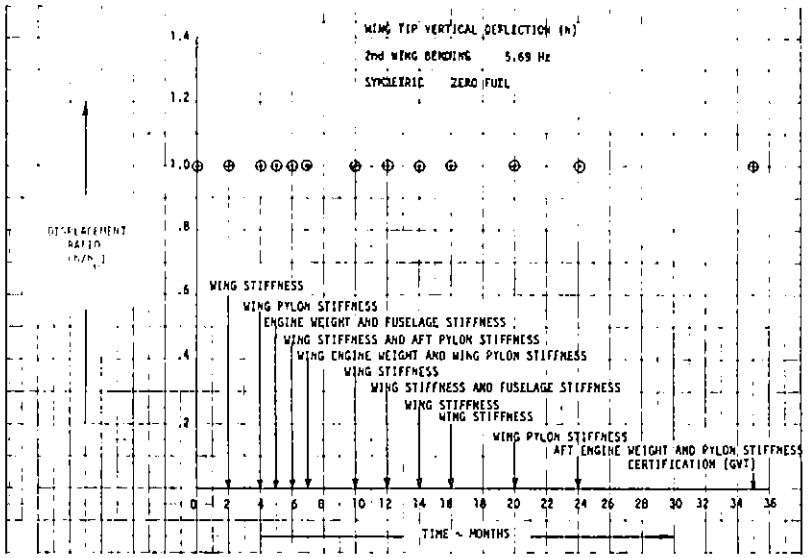

FIGURE 111. EVOLUTION OF DISPLACEMENT RATIO h

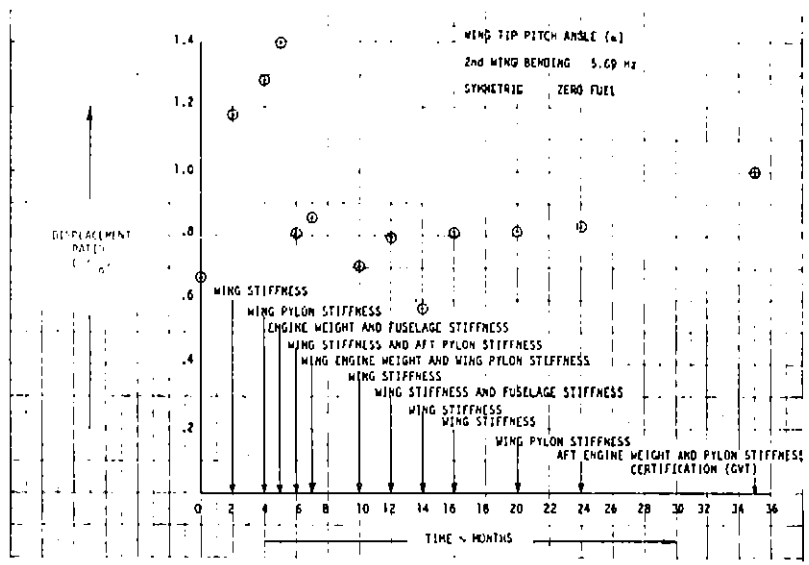

FIGURE 112. EVOLUTION OF DISPLACEMENT RATIO α

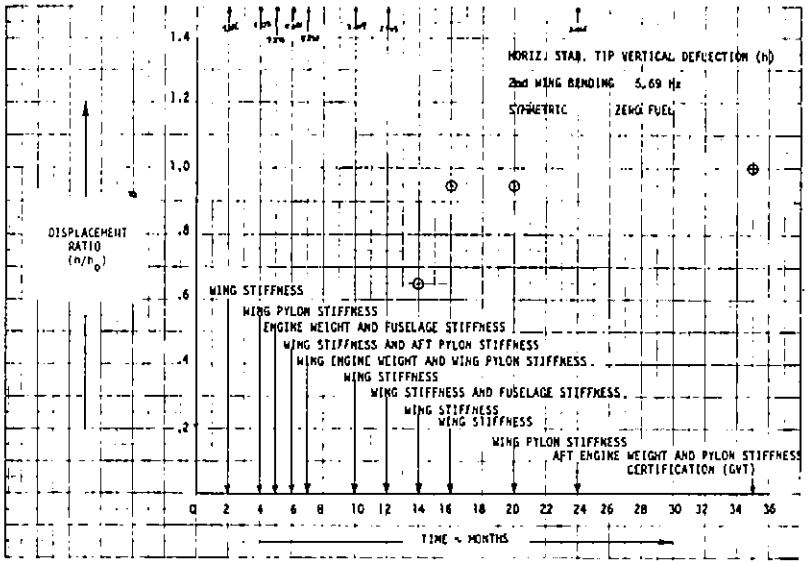

FIGURE 113. EVOLUTION OF DISPLACEMENT RATIO h

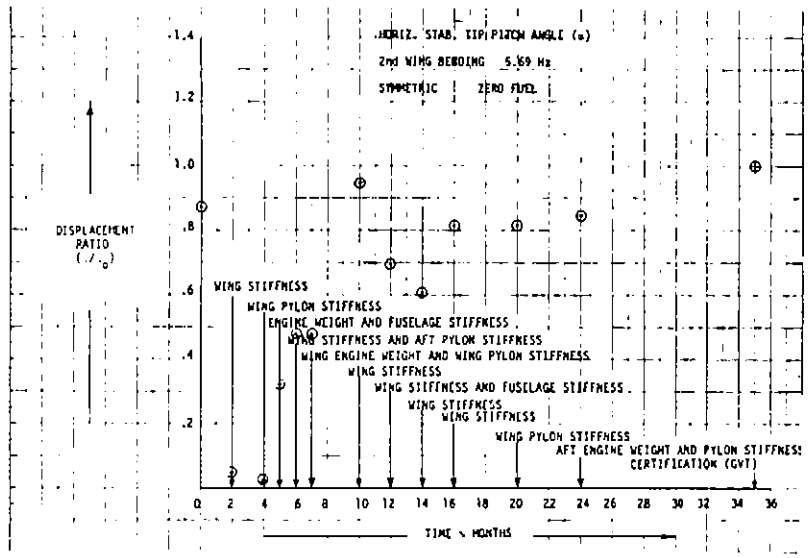

FIGURE 114. EVOLUTION OF DISPLACEMENT RATIO α

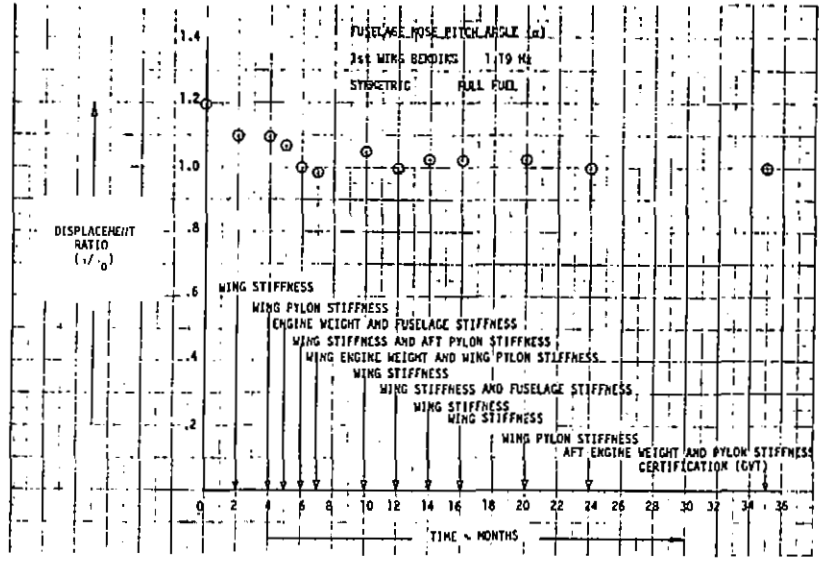

FIGURE 115. EVOLUTION OF DISPLACEMENT RATIO α

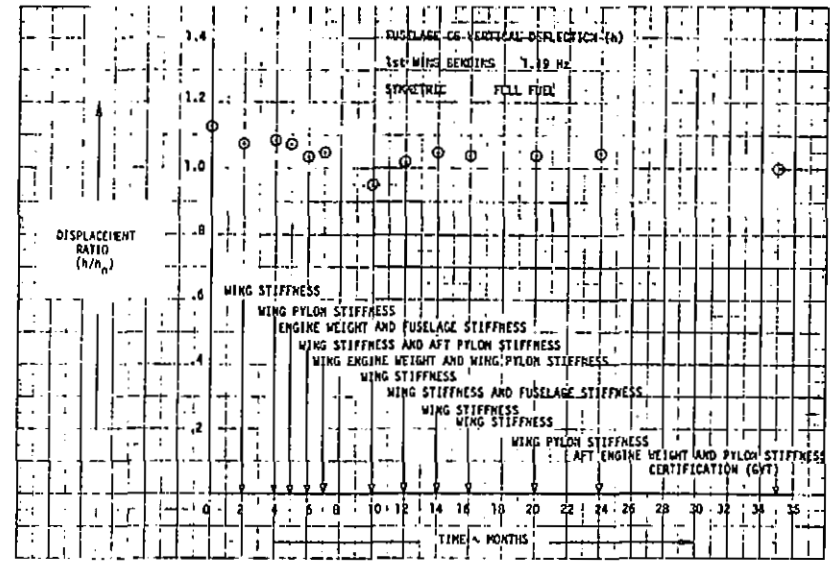

FIGURE 116. EVOLUTION OF DISPLACEMENT RATIO h

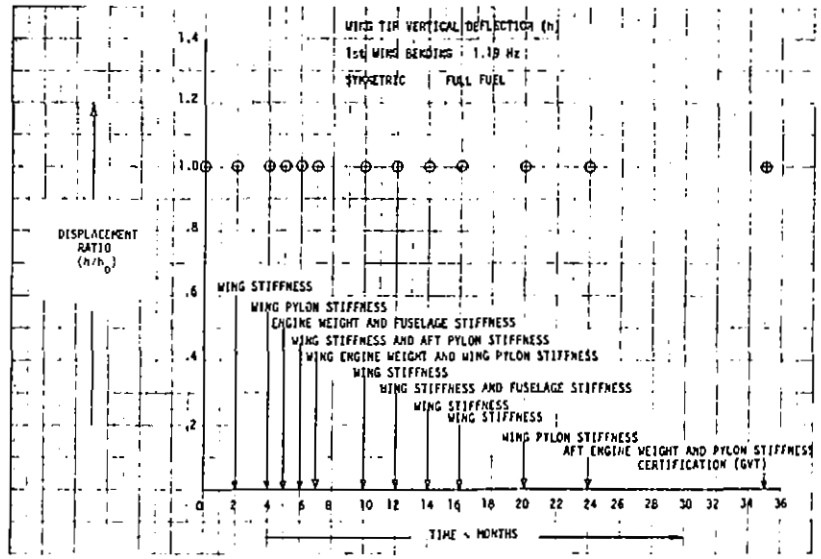

FIGURE 117. EVOLUTION OF DISPLACEMENT RATIO WING h

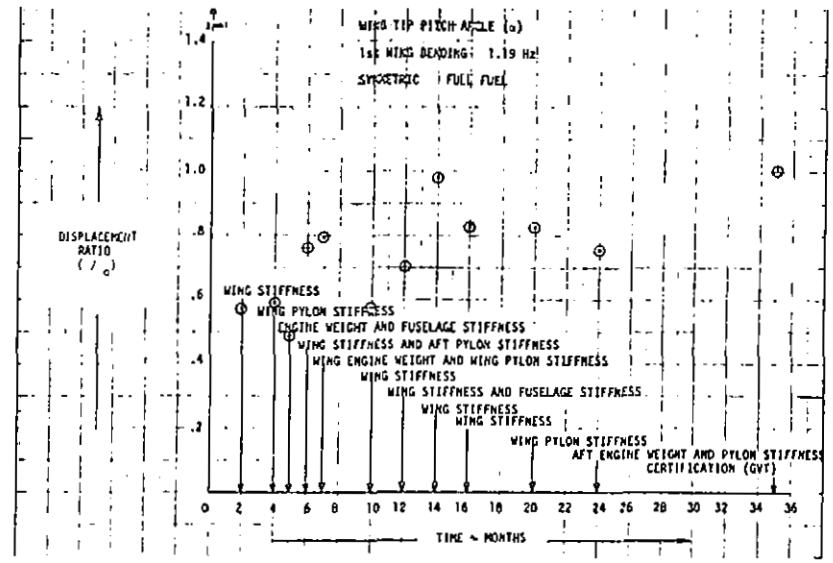

FIGURE 118. EVOLUTION OF DISPLACEMENT RATIO WING α

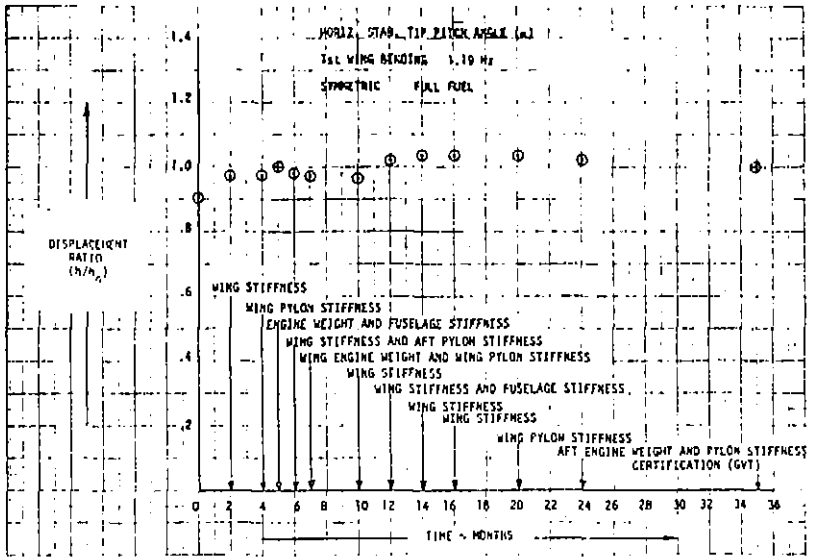

FIGURE 119. EVOLUTION OF DISPLACEMENT RATIO h

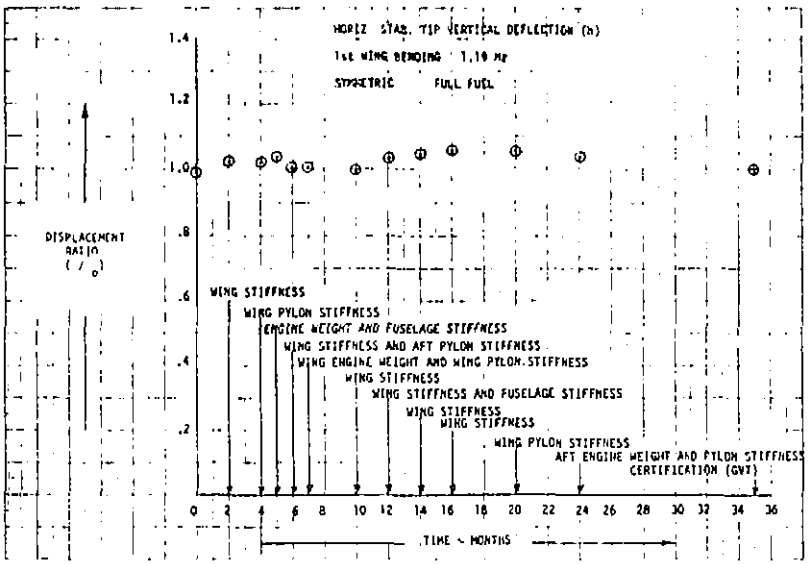

FIGURE 120. EVOLUTION OF DISPLACEMENT RATIO α

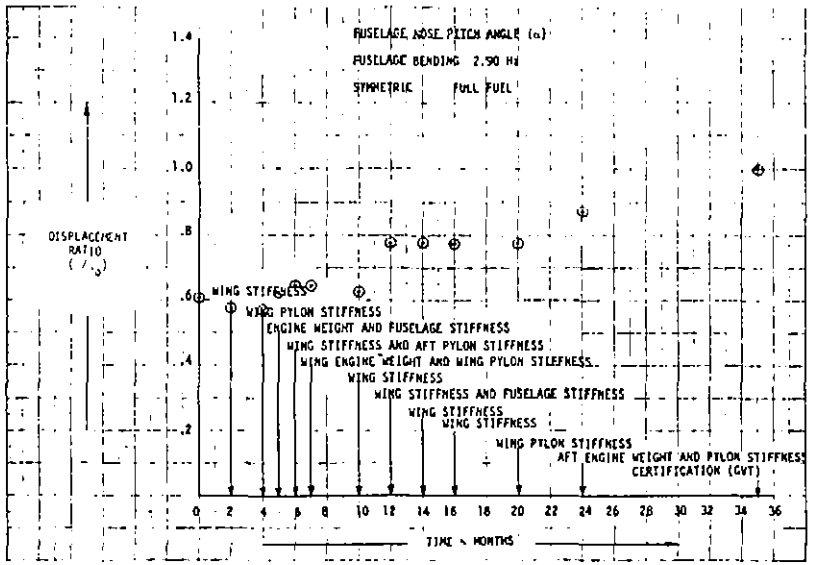

FIGURE 121. EVOLUTION OF DISPLACEMENT RATIO α

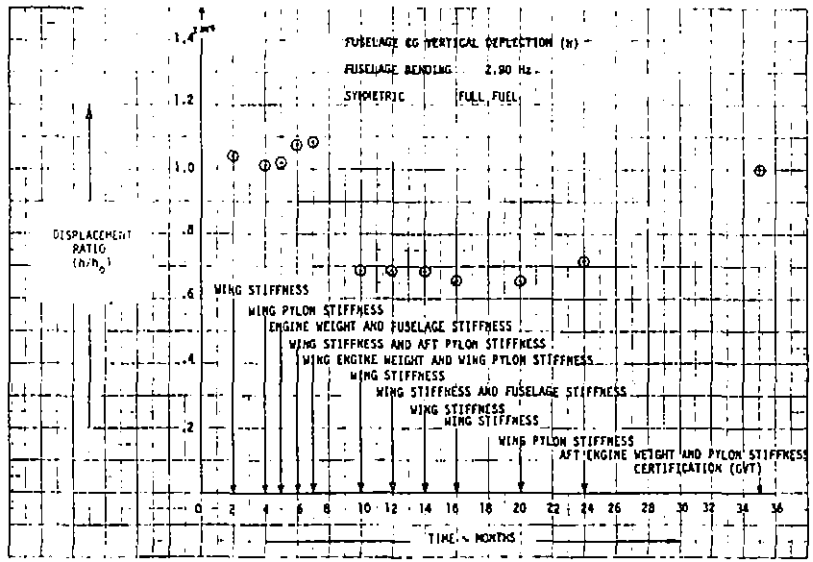

FIGURE 122. EVOLUTION OF DISPLACEMENT RATIO h

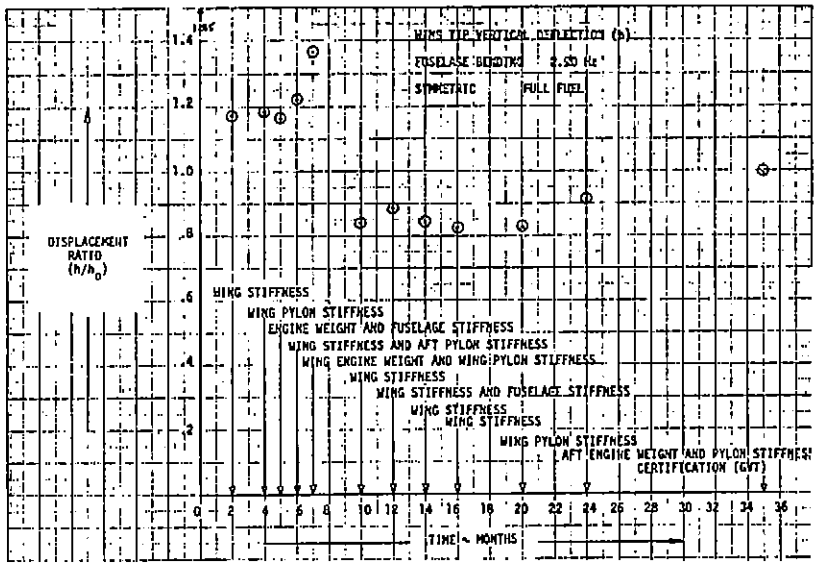

FIGURE 123. EVOLUTION OF DISPLACEMENT RATIO h

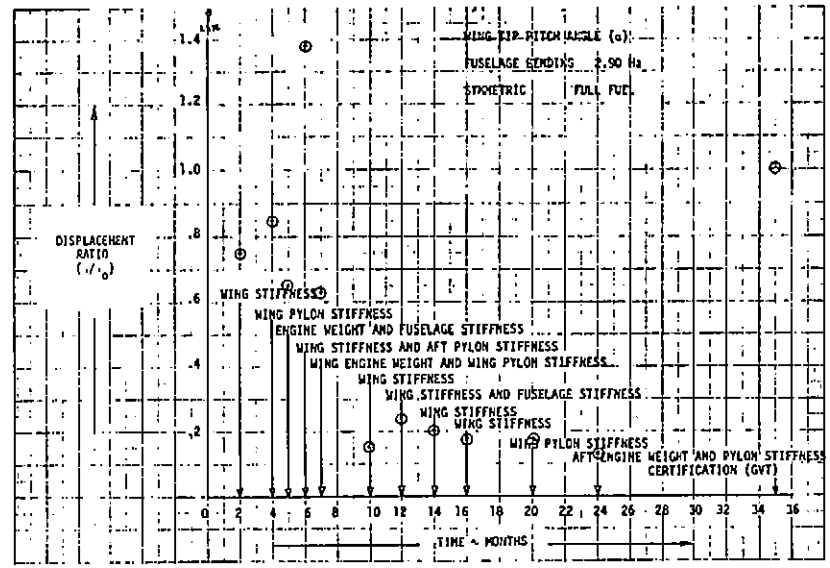

FIGURE 124. EVOLUTION OF DISPLACEMENT RATIO α

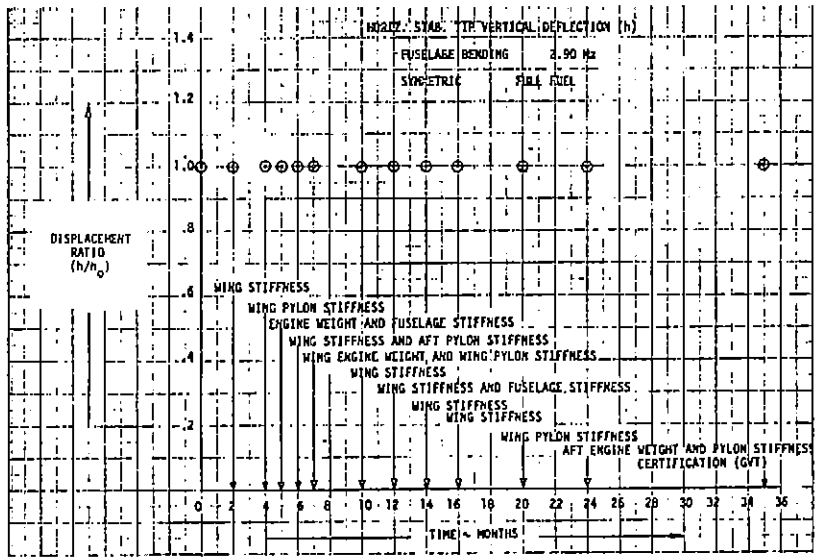

FIGURE 125. EVOLUTION OF DISPLACEMENT RATIO h

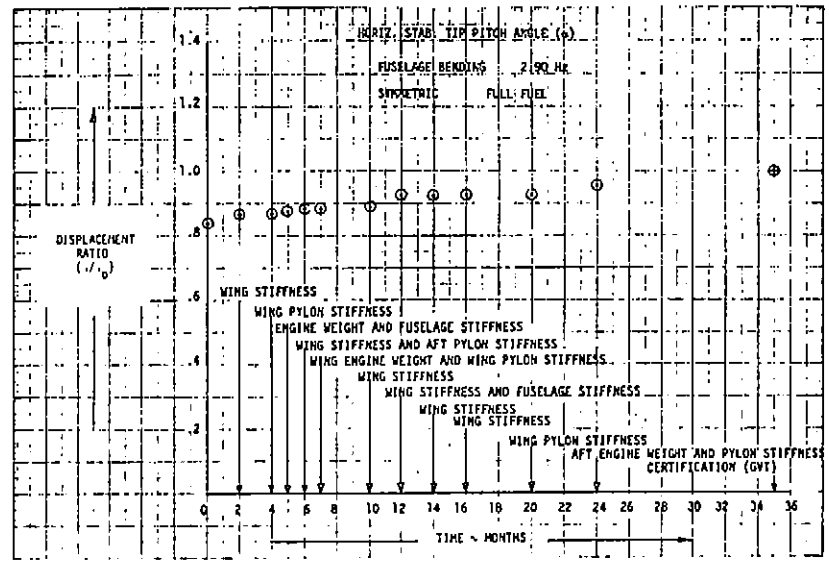

FIGURE 126. EVOLUTION OF DISPLACEMENT RATIO α

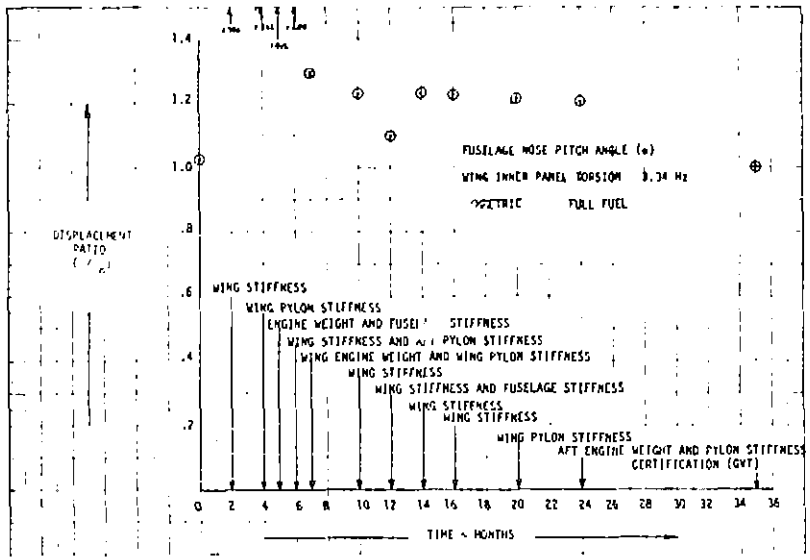

FIGURE 127. EVOLTUION OF FUSELAGE α DISPLACEMENT RATIO

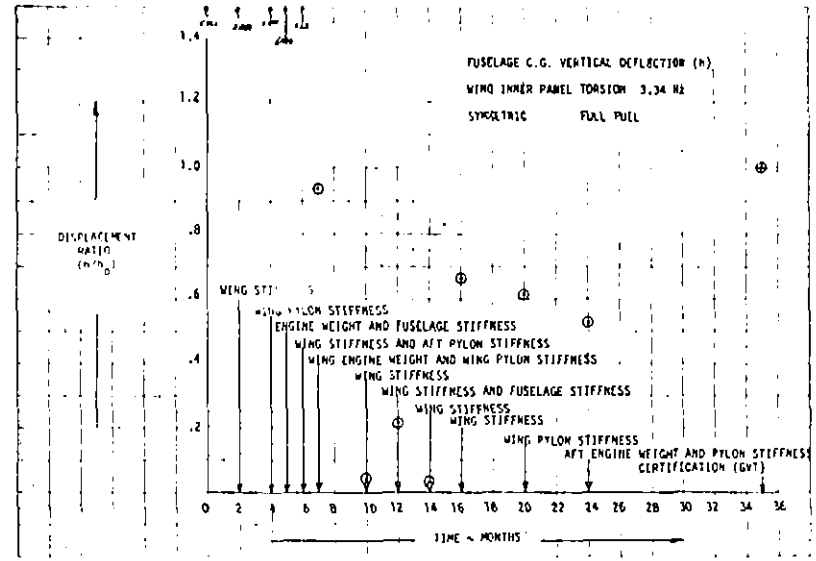

FIGURE 128. EVOLUTION OF DISPLACEMENT RATIO h

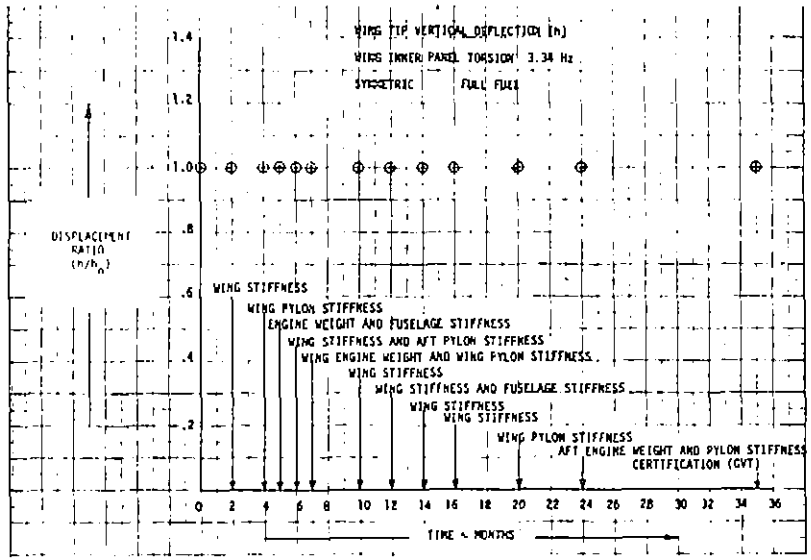

FIGURE 129. EVOLUTION OF DISPLACEMENT RATIO WING h

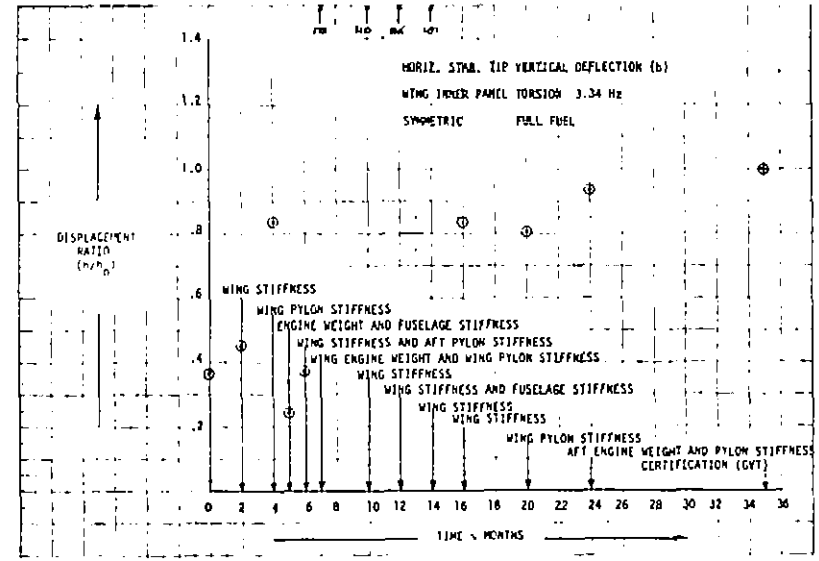

FIGURE 130. EVOLUTION OF DISPLACEMENT RATIO h

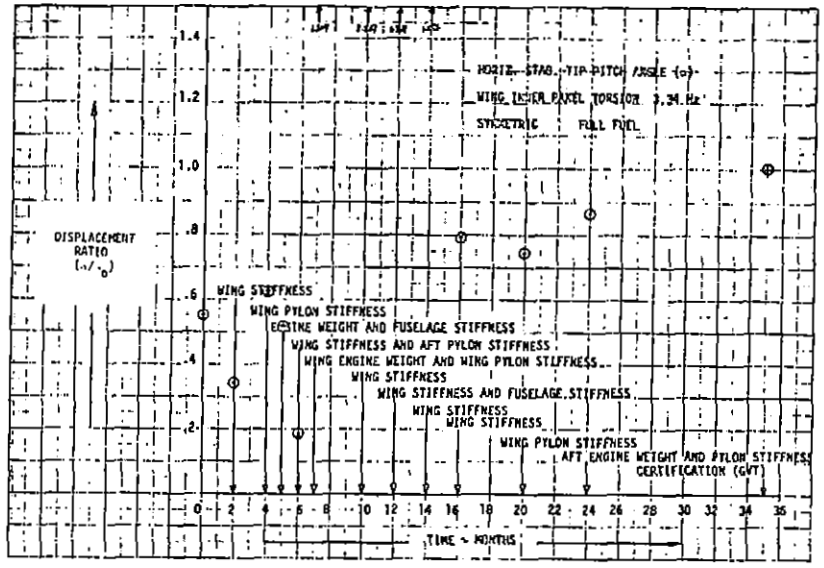

FIGURE 131. EVOLUTION OF DISPLACEMENT RATIO α

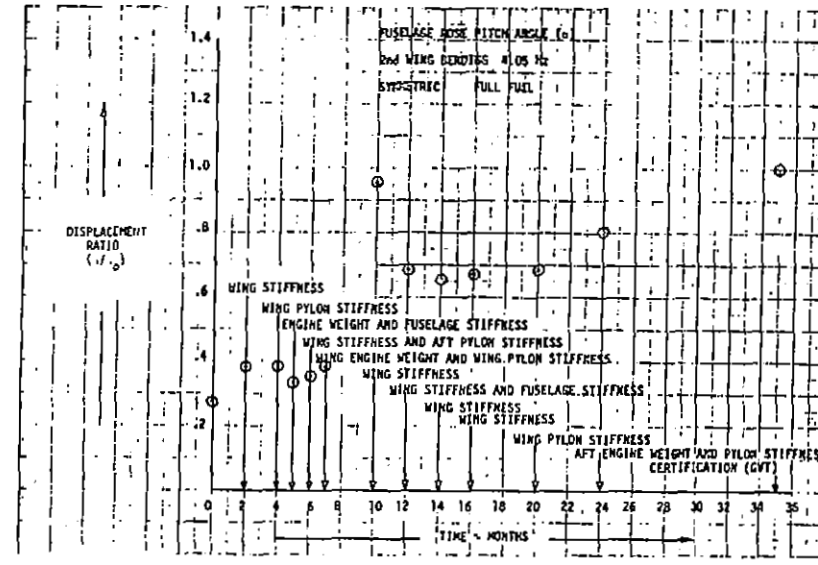

FIGURE 132. EVOLUTION OF DISPLACEMENT RATIO α

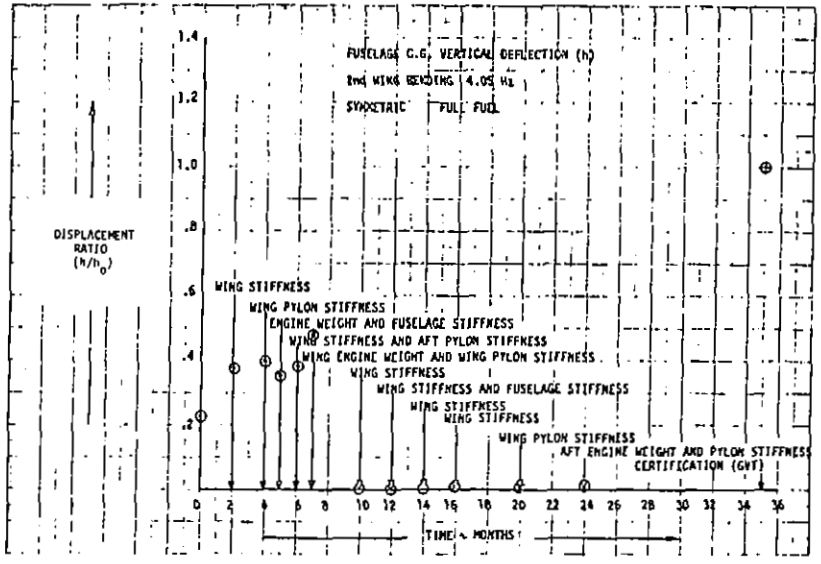

FIGURE 133. EVOLUTION OF DISPLACEMENT RATIO h

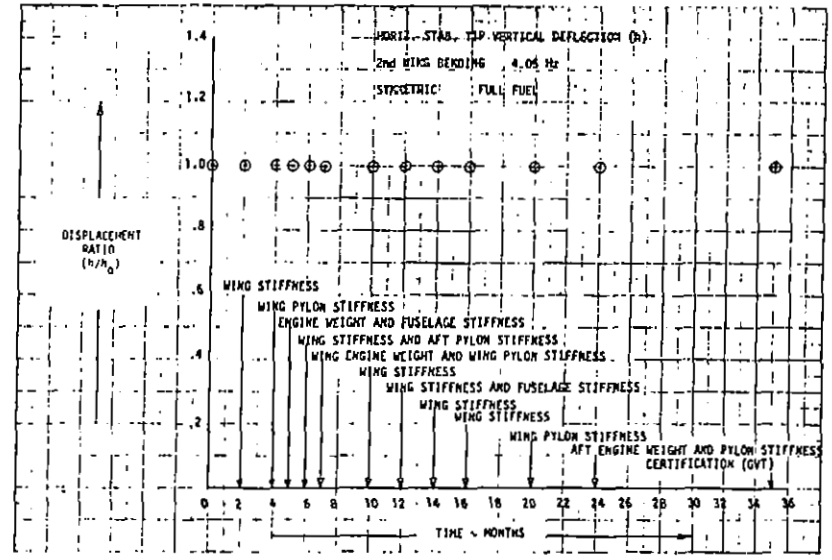

FIGURE 134. EVOLUTION OF DISPLACEMENT RATIO h

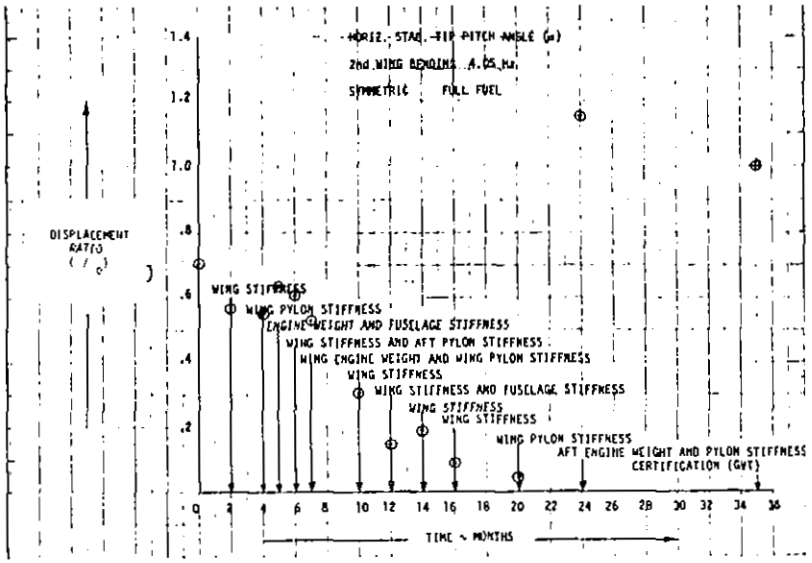

FIGURE 135. EVOLUTION OF DISPLACEMENT RATIO α

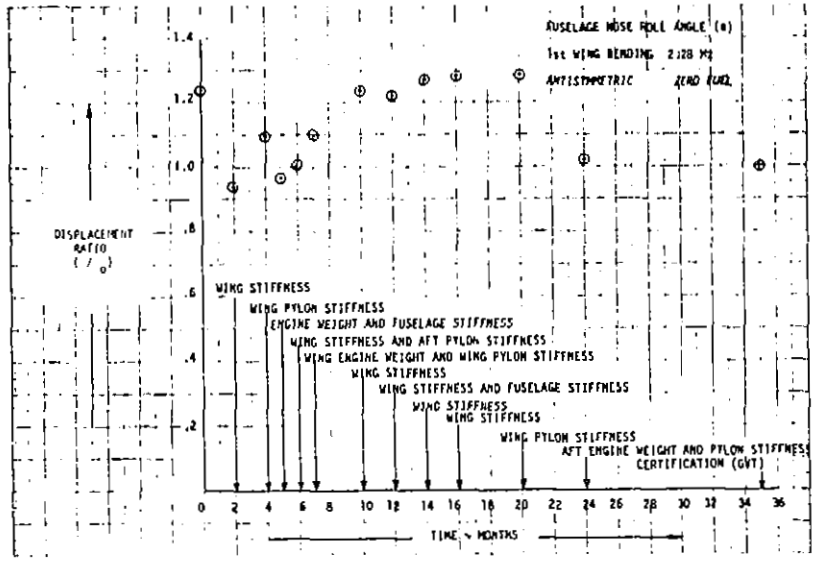

FIGURE 136. EVOLUTION OF DISPLACEMENT RATIO θ

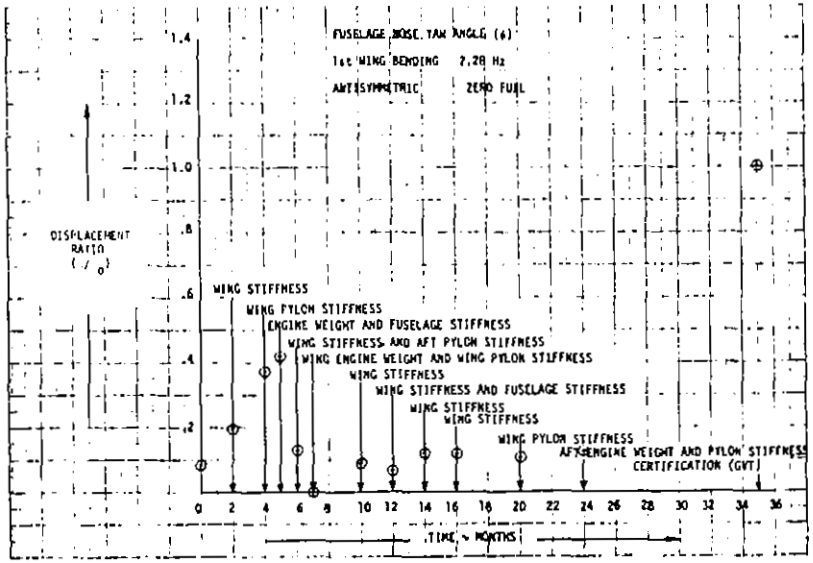

FIGURE 137. EVOLUTION OF DISPLACEMENT RATIO ψ

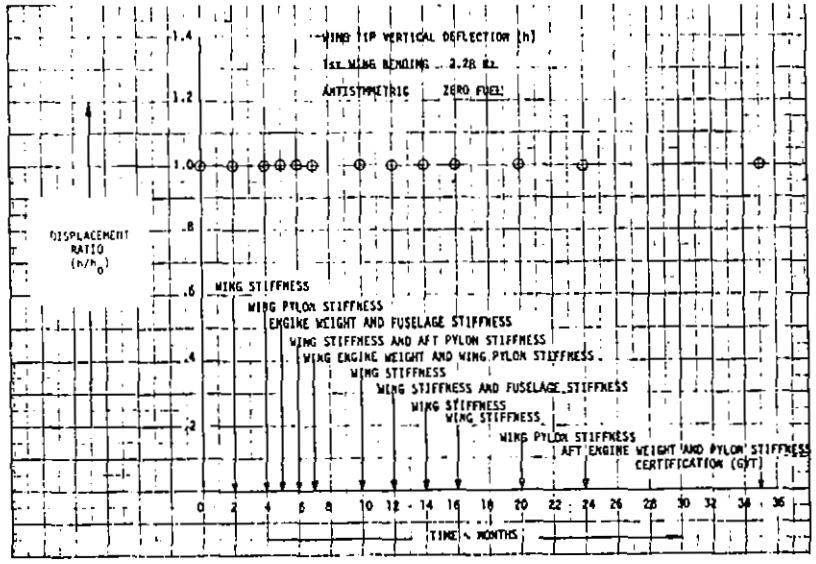

FIGURE 138. EVOLUTION OF DISPLACEMENT RATIO h

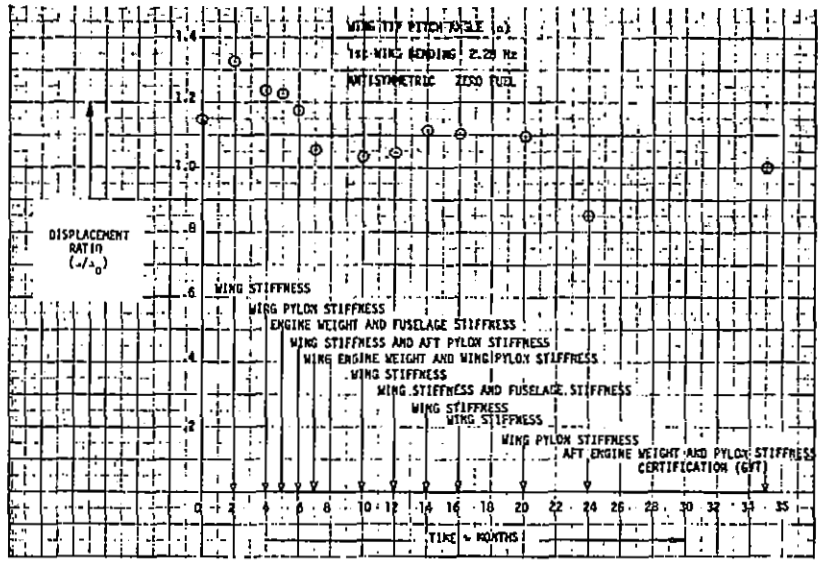

FIGURE 139. EVOLUTION OF DISPLACEMENT RATIO α

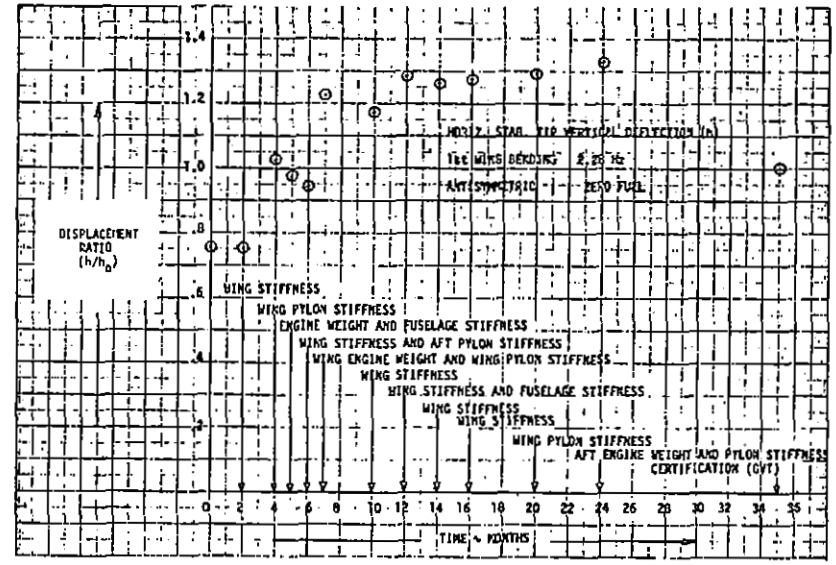

FIGURE 140. EVOLUTION OF DISPLACEMENT RATIO h

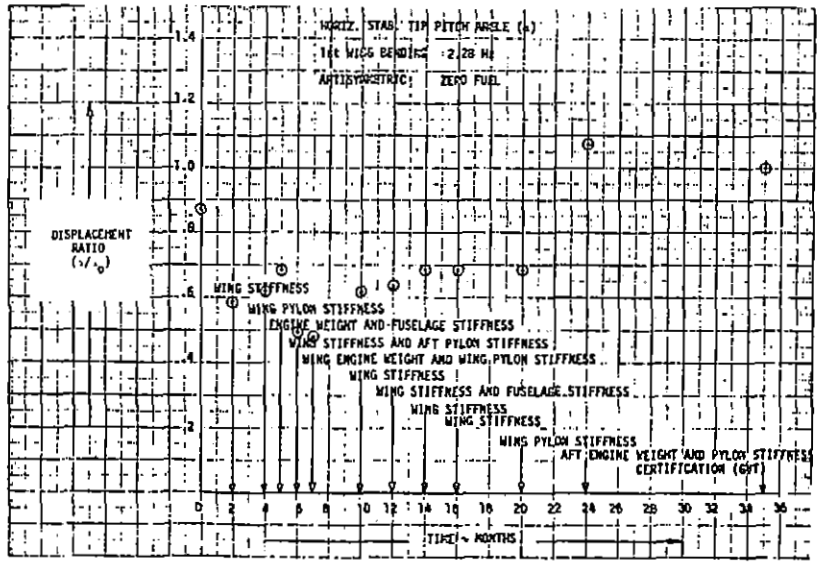

FIGURE 141. EVOLUTION OF DISPLACEMENT RATIO α

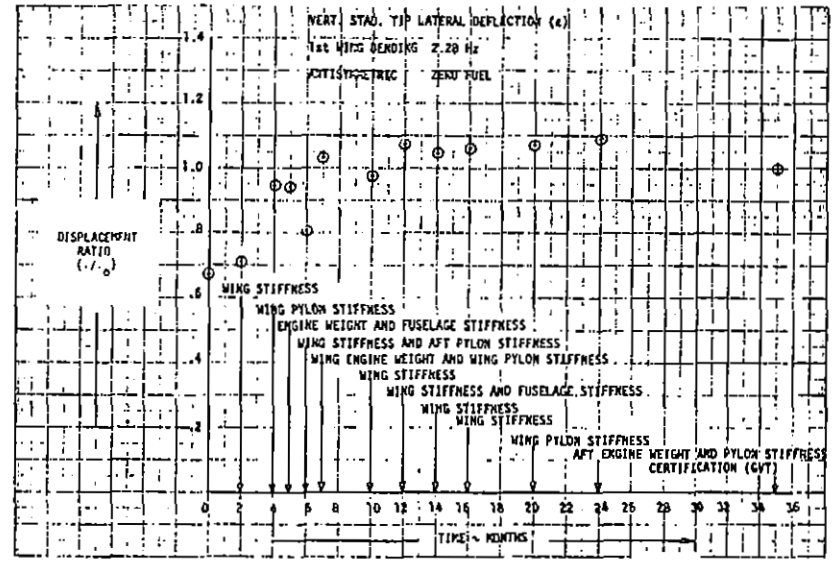

FIGURE 142. EVOLUTION OF DISPLACEMENT RATIO ℓ

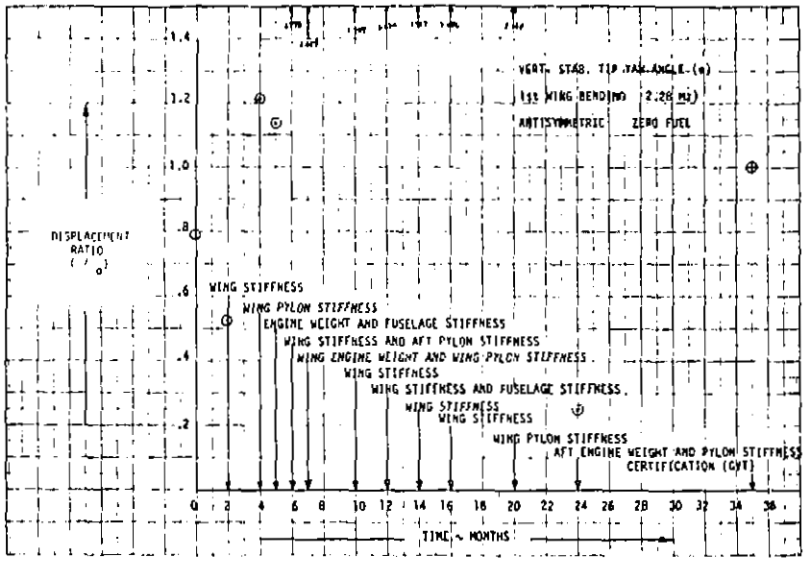

FIGURE 143. EVOLUTION OF DISPLACEMENT RATIO ψ

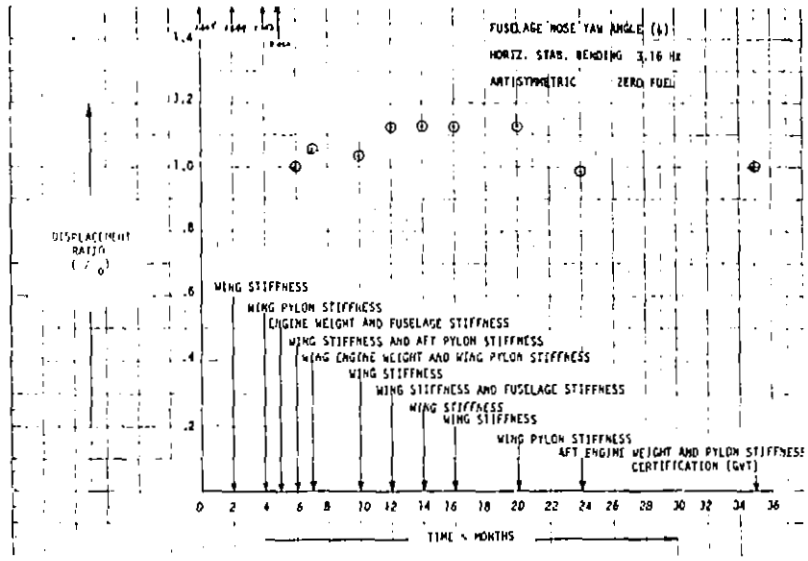

FIGURE 144. EVOLUTION OF DISPLACEMENT RATIO ψ

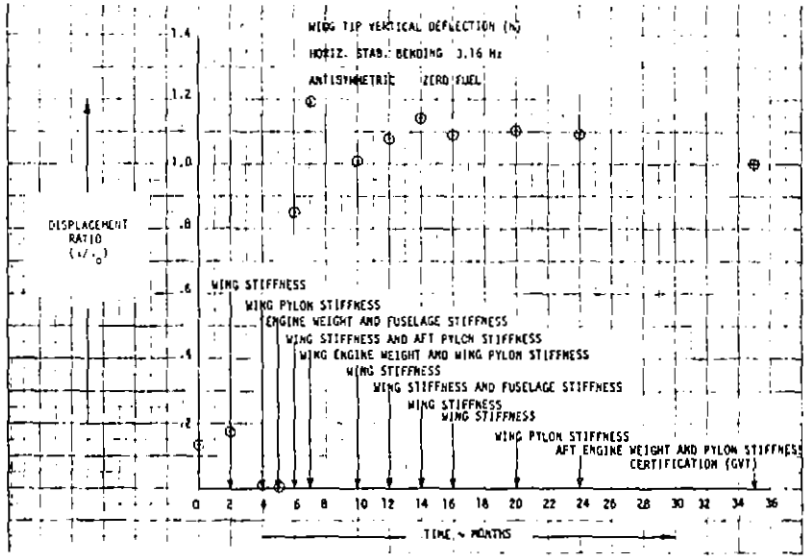

FIGURE 145. EVOLUTION OF DISPLACEMENT RATIO α

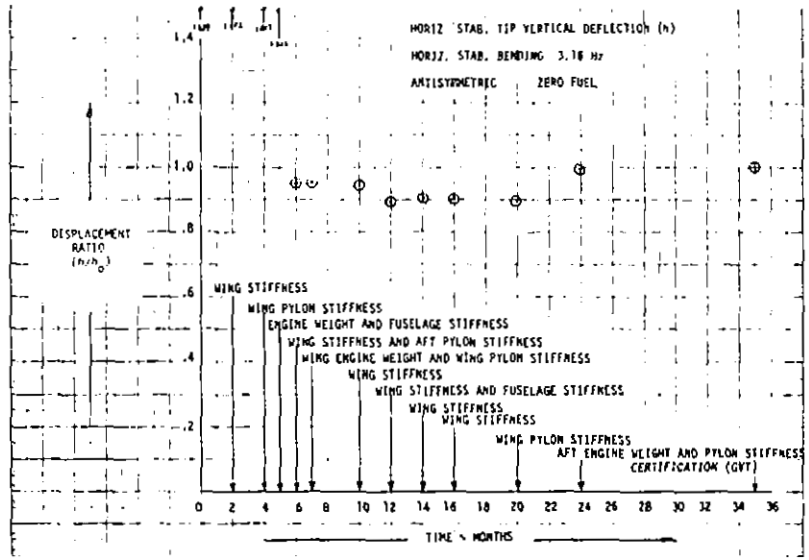

FIGURE 146. EVOLUTION OF DISPLACEMENT RATIO h

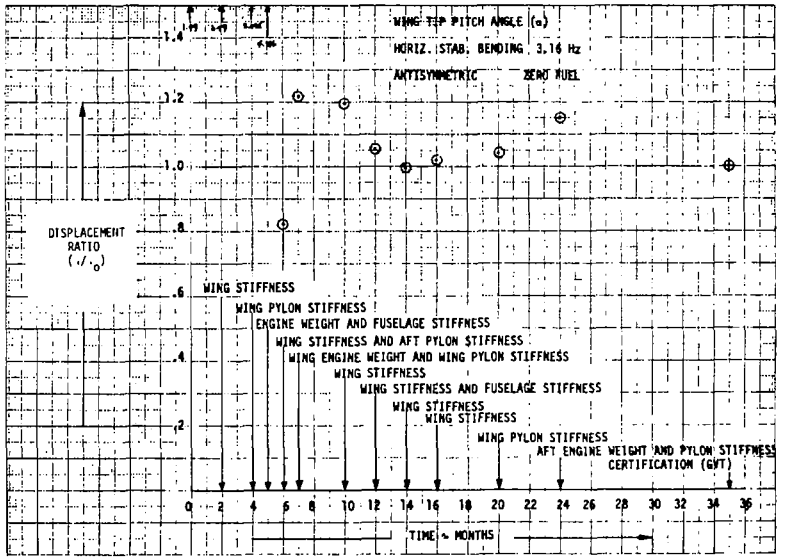

FIGURE 147. EVOLUTION OF DISPLACEMENT RATIO α

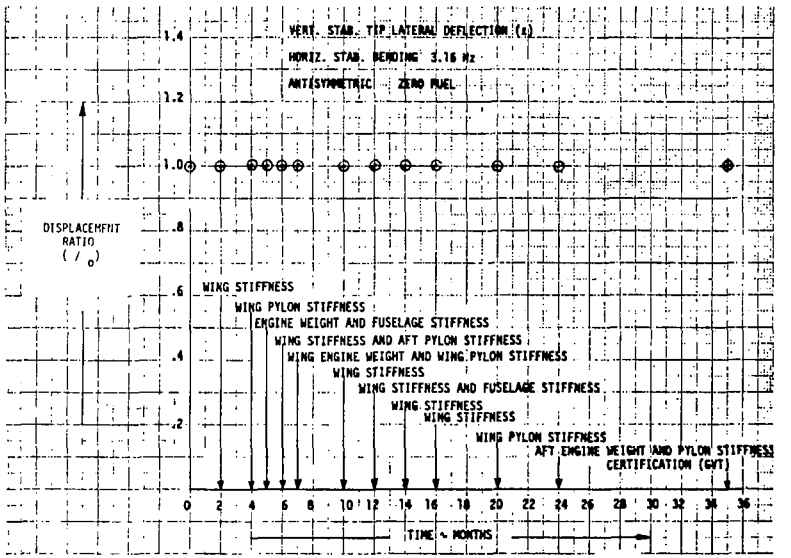

FIGURE 148. EVOLUTION OF DISPLACEMENT RATIO ℓ

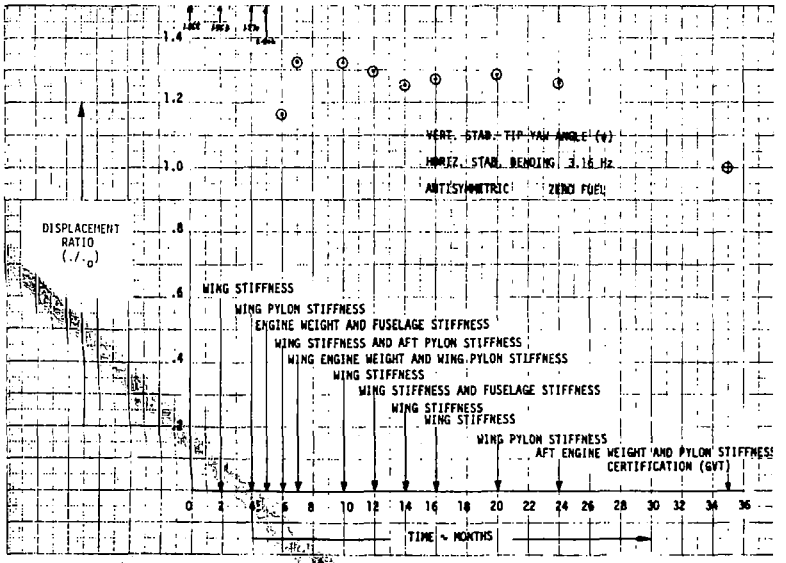

FIGURE 149. EVOLUTION OF DISPLACEMENT RATIO ψ

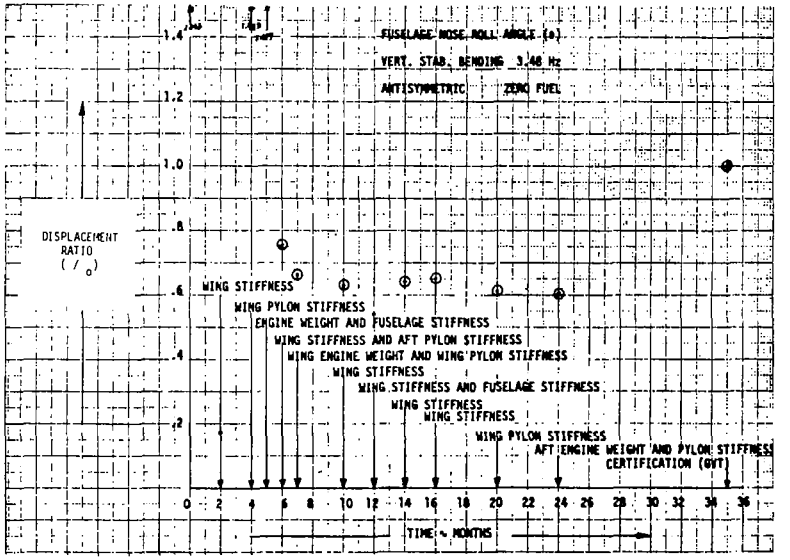

FIGURE 150. EVOLUTION OF DISPLACEMENT RATIO θ

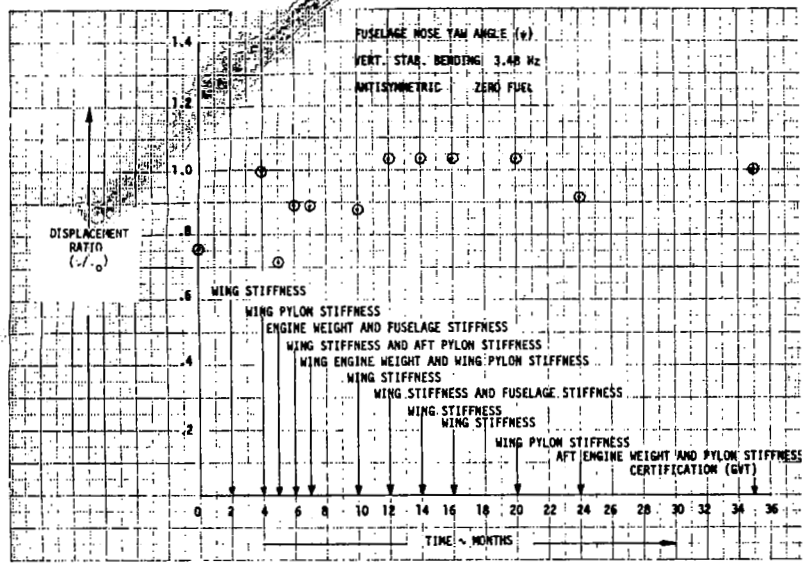

FIGURE 151. EVOLUTION OF DISPLACEMENT RATIO ψ

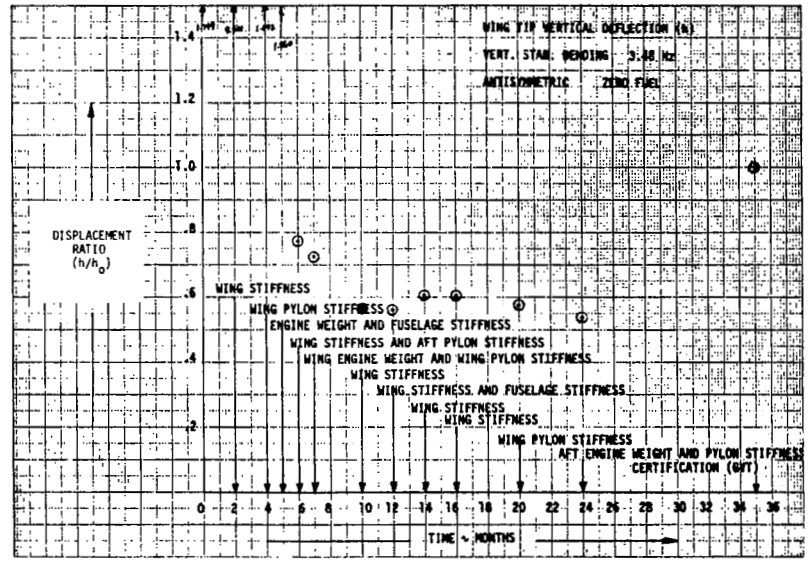

FIGURE 152. EVOLUTION OF DISPLACEMENT RATIO h

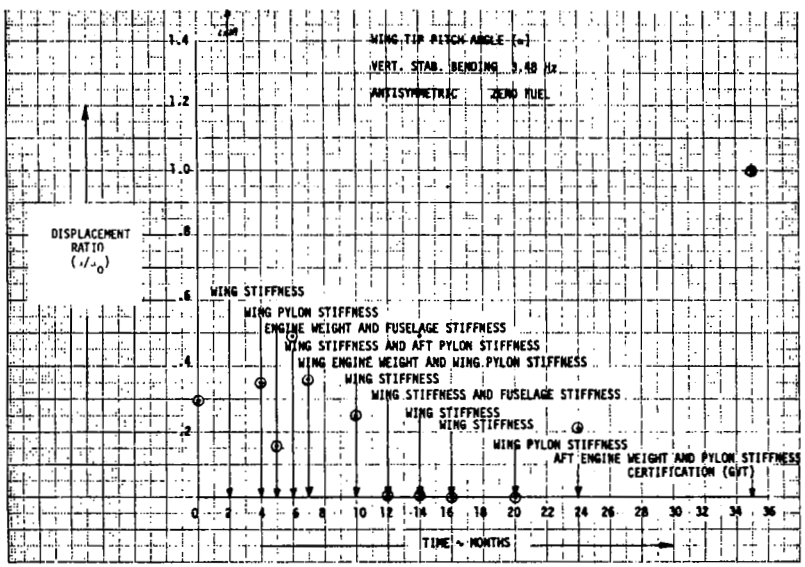

FIGURE 153. EVOLUTION OF DISPLACEMENT RATIO α

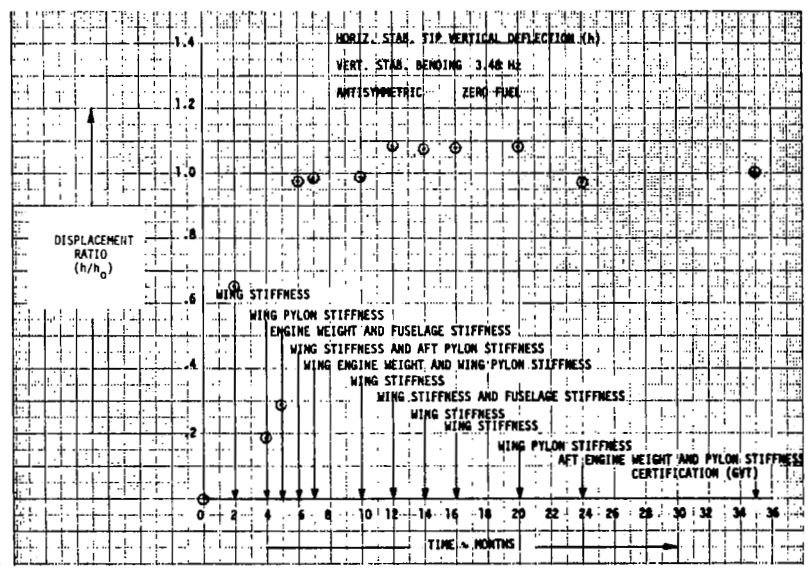

FIGURE 154. EVOLUTION OF DISPLACEMENT RATIO h

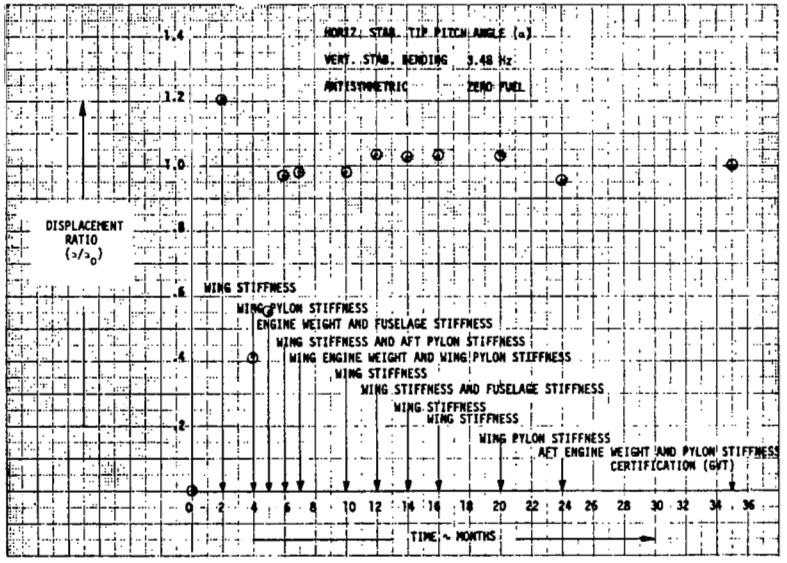

FIGURE 155. EVOLUTION OF DISPLACEMENT RATIO α

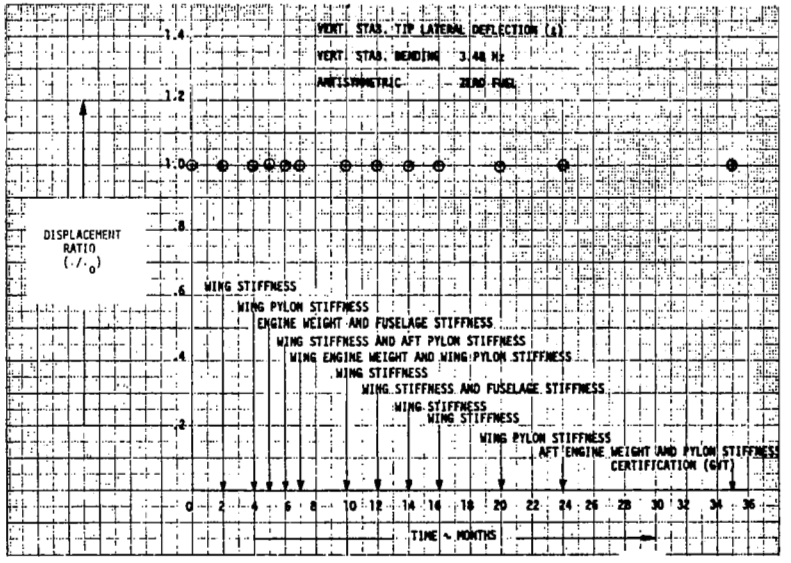

FIGURE 156. EVOLUTION OF DISPLACEMENT RATIO ℓ

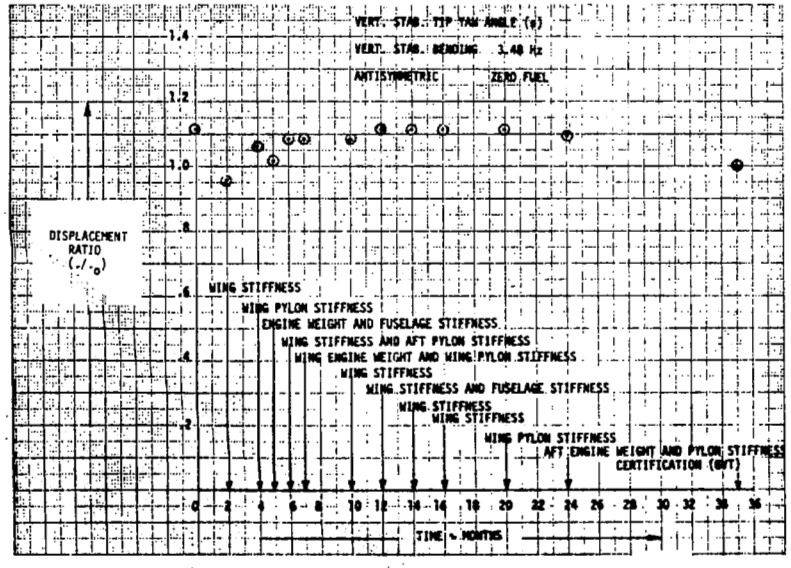

FIGURE 157. EVOLUTION OF DISPLACEMENT RATIO ψ

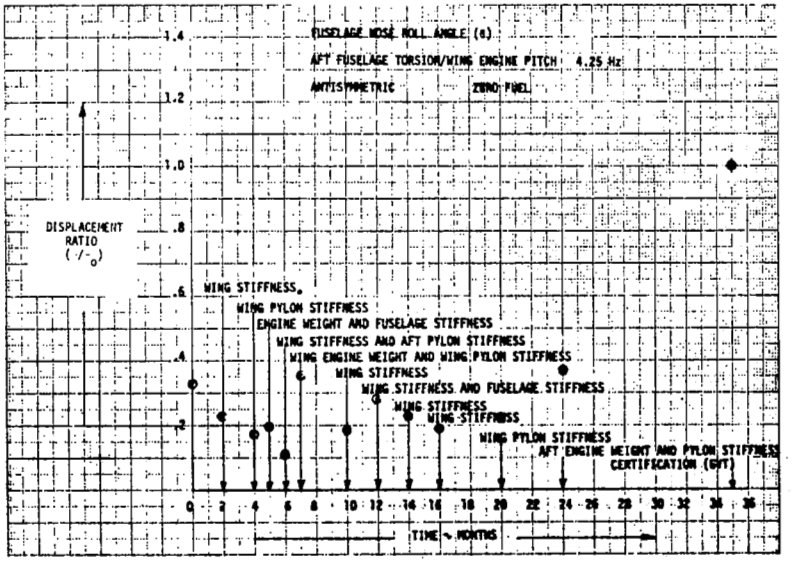

FIGURE 158. EVOLUTION OF DISPLACEMENT RATIO θ

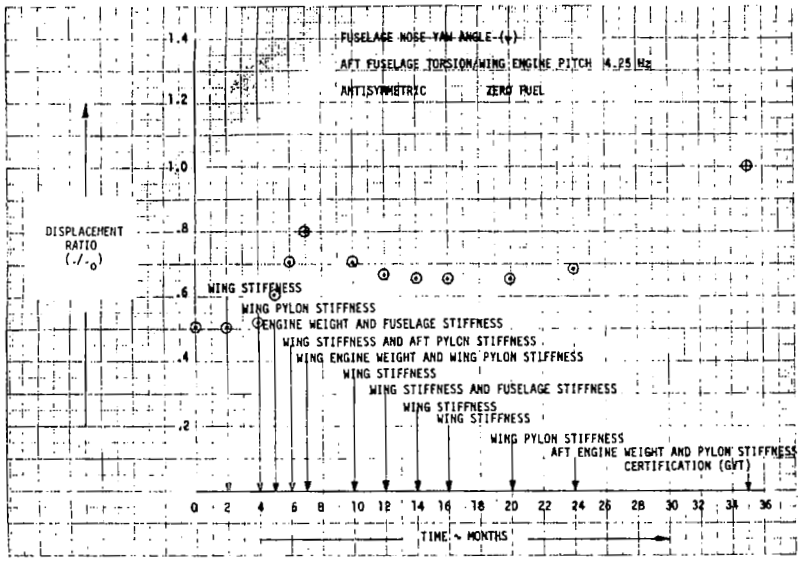

FIGURE 159. EVOLUTION OF DISPLACEMENT RATIO ψ

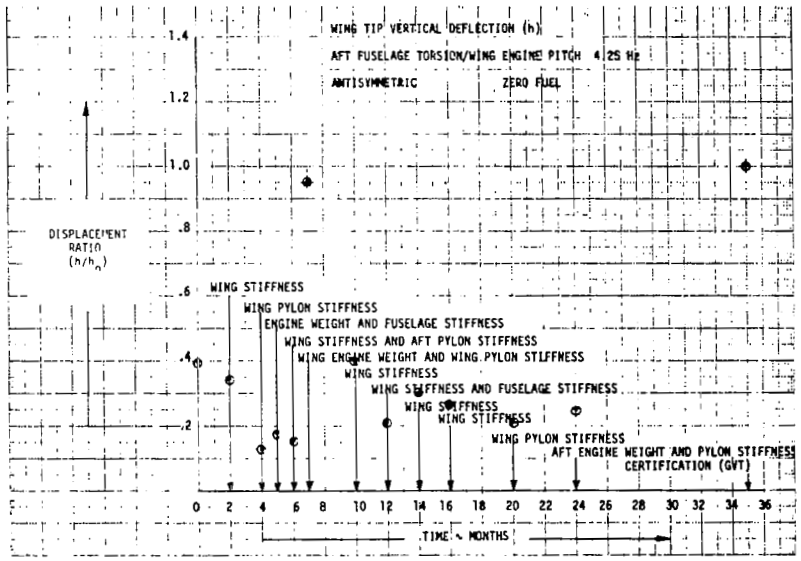

FIGURE 160. EVOLUTION OF DISPLACEMENT RATIO h

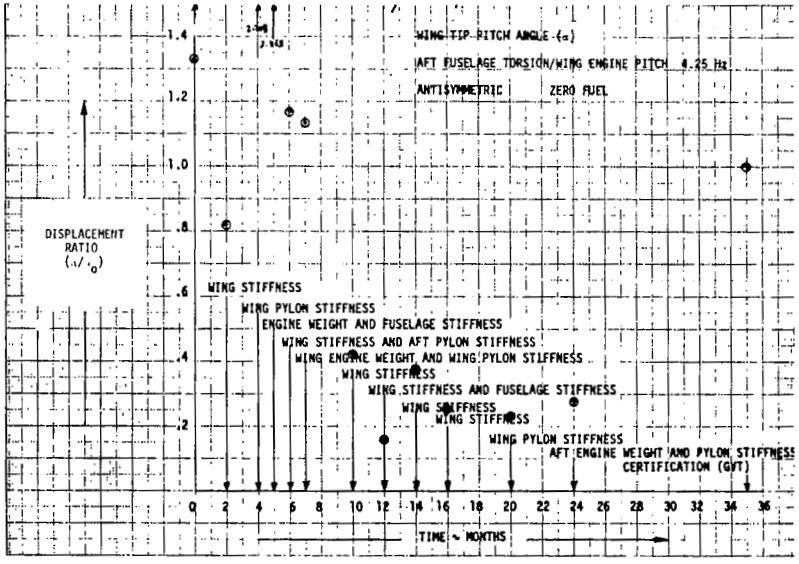

FIGURE 161. EVOLUTION OF DISPLACEMENT RATIO α

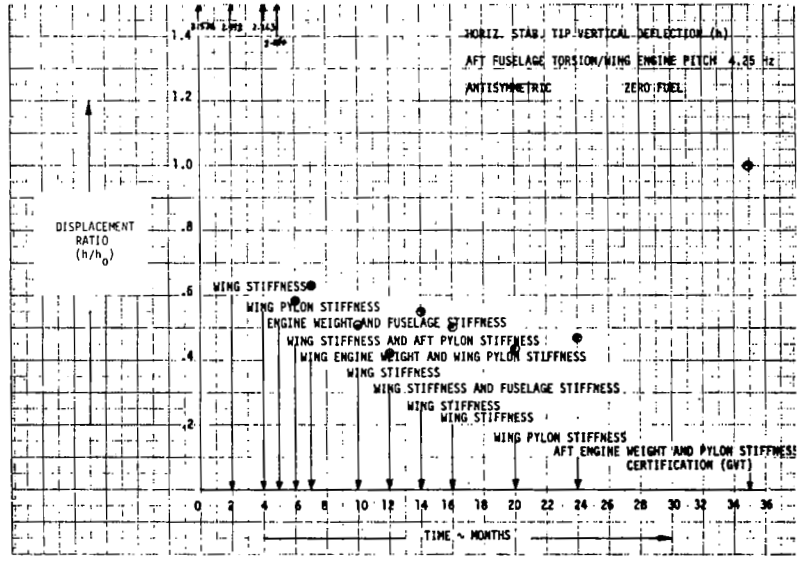

FIGURE 162. EVOLUTION OF DISPLACEMENT RATIO h

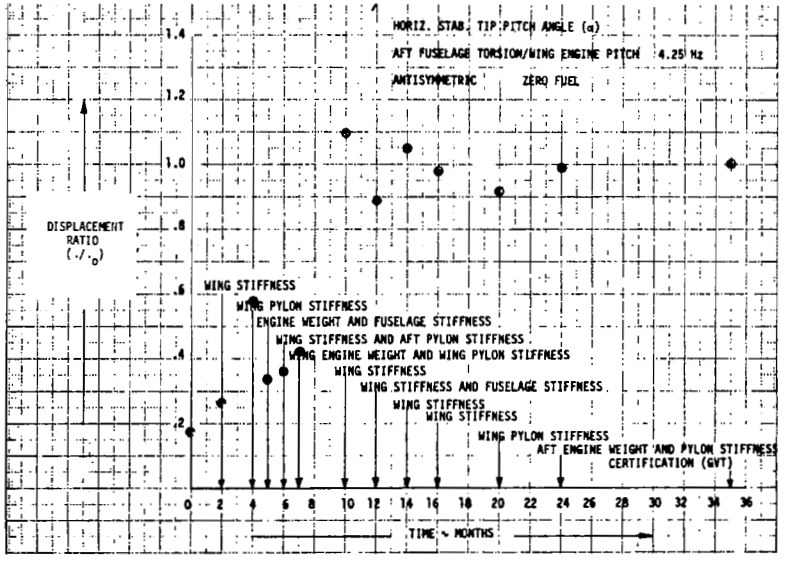

FIGURE 163. EVOLUTION OF DISPLACEMENT RATIO α

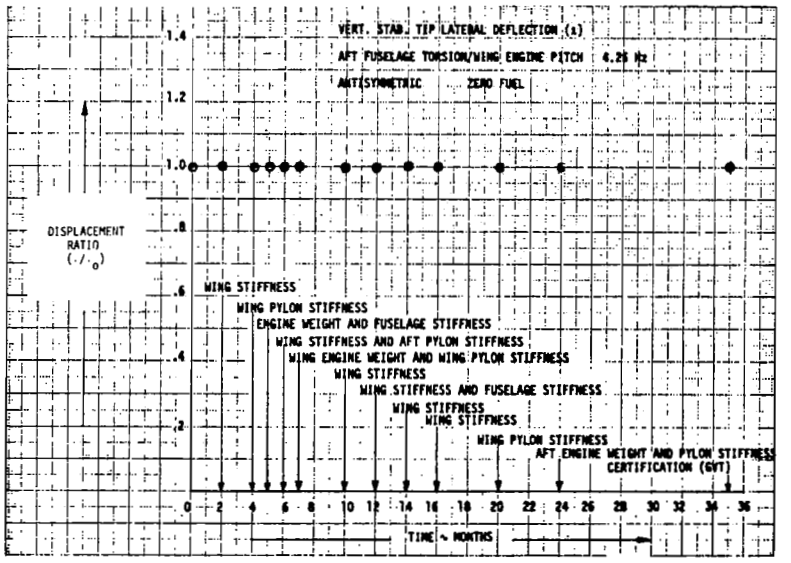

FIGURE 164. EVOLUTION OF DISPLACEMENT RATIO ℓ

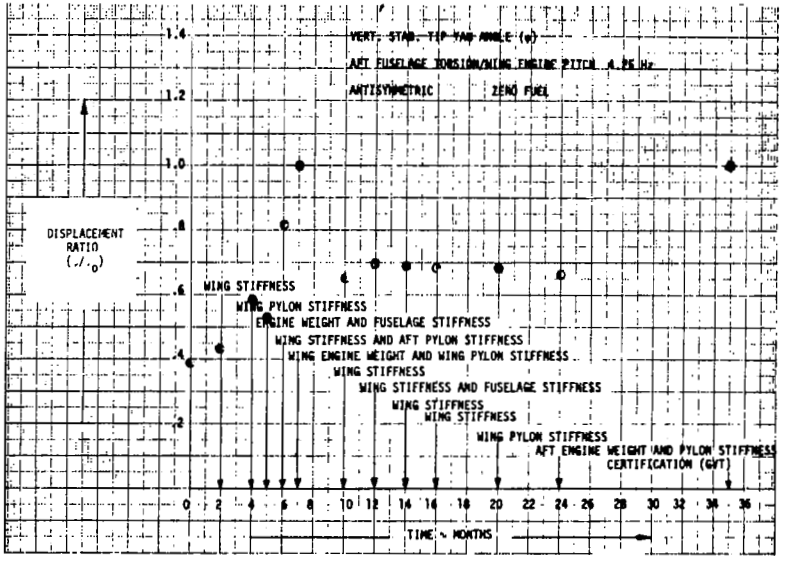

FIGURE 165. EVOLUTION OF DISPLACEMENT RATIO ψ

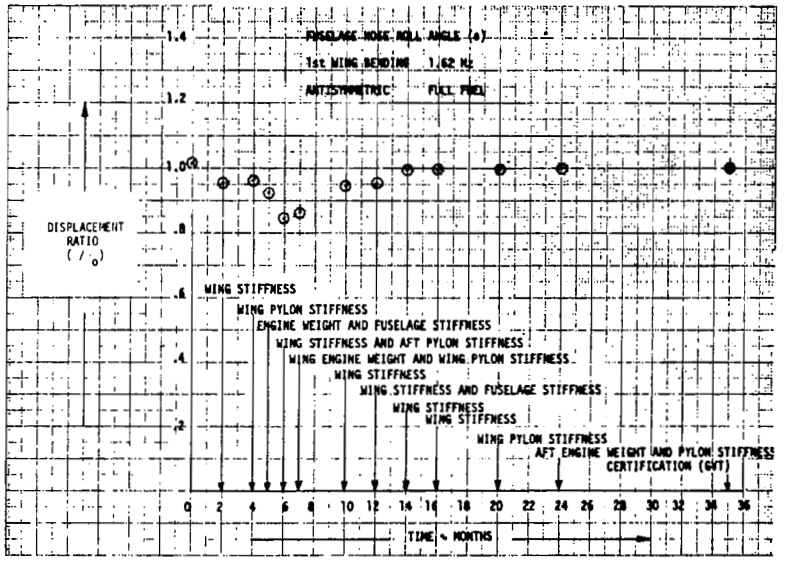

FIGURE 166. EVOLUTION OF DISPLACEMENT RATIO θ

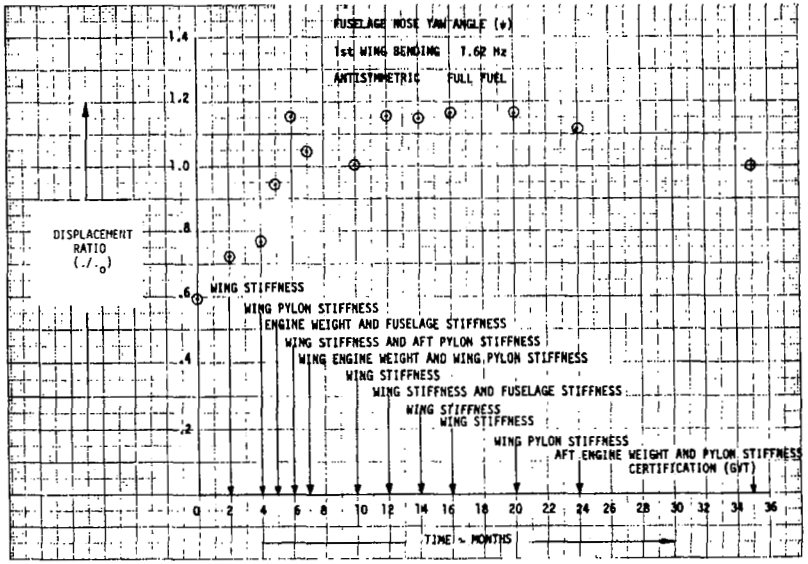

FIGURE 167. EVOLUTION OF DISPLACEMENT RATIO ψ

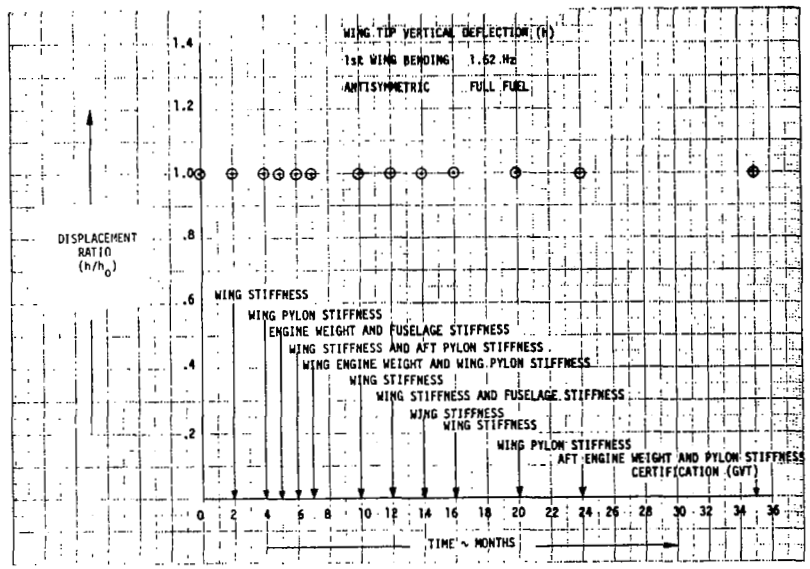

FIGURE 168. EVOLUTION OF DISPLACEMENT RATIO h

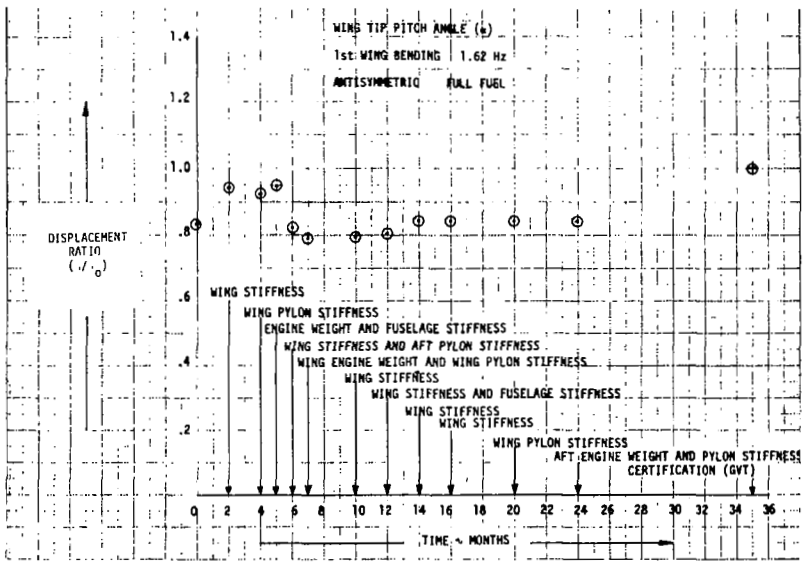

FIGURE 169. EVOLUTION OF DISPLACEMENT RATIO α

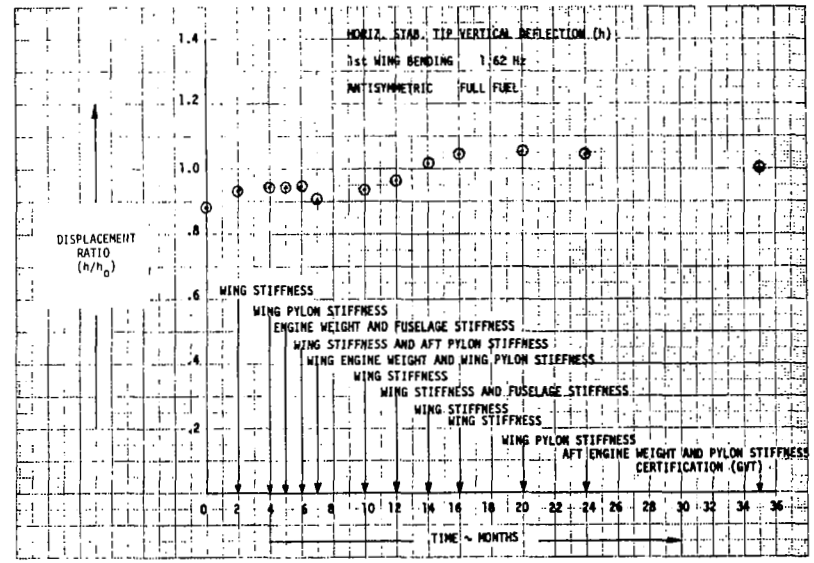

FIGURE 170. EVOLUTION OF DISPLACEMENT RATIO h

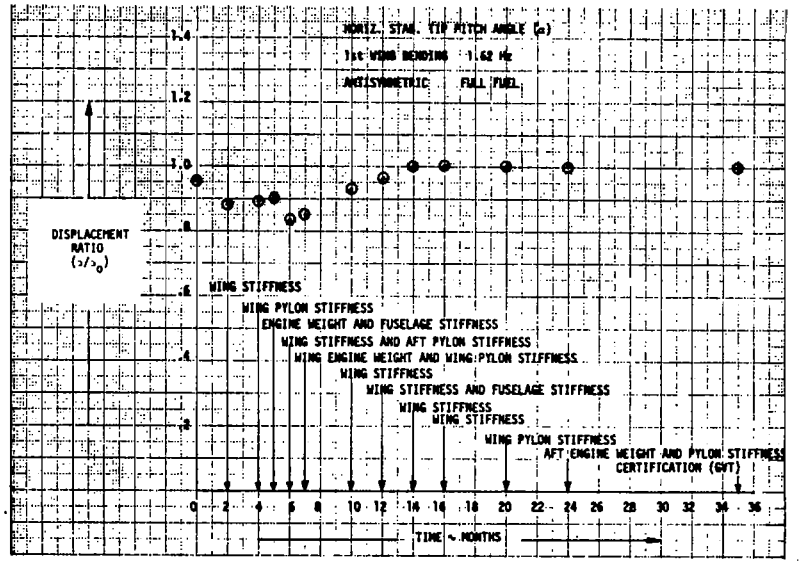

FIGURE 171. EVOLUTION OF DISPLACEMENT RATIO α

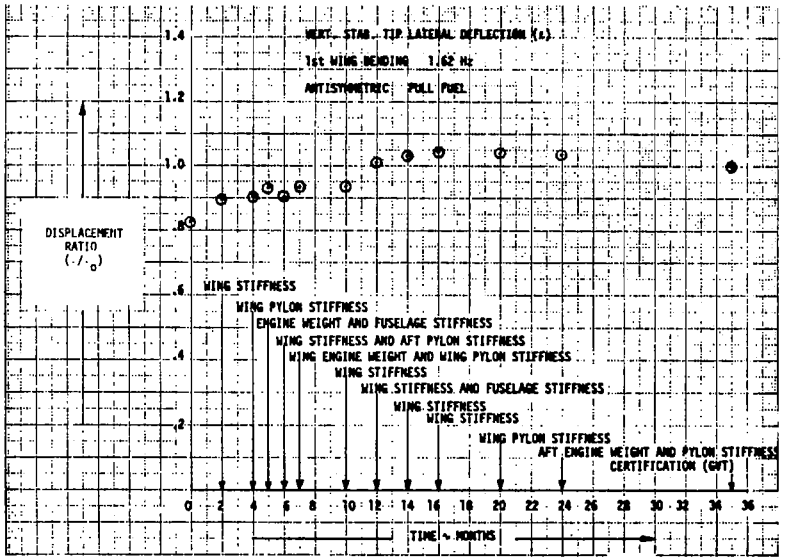

FIGURE 172. EVOLUTION OF DISPLACEMENT RATIO ℓ

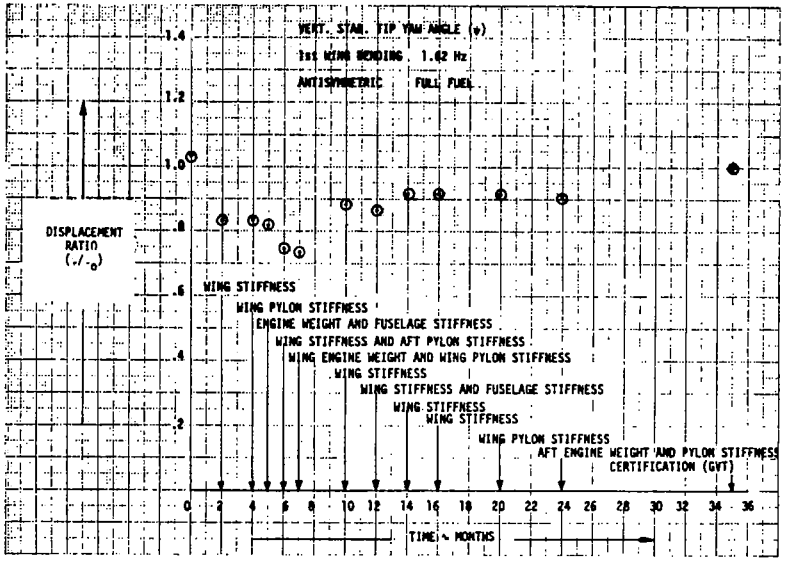

FIGURE 173. EVOLUTION OF DISPLACEMENT RATIO ψ

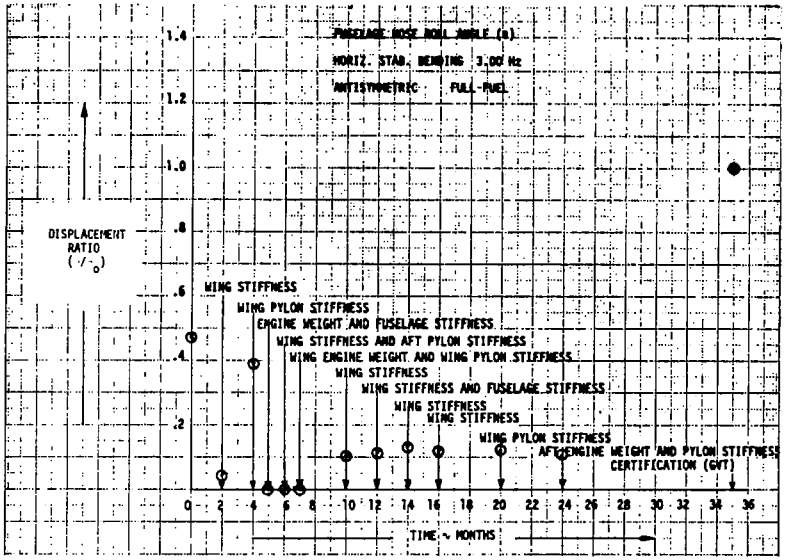

FIGURE 174. EVOLUTION OF DISPLACEMENT RATIO θ

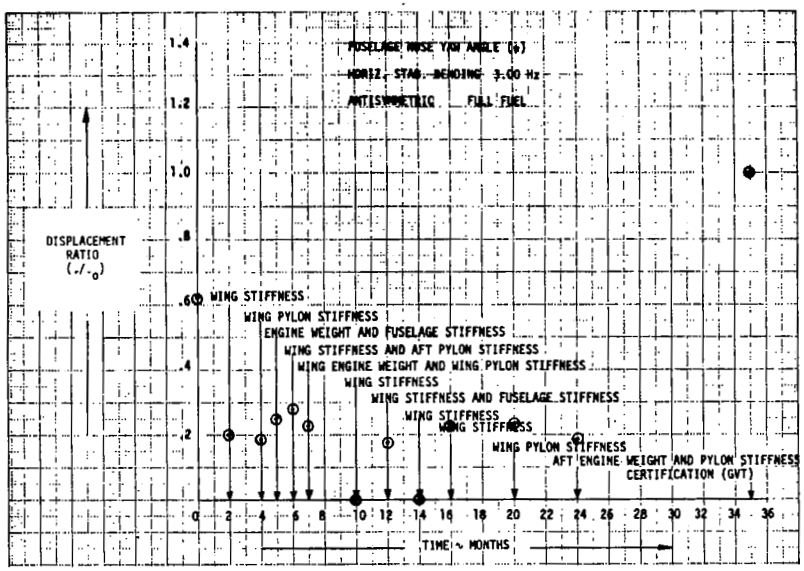

FIGURE 175. EVOLUTION OF DISPLACEMENT RATIO ψ

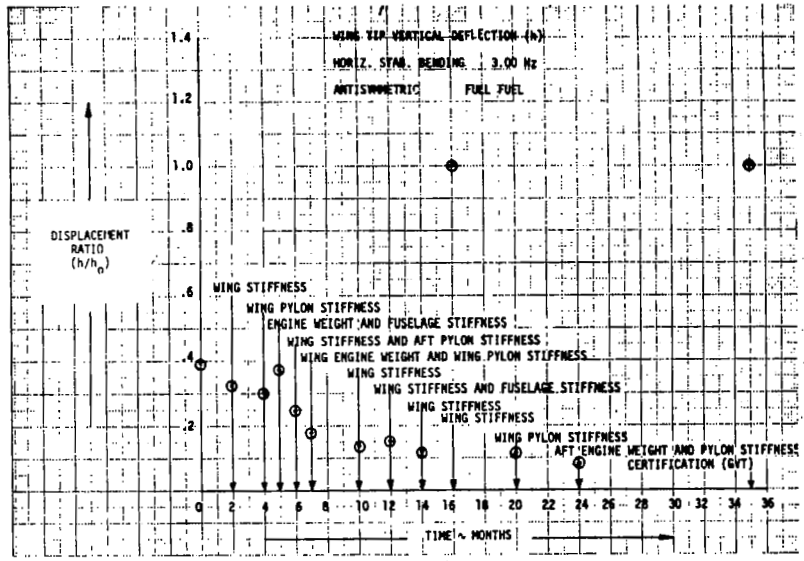

FIGURE 176. EVOLUTION OF DISPLACEMENT RATIO h

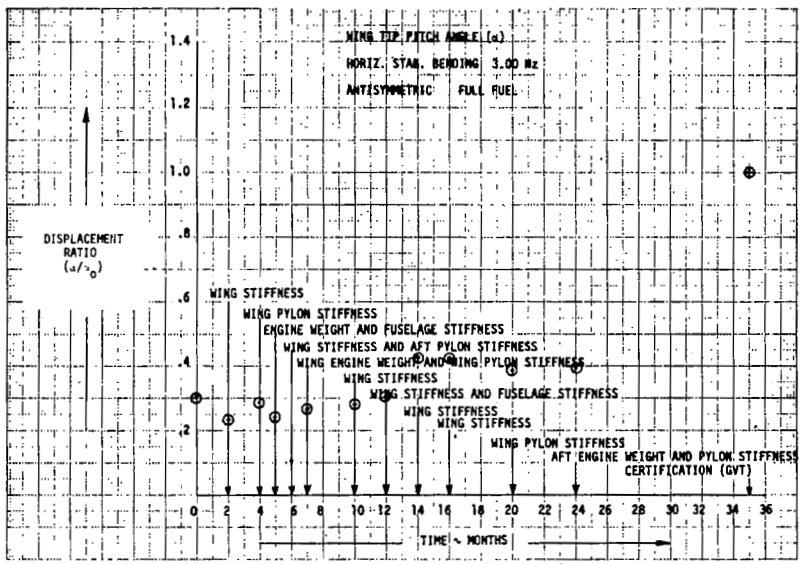

FIGURE 177. EVOLUTION OF DISPLACEMENT RATIO α

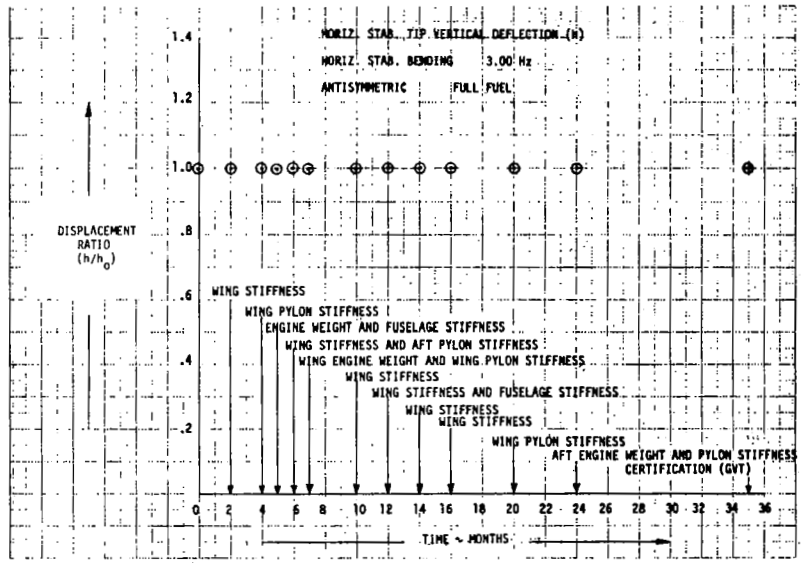

FIGURE 178. EVOLUTION OF DISPLACEMENT RATIO h

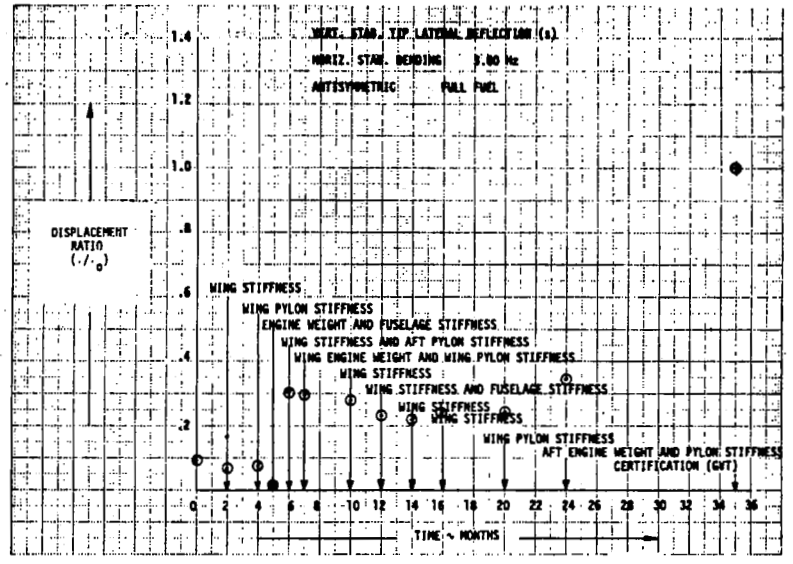

FIGURE 179. EVOLUTION OF DISPLACEMENT RATIO ℓ

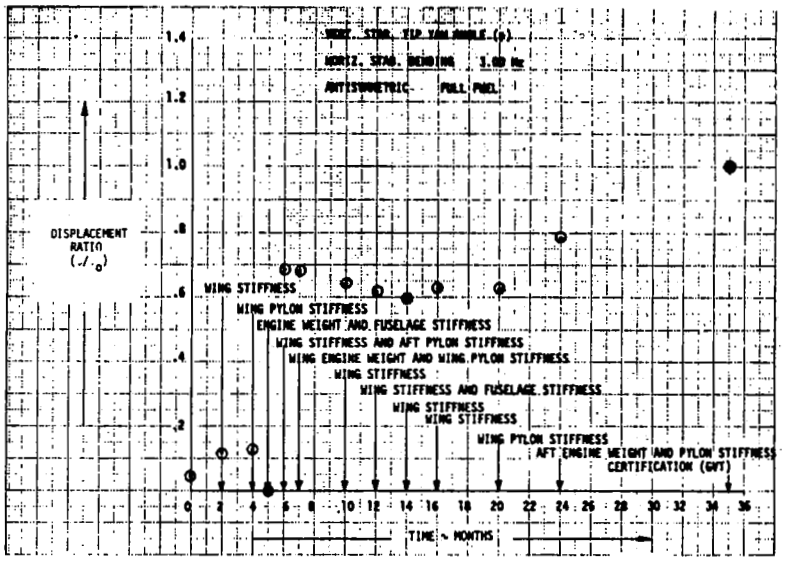

FIGURE 180. EVOLUTION OF DISPLACEMENT RATIO ψ

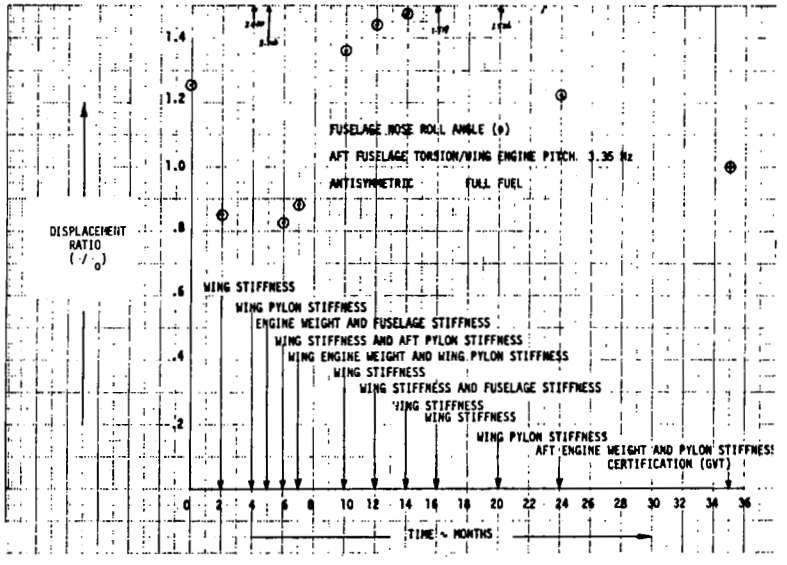

FIGURE 181. EVOLUTION OF DISPLACEMENT RATIO θ

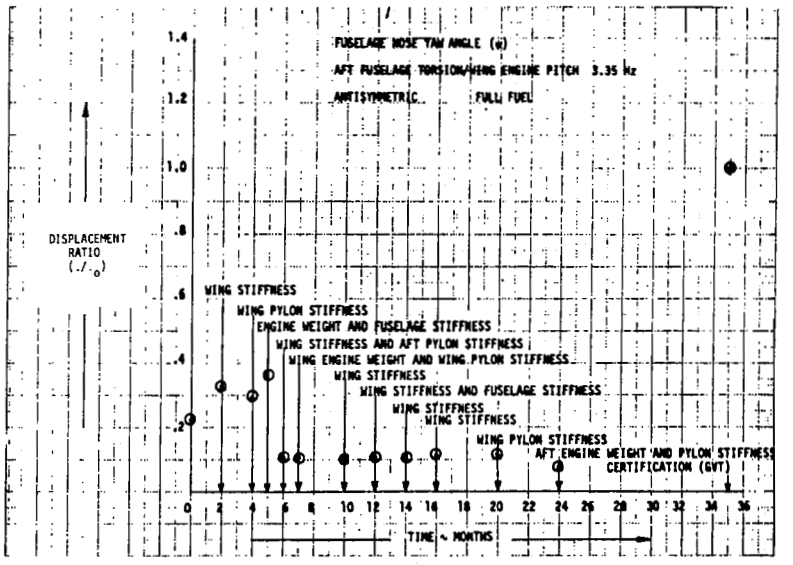

FIGURE 182. EVOLUTION OF DISPLACEMENT RATIO ψ

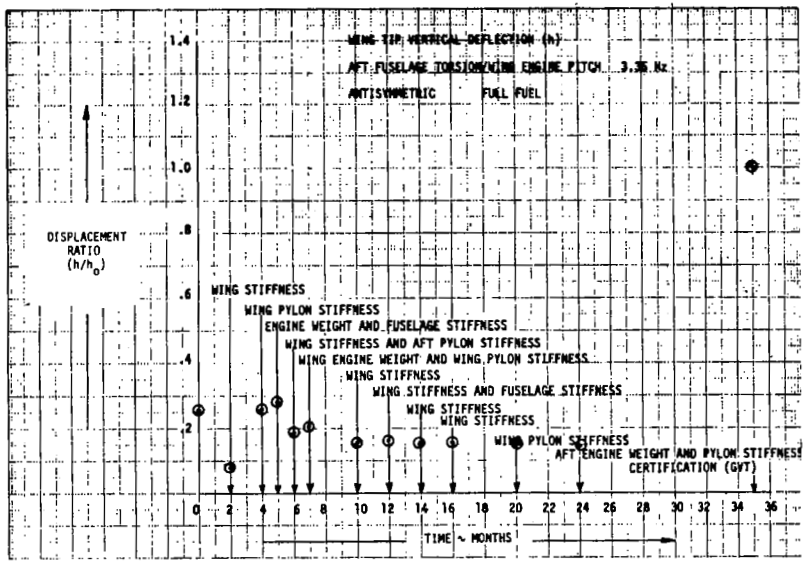

FIGURE 183. EVOLUTION OF DISPLACEMENT RATIO h

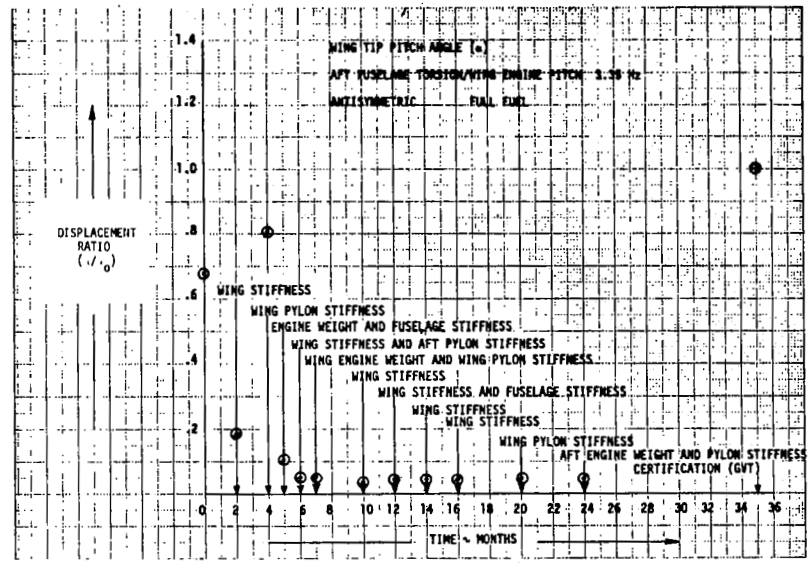

FIGURE 184. EVOLUTION OF DISPLACEMENT RATIO α

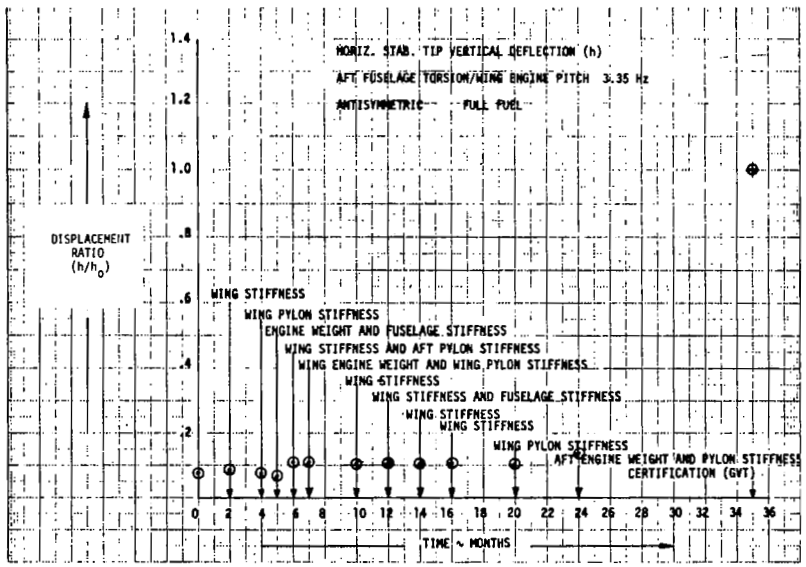

FIGURE 185. EVOLUTION OF DISPLACEMENT RATIO h

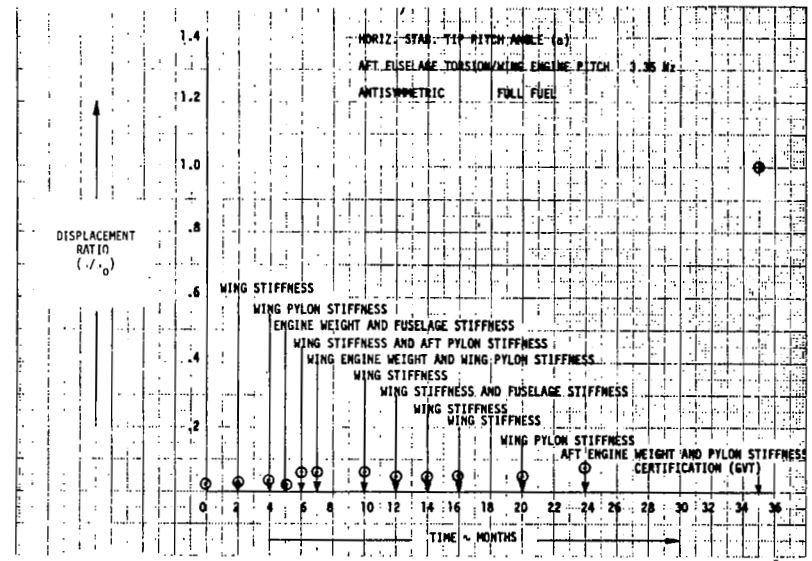

FIGURE 186. EVOLUTION OF DISPLACEMENT RATIO α

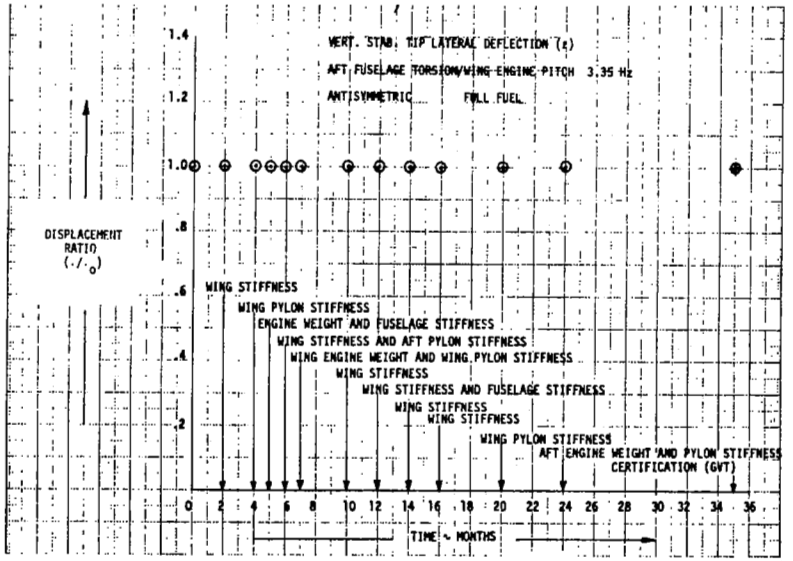

FIGURE 187. EVOLUTION OF DISPLACEMENT RATIO ℓ

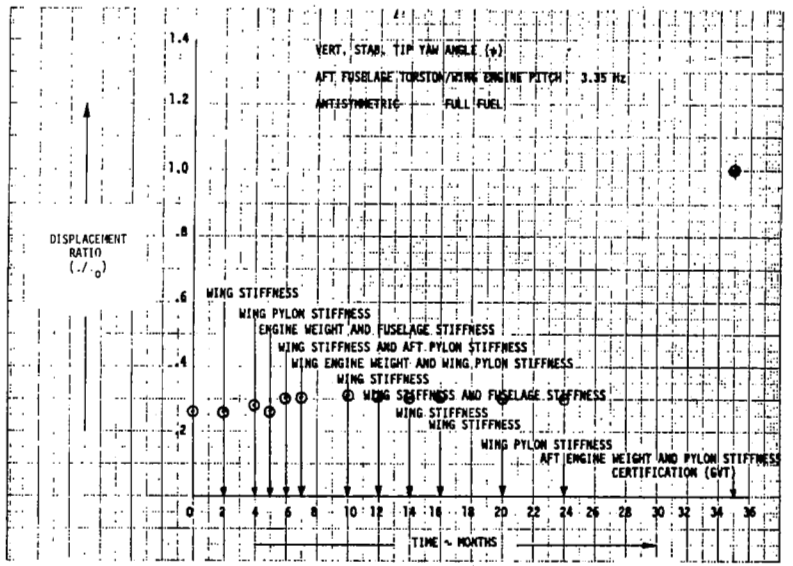

FIGURE 188. EVOLUTION OF DISPLACEMENT RATIO ψ

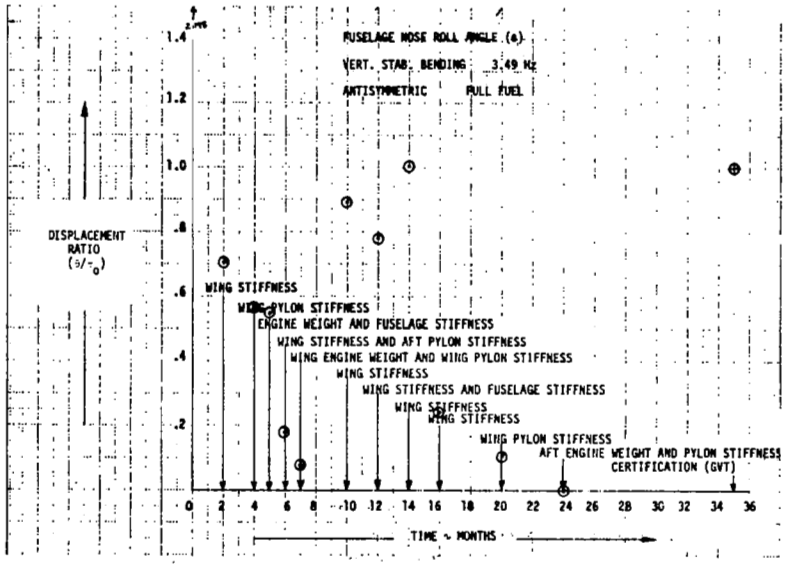

FIGURE 189. EVOLUTION OF DISPLACEMENT RATIO θ

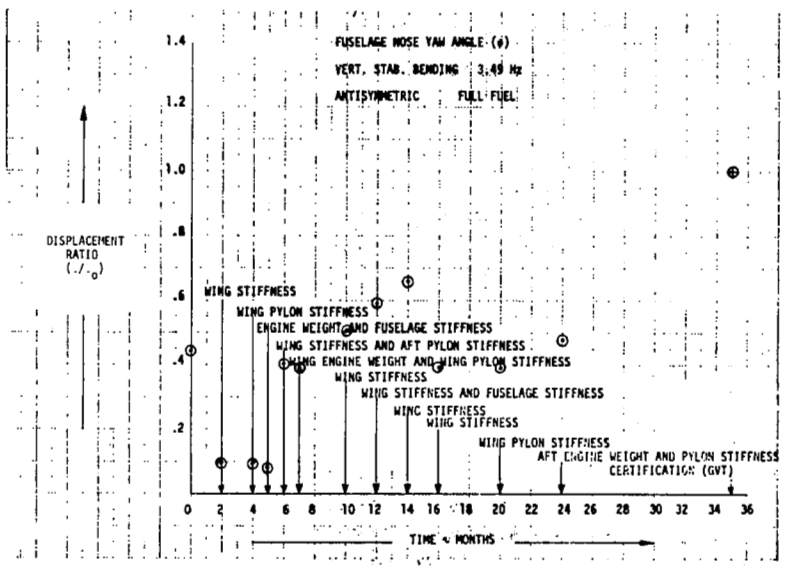

FIGURE 190. EVOLUTION OF DISPLACEMENT RATIO ψ

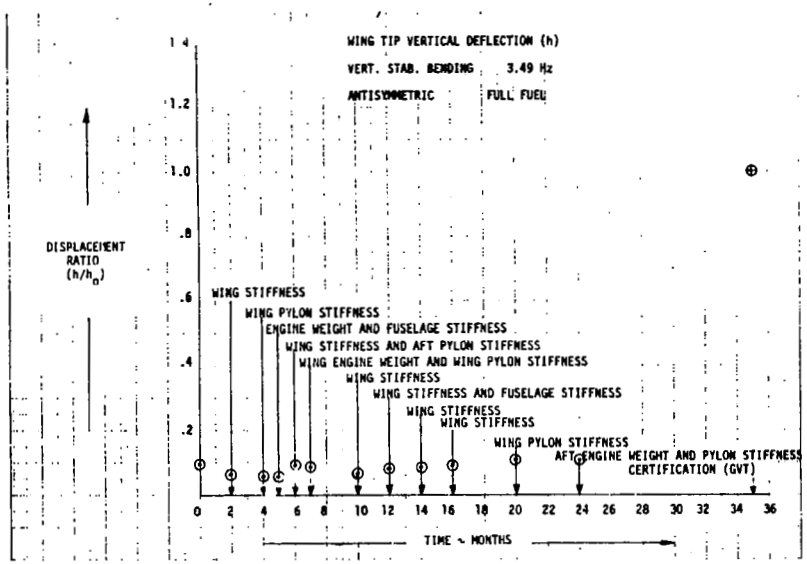

FIGURE 191. EVOLUTION OF DISPLACEMENT RATIO h

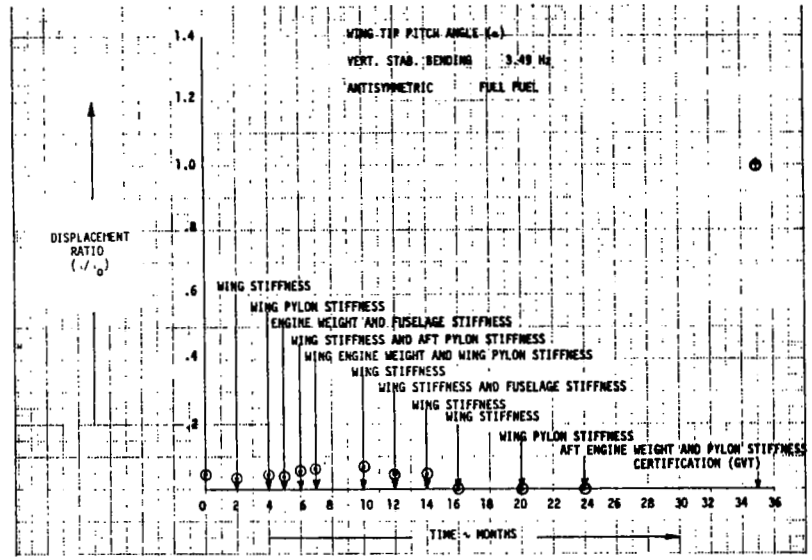

FIGURE 192. EVOLUTION OF DISPLACEMENT RATIO α

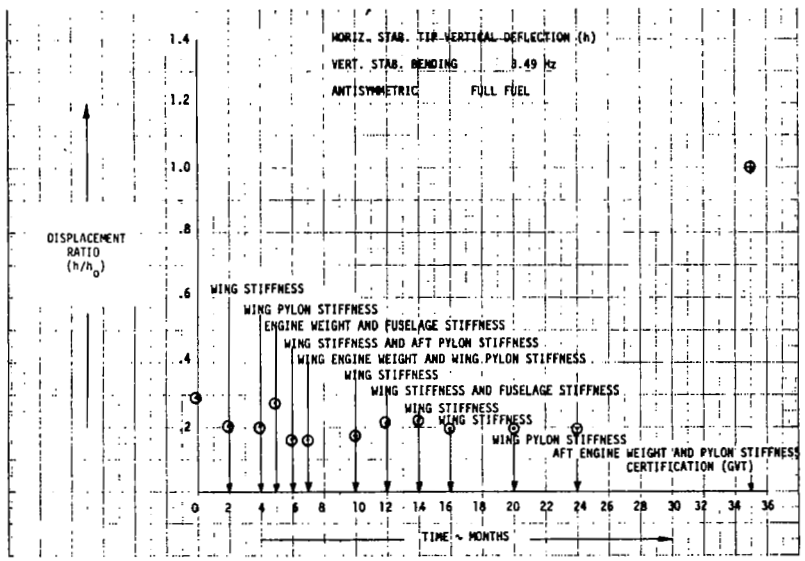

FIGURE 193. EVOLUTION OF DISPLACEMENT RATIO h

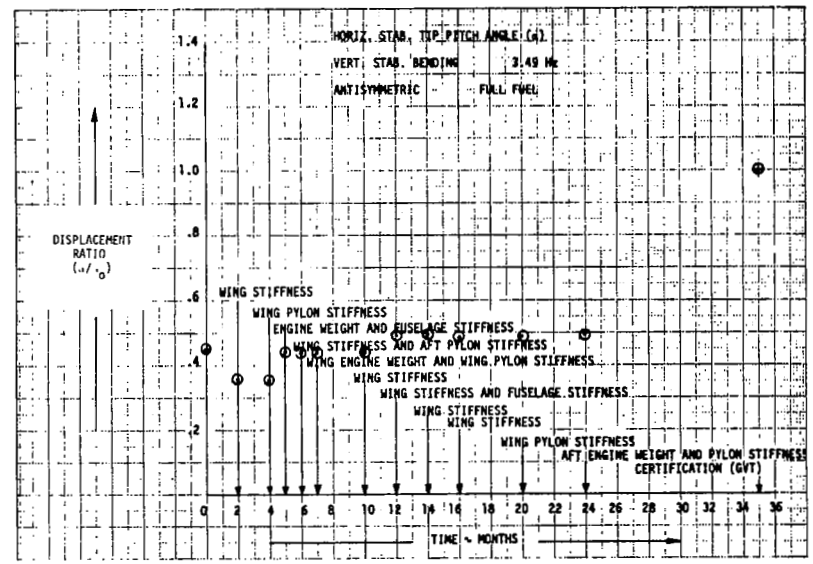

FIGURE 194. EVOLUTION OF DISPLACEMENT RATIO α

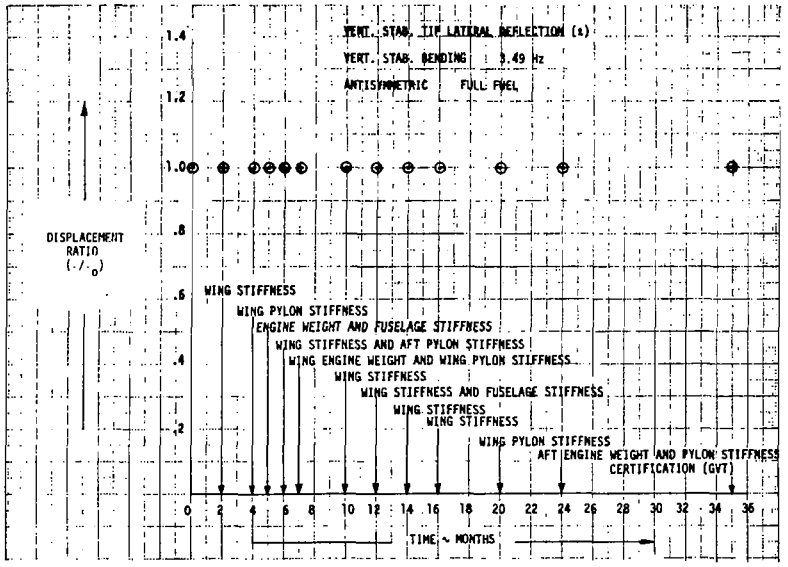

FIGURE 195. EVOLUTION OF DISPLACEMENT RATIO ℓ

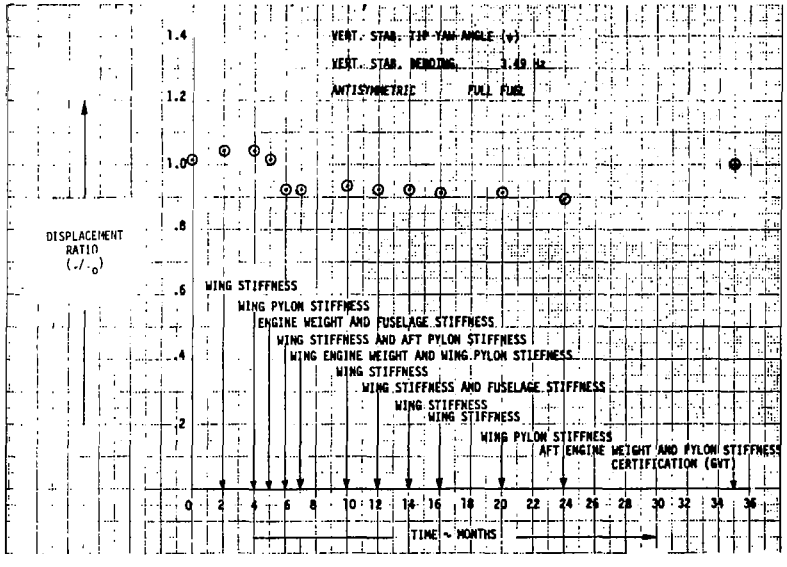

FIGURE 196. EVOLUTION OF DISPLACEMENT RATIO ψ

SECTION 4

SOME POSSIBLE APPLICATIONS

As noted previously, this report is intended to provide a data base for the control system designer so that he can estimate the likelihood that an advanced system will provide its intended function at first flight in the presence of uncertainties in plant and control system dynamics. The specific application of these data will depend on the designer's favorite analytical tools and the general design approach used by a manufacturer. This section will suggest a few ways of using these data. As will be apparent, the assessment of stability margins will be reasonably straight-forward, but the estimation of flying qualities is not quite as easy. Reference 4 gives some results of recent transport simulator handling qualities tests. It is apparent that conflict exists between various popular handling qualities measures, so the system designer will need to use several yardsticks to measure the effects of these reported parameter variations.

CLASSICAL SERVO ANALYSIS APPLICATIONS

Normally the system designer uses classical analysis methods to a first-cut definition of a system based on nominal aerodynamics and an exact specification of control dynamics. A second iteration then considers the change in closed-loop dynamics and system performance due to plant and controller parameter variation. The classical analyst depends on the visibility of system characteristics via root-locus, Bode, and time history plots to aid him in the system design, so it would be desirable to reflect the effects of parameter variability graphically.

If we consider a simple pitch axis problem, the aircraft nominal open-loop dynamics might appear as shown in Figure 197.

The tuck/subsidence, short-period, actuator and first structural modes (nominal) are shown along with the pitch to elevator numerator. The control system designer may be interested in an attitude-hold system for this aircraft and would then make the usual rate plus position closure as shown in Figure 198.

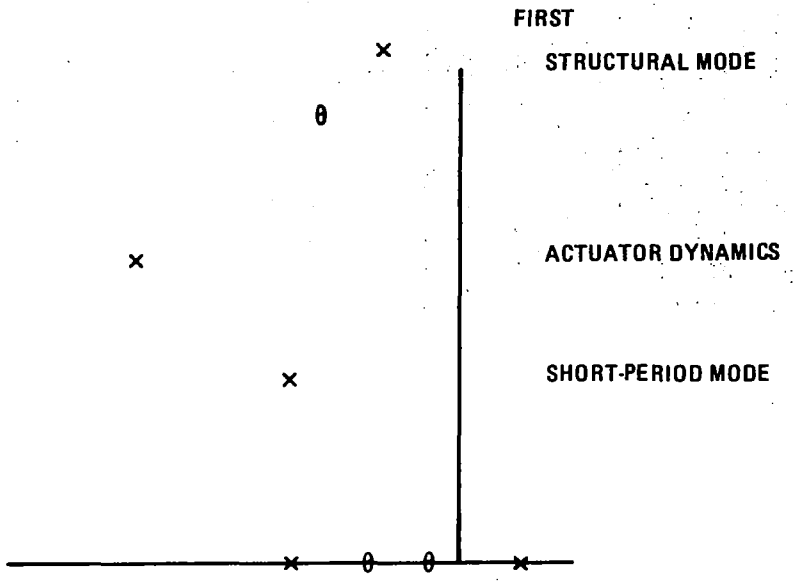

FIGURE 197. TYPICAL LONGITUDINAL ROOT LOCATION

The nominal closed-loop system is well behaved and performs to specification, but the effects of variations in the system parameters are not obvious.

Past work has established the mathematics for assessing the effects of uncertainties on closed-loop characteristics (e.g., Reference 8) but these methods have been so tedious for higher order systems that they have not been generally applied. Computer capacity and speed are now sufficient to allow sensitivity methods such as those developed in reference 8 to be programmed. A Monte Carlo parameter variational approach could be used to establish the "envelopes" of open-loop and closed-loop system parameters for expected plant parameter variations as sketched in Figure 199.

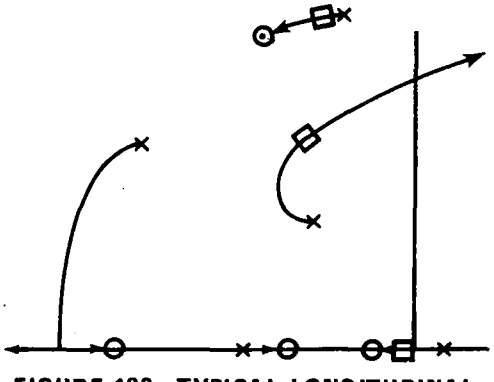

FIGURE 198. TYPICAL LONGITUDINAL SYSTEM ROOT LOCUS

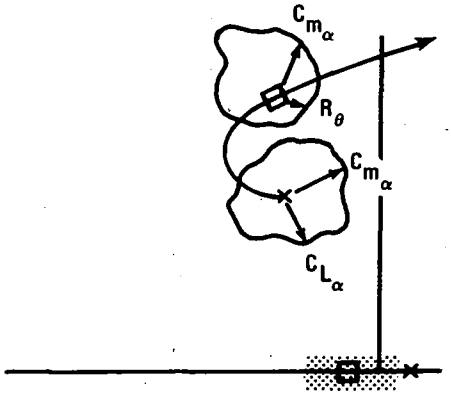

FIGURE 199. CLOSED-LOOP ROOT VARIATION

The designer's task will be to design the system such that $\zeta_{min} < \zeta < \zeta_{max}$, etc., to satisfy the basic flying qualities and structural criteria. Where the modes being stabilized are potentially "flight critical" (e.g., the first-order divergence or second-order low-damped modes shown in Figure 199 could possibly result in unacceptable characteristics), the designer will take all possible assurances that the total pilot/vehicle system will perform reasonably well before the first flight opportunity arrives.

STATE-SPACE SYNTHESIS METHODS

In an initial design exercise, state-space methods are now often used in the form of linear-quadratic-Gaussian synthesis procedures for quickly identifying candidate control systems (References 5 and 6). With estimates of plant uncertainties available, state-space methods can be employed to determine eigenvalue sensitivities in addition to time response and frequency response sensitivities already discussed. Sensitivities may be determined for individual as well as statistically selected combinations of parameter variations. Alternative control system configurations which yield approximately equivalent dynamic performance characteristics are easily synthesized using state-space methods. The sensitivity of these systems to plant parameter variations offer criteria for selection of a particular configuration.

Eigenvalue sensitivities can be obtained from a pole placement synthesis program which employs a first order perturbation approximation to relate changes in the closed-loop system coefficient matrix, A, to changes in the system eigenvalues, Λ.

The matrix equation employed is:

$$D\ \Delta a \simeq \Delta\lambda$$

Where D is the eigenvalue sensitivity matrix, Δa is a vector consisting of the system parameter variations, and $\Delta\lambda$ is a vector consisting of the eigenvalue changes. The sensitivities of the eigenvalues to parameter variations from the nominal values may be determined merely by examining the matrix, D. D would be calculated for various control configurations, and would also be recalculated for cases where the parameters are varied from the nominal values. (Note that Δa consists of the non-zero elements of the matrix ΔA).

The off-nominal sensitivity matrix is obtained by calculating D using the matrix $(A + \Delta A)$ rather than the nominal matrix A.)

PARAMETER IDENTIFICATION AND ADAPTIVE CONTROL APPROACH

Yet another system design philosophy could be to conduct an exercise that shows the aircraft/control system has closed-loop dynamics meeting the designer's specification for the entire range of plant dynamics described by the plant parameters with their expected variation. Such a system might be required to converge within a fixed period of time (which would be much less than the time for control problems to develop) from any and all corners of the open-loop dynamic envelope of Figure 199, and at all flight conditions. The approach would represent a significant departure from the previous two approaches where control system gains are assumed fixed at a specific flight condition.

Such a system design would employ parameter identification techniques to determine plant parameters and to update the control laws in response to on-line measurements of the plant states. A comprehensive bibliography on the system identification problem is contained in Reference 7.

POSSIBLE STATISTICAL USAGE OF STRUCTURAL DYNAMIC RESULTS

The previously described study utilizes only one airplane as a basis for parameter variability determination. The lack of data for a large number of airplanes is compensated to a great extent by the consideration of parameter variability within a reasonably large group of different flexible modes.

For each modal parameter, a measure of variability can be established by bringing the results together from each of the modes. Let $r_{ij}(t)$ denote the value at time t of any of the parameter ratios expressed in the plots. The subscripts indicate that the result for the i-th parameter is being considered for the j-th flexible mode and $\dot{r}_{ij}(t) \to 1$ as $t \to T$, where T denotes the durations to certification. If $b_i(t)$ signifies the average of the logarithms of the i-th parameter values over the modes (i.e., over j), then

$$b_i(t) = \frac{1}{M} \sum_{j=1}^{M} \log r_{ij}(t)$$

M is the number of modes presented in the plots in a defined category (e.g. symmetric, zero fuel) and $b_i(t)$ is the bias tendency of the log of the i-th parameter at time t in the design cycle. Then the variability can be measured by $v_i(t)$, where

$$V_i^2(t) = \frac{1}{(M-1)} \sum_{j=1}^{M} [\log r_{ij}(t) - b_i(t)]^2$$

Having the bias and variability estimates for each parameter, combinations of parameter magnitudes can be selected for investigating the control system design. In studying the airplane performance to control and external inputs, the parameters used for the airplane can be selected as follows: If $p_{ij}(t)$ is the value determined at time t for the i-th parameter of the j-th mode, then a set of nominal parameter values $n_{ij}(t)$ can be obtained as

$$\log n_{ij}(t) = \log p_{ij}(t) - b_i(t); \quad i = 1, \ldots, N^*$$
$$j = 1, \ldots, M^*$$

A set of extreme parameter values $e_{ij}(t)$ are given by

$$\log e_{ij}(t) = \log p_{ij}(t) - b_i(t) \pm 3\, v_i(t); \; i = 1, \ldots, N^*$$
$$j = 1, \ldots, M^*$$

(The number of airplane flexible modes M* used for the control system design may be different than the number M defined above. N* is the number of parameters pertinent to the M* modes).

The determination of parameter combinations from the $P = M^* \cdot N^*$ parameters can be done as follows: In one combination all parameters can be set at their nominal values. For the other 2P combinations, (P - 1) of the parameters are set at their nominal values while the remaining parameter is set at each of its extremes. This simple scheme gives 2P + 1 parameter combinations.

In a previous discussion, it is indicated that a Monte Carlo procedure can be used in selecting the parameters. In this approach it can be assumed that the $\log r_{ij}(t)$ have independent normal distributions with mean $b_i(t)$ and standard deviation $v_i(t)$. From a table of random numbers, values of $\log r_{ij}(t)$ are drawn for each of the P parameters. Now $p_{ij}(t)$ is the value of the parameter

determined at time t in the design cycle. Let $p^r_{ij}(t)$ be a randomly determined value for the same parameter. This value can be found as follows from the randomly selected $r_{ij}(t)$ value:

$$p^r_{ij}(t) = n_{ij}(t) \cdot r_{ij}(t)$$

where $n_{ij}(t)$ is previously defined. The number of combinations required for a Monte Carlo approach will at least be as large as that used in the above simple scheme.

The usages of the plotted results that have been discussed above can be further clarified by considering the following airplane openloop differential equations for the flexible modes: The equation for the j-th mode, in symbolic form, is

$$\sum_{\alpha=1}^{A} [(\delta_{\alpha j}\, \bar{m}_j + C^a_{j\alpha})\, \ddot{q}_\alpha(t) + (4\pi \delta_{\alpha j}\, \zeta_j\, \bar{m}_j f_j + C^v_{j\alpha})\, q_\alpha(t)$$

$$+ (4\pi^2 \delta_{\alpha j}\, \bar{M}_j\, f_j^2 + C^d_{j\alpha})\, q_\alpha(t)] = \sum_{\beta=1}^{B} F_\beta(t)\, \phi_{\beta j}$$

$$(\delta_{\alpha j} = 1 \text{ for } \alpha = j;\ = 0 \text{ otherwise}) \qquad j = 1, \ldots, M^*$$

This second order equation can be converted into two first order equations for the state-space formulation. This transformation is straight-forward and will not be done here. The parameters expressed in the above equations represent the following for the j-th mode:

$\bar{m}_j$ - generalized mass

ζ_j - critical damping factor

f_j - natural frequency

$\phi_{\beta j}$ - modal coordinate at location

$C^a_{j\alpha}$, $C^v_{j\alpha}$, $C^d_{j\alpha}$ - generalized unsteady aerodynamic coefficient matrix elements associated, respectively, with aerodynamic forces produced by accelerations, velocities and displacements.

The time-dependent quantity $q_\alpha(t)$ is the generalized displacement for the α-th mode. $\dot{q}_\alpha(t)$ and $\ddot{q}_\alpha(t)$ are the associated first and second time derivatives. $F_\beta(t)$ is an external time-varying force acting on the mode shapes at the number β modal coordinate.

The number, A, of modes over which the left-hand side summation is conducted equals the number of flexible plus rigid body modes being considered. The number of modal coordinates B for the right-hand side summation is given by the size of the modal eigenvectors. The number of parameters N* necessary to define each modal equation is at most 3 + 3A + B. (A modal coordinate $\phi_{\beta j}$ is not needed if no force is associated with it).

The N* parameters for the j-th mode can be placed in the j-th column of a matrix array. The i-th row element of this column is the parameter quantity p_{ij} previously defined. Since the parameters pertain to a particular time t in the design, they are designated as $p_{ij}(t)$. No data has been presented in this report for the parameter $p_{ij}(t) = \zeta_j$ to calculate its bias or variability. Its value selected for any control system study will then remain fixed at its determined value. A similar statement applies to each of the coefficients $C^a_{j\alpha}$, $C^v_{j\alpha}$ and $C^d_{j\alpha}$. Thus of the possible set of N* parameters for the j-th modal equation, the results in the given plots will provide bias and variabilty information for at most 2 + B of the parameters.

CONCLUSIONS AND RECOMMENDATIONS

Based upon the uncertainty investigation over the design period of a single large transport aircraft the following conclusions are made:

1. The largest variation in modal parameters occurs during the early design phase, reflecting major design changes.
2. Analyses performed after the early design phase show less variation in modal parameters, reflecting minor modification to the airplane design data.

3. No discernable trend was seen in the parameter uncertainties between fuel condition or airplane symmetry.
4. The modal generalized mass and displacement parameters show much larger variations than do the modal frequency parameters and are of limited use except as input to further response analyses.
5. The magnitude of the input modal displacement ratio shows little or no correlation to the magnitude of the output response acceleration ratio.
6. By the time the basic design characteristics have stabilized, the structural dynamic modal characteristics can be predicted adequately for use in the control system design.
7. The generalized mass and modal amplitudes, by themselves, do not provide insight to the airplane flight response characteristics.

The modal parameter uncertainty results presented herein represent a starting point for further studies. Recommendations are as follows:

1. The preferred location of sensors is often at nodal or antinodal points. The uncertainty of these points should be determined to enable optimum sensor placement at an early part of the design cycle.
2. The effect of variations in airplane (i.e. plant) parameters on airplane flight control should be evaluated in a follow-on phase. The parameters whose variations produce the most pronounced effects should be identified. Control system designs should then be studied to determine the extent to which these sensitivities can be reduced. The proper positioning of sensors and control surfaces would be part of this study along with the design of the control system.
3. The effect of unsteady aerodynamics uncertainties should be investigated for the purpose of not only improving control system functions but for the immediate problem of flutter prevention.

APPENDIX A

BODY AXES EQUATIONS OF MOTION

Longitudinal Set:

$$\dot{u} = - W_o q - g\theta \cos \theta_o + X_u u + X_q q + X_w w + X_{\dot{w}} \dot{w} + X_{\delta_e} \delta_e$$

$$\dot{w} = U_o q - g\theta \sin \theta_o + Z_u u + Z_q q + Z_w w + Z_{\dot{w}} \dot{w} + Z_{\delta_e} \delta_e$$

$$\dot{q} = M_u u + M_q q + M_w w + M_{\dot{w}} \dot{w} + M_{\delta_e} \delta_e$$

Lateral-Directional Set:

$$\dot{v} = - U_o r + W_o p + g\psi \sin \theta_o + G\phi \cos \theta_o + Y_r r + Y_v v + Y_p p + Y_{\delta_a} \delta_a + Y_{\delta_r} \delta_r + Y_{\delta_{sp}} \delta_{sp}$$

$$\dot{p} = \dot{r} \frac{I_{xz}}{I_x} + L_r r + L_v v + L_p p + L_{\delta_a} \delta_a + L_{\delta_r} \delta_r + L_{\delta_{sp}} \delta_{sp}$$

$$\dot{r} = \dot{p} \frac{I_{xz}}{I_z} + N_v v + N_r r + N_p p + N_{\delta_a} \delta_a + N_{\delta_r} \delta_r + N_{\delta_{sp}} \delta_{sp}$$

APPENDIX B

DEFINITION OF COEFFICIENTS OF EQUATIONS OF MOTION (DIMENSIONAL STABILITY DERIVATIVES)

$$W_o = \alpha_o U_o$$

$$X_u = \frac{\rho US}{m}(-C_{D_u} - C_D$$

$$X_q = \frac{\rho US\bar{c}}{4m} C_{D_q}$$

$$X_w = \frac{\rho US}{2m}(C_L - C_{D_\alpha})$$

$$X_{\dot{w}} = -\frac{\rho S\bar{c}}{4m} C_{D_{\dot{\alpha}}}$$

$$X_{\delta_e} = \frac{\rho U^2 S}{2m} C_{D_{\delta_e}}$$

$$Z_u = \frac{\rho US}{m}(-C_{L_u} - C_L)$$

$$Z_q = \frac{\rho US\bar{c}}{4m} C_{L_q}$$

$$Z_w = \frac{\rho US}{2m}(-C_{L_\alpha} - C_D)$$

$$Z_{\dot{w}} = -\frac{\rho S\bar{c}}{4m} C_{L_{\dot{\alpha}}}$$

$$Z_{\delta_e} = \frac{\rho U^2 S}{2m} C_{L_{\delta_e}}$$

$$M_u = \frac{\rho US\bar{c}}{I_y}(C_{m_u} + C_m)$$

$$Y_r = \frac{\rho USb}{4m} C_{y_r}$$

$$Y_v = \frac{\rho US}{2m} Cy$$

$$Y_p = \frac{\rho USb}{4m} C_{y_p}$$

$$Y_{\delta_a} = \frac{\rho U^2 S}{2m} \epsilon_{y_{\delta_a}}$$

$$Y_{\delta_r} = \frac{\rho U^2 S}{2m} C_{y_{\delta_r}}$$

$$L_r = \frac{\rho USb^2}{4I_x} C_{\ell_r}$$

$$L_v = \frac{\rho USb}{2I_x} C_{\ell_\beta}$$

$$L_p = \frac{\rho USb^2}{4I_x} C_{\ell_p}$$

$$L_{\delta_a} = \frac{\rho U^2 Sb}{2I_x} C_{\ell_{\delta_a}}$$

$$L_{\delta_r} = \frac{\rho U^2 Sb}{2I_x} C_{\ell_{\delta_r}}$$

$$N_v = \frac{\rho USb}{2Iz} C_n$$

$$N_r = \frac{\rho USb^2}{4I_z} C_{n_r}$$

$$M_q = \frac{\rho U S \bar{c}^2}{4 I_y} C_{m_q}$$

$$M_w = \frac{\rho U S \bar{c}}{2 I_y} C_m$$

$$M_{\dot{w}} = \frac{\rho S \bar{c}^2}{4 I_y} C_{m_{\dot{\alpha}}}$$

$$M_{\delta_e} = \frac{\rho U^2 S \bar{c}}{2 I_y} C_{m_{\delta_e}}$$

$$N_p = \frac{\rho U S b^2}{4 I_z} C_{n_p}$$

$$N_{\delta_r} = \frac{\rho U^2 S b}{2 I_z} C_{n_{\delta_r}}$$

$$N_{\delta_a} = \frac{\rho U^2 S b}{2 I_z} C_{n_{\delta_a}}$$

$$N_{\delta_{sp}} = \frac{\rho U^2 S b}{2 I_z} C_{n_{\delta_{sp}}}$$

$$L_{\delta_{sp}} = \frac{\rho U^2 S b}{2 I_x} C_{\ell_{\delta_{sp}}}$$

$$Y_{\delta_{sp}} = \frac{\rho U^2 S}{2 m} C_{y_{\delta_{sp}}}$$

REFERENCES

1. Finck, R.D.; Ellison, D.E.; and Malthan, L.V., et al.: USAF Stability And Control Datcom. October 1960, revised January 1974.

2. DeYoung, J.; and Harper, C.W.: "Theoretical Span Loading at Subsonic Speeds for Wings Having Arbitrary Plan Form." NACA TR-921, 1948.

3. Hedman, S.G.: "Vortex Lattice Method for Calculation of Quasi Steady State Loadings on Thin Elastic Wings in Subsonic Flow." Report 105, The Aeronautical Research Institute of Sweden, October 1965.

4. Rickard, W.W.: "Longitudinal Flying Qualities in the Landing Approach." Proceedings of the 12th Annual Conference on Manual Control, May 1976.

5. Kriechbaum, G.K.L.; and Stineman, R.W.: "Design of Desirable Airplane Handling Qualities via Optimal Control." J. Aircraft. Vol. 9, No. 5, May 1972.

6. Markland, C.A.: "Optimal Model-Following Control System Synthesis Techniques." Proc. I.E.E., Vol. 117, No. 3, March 1970.

7. Astrom, K.J.; and Eykhoff, P.: "System Identification" - A Survey, Automatic, Vol. 7, pp. 123-162, 1971.

8. McRuer, D.J.; and Stapleford, R.L.: "Sensitivity and Modal Response for Single-Loop and Multi-Loop Systems." ASD-TDR-62-812, January 1963.

9. Vandierendonck, A.J.: "Design Method for Fully Augmented Systems for Variable Flight Conditions." AFFDL-TR-71-152, January 1972.

*U.S. GOVERNMENT PRINTING OFFICE: 1977 - 735-004/33